Determination of immunomodulatory bioactivity biomarkers and mechanistic insights in umbilical cord mesenchymal stromal cells

Submitted by

Dylan Siriwardena

Thesis submitted to the Faculty of Graduate and Postdoctoral Studies in partial fulfillment of the M.Sc. program in Cellular and Molecular Medicine

University of Ottawa Faculty of Medicine Department of Cellular and Molecular Medicine

Supervisor: William Stanford, PhD

Submitted: November 24, 2018

Ottawa, Ontario, Canada

Abstract

Detrimental immune and inflammatory responses contribute to the pathogenesis of various conditions, including Crohn's disease, Lupus, and sepsis.[1,2,3] Unfortunately, novel treatments for detrimental immune and inflammatory responses have been met with little success. Mesenchymal stromal cells (MSCs) represent a promising cellular therapy to treat immune and inflammatory disorders due to their ability to suppress the immune system. However, despite their promise, clinical trials that have employed MSC cellular therapies have produced varying and sometimes conflicting results. These discrepancies have been partially attributed to the cellular heterogeneity within MSC populations. To address these discrepancies, I performed transcriptomic and proteomic analysis of MSCs with varying immunomodulatory capacity to identify robust immunomodulatory biomarkers and gain better mechanistic insights into MSC immunomodulatory function. In this study, MSCs with differing immunomodulatory function were identified and the effect of *in vitro* passaging and proinflammatory induction on immunomodulatory ability was characterized. To characterize MSC immunomodulatory control mechanisms, RNA sequencing and proteomic analyses were performed on MSCs with different immunomodulatory capabilities. These analyses enabled the identification of potential immunomodulatory biomarkers and regulatory mechanisms. Finally, to test the therapeutic efficacy of immunomodulatory MSC subpopulations, I developed a humanize mouse model for sepsis. Overall, this work contributes to our understanding of MSC immunomodulation and to the development of a robust MSC cellular therapeutics.

Acknowledgements

First and foremost, to Dr. William Stanford and Dr. Caryn Ito, thank you for your mentorship and kindness, without which this project would not have been possible. I would not be the researcher I am today without your guidance. To Dr. Carolina Ilkow and Dr. Bernard Thébaud, thank you for your valuable suggestions, which were instrumental to the development of the project. To Dr. Julien Yockell-Lelievre, thank you for your expertise and intriguing problems. I will miss our conversations on science and more. To Angela Raymond and Carole Dore, thank you for your infinite patience. Neither I or the lab would still be in one piece without your help. To my fellow lab members, thank you for all the useful suggestions and friendly environment. To Priya Chandran, Winston Cheung, and Chandarong Choey, thank you for your significant contributions to the project. To Nader El-Sayes and the bois, thank you for keeping me sane in the face of research. To Zhaoyi Chen, thank you for your kindness and support. Without your snacks, beatings and unending support, my thesis would still be unwritten. Lastly, to Amma, Appachchi, and Akki, thank you for the love you have given me over the past 25 years. Everything I have achieved was only made possible by your guidance.

Table of Contents

List of Abbreviations

ALT	Alanine transaminase	**FBS**	Fetal bovine serum
AST	Aspartate transaminase	**FDR**	False discovery rate
BM	Bone marrow	**GO**	Gene ontology
BM-MSC	Bone marrow MSCs	**grB**	granzyme B
CD	Cluster of differentiation	**GVHD**	Graft versus host disease
CFSE	Carboxyfluorescein succinimidyl ester	**helper T cells**	Th
CFU	Colony forming unit	**HSPC**	Hematopoietic stem and progenitor cell
CLP	Cecal ligation and puncture	**HUCPVC**	Human umbilical cord perivascular cell
COX-2	Cyclo-oxygenase 2	**IDO**	Indoleamine-pyrrole 2,3-dioxygenase
CPDA-1	Citrate phosphate dextrose adenine anti-coagulant	**IL**	Interleukin
CS	Cecal slurry	**INFγ**	Interferon gamma
CSP	Cecal slurry and puncture model	**LC-MS**	Liquid chromatography-tandem mass spectrometry
DEG	Differentially expressed gene	**lncRNAs**	long non-coding RNAs
DIIRs	Detrimental immune and inflammatory responses	**LPS**	Lipopolysaccharides
EDTA	Ethylenediaminetetraacetic acid	**MHC**	Major histocompatability complex
ER	Endoplasmic reticulum	**MPO**	Myeloperoxidase
ER/G	ER and Golgi apparatus	**MSCs**	Mesenchymal stromal cell

NK cell	Natural killer cell	**RBC**	Red blood cell
NRG	NOD-Rag1^{null} IL2rγ^{null}	**SERPINs**	Serpin protease inhibitors
NSG	NOD-*scid* IL2Rγ^{null}	**TNFα**	Tumor necrosis factor α
PB	Peripheral blood	**TRT**	Tissue regeneration therapeutics
PBS	Phosphate-buffered saline	**UCB**	Umbilical cord blood
PDX	Patient derived xenograft	**UC-MSC**	Umbilical cord MSC
PGE2	Prostaglandin E2	**WJ-MSC**	Wharton's Jelly MSC
pro-T	Human progenitor T		

List of Figures

List of Tables

1.0 Introduction

1.1 Mesenchymal stromal cells

Human mesenchymal stromal cells (MSCs) were first discovered as a rare population of clonal multipotent cells found in the bone marrow.[1,2] MSCs are classically defined by their ability to differentiate into osteogenic, adipogenic, and chondrogenic lineages, their adherence to plastic, and expression of $CD105^+$, $CD73^+$, and $CD90^+$, while lacking hematopoietic markers such as, $CD45^-$, $CD34^-$, $CD14^-$, and $CD11b^-$.[1–4] Other potential markers have been identified since the discovery of MSCs, including $CD79a^-$ or $CD19^-$ and $HLA\text{-}DR^-$.[2,5] Currently, MSCs are predominantly isolated from three sources: adipose tissue, bone marrow, and umbilical cord. However, cells exhibiting MSC characteristics have been isolated from nearly all adult tissues and are closely associated with perivascular cells.[5] Given their multipotent potential and origin, bone marrow MSCs (BM MSCs) were initially applied as a regenerative cellular therapy for osteogenic disorders such as osteogenesis imperfecta.[6–8]

1.2 MSC immunomodulation

Recently, MSCs have been emerging as a promising, novel autologous cellular therapy for immune and inflammatory disorders.[1,9] Indeed, MSCs have been observed to have immunomodulatory activity, repressing both the adaptive and innate immune responses (**Figure 1**).[2–4,7,10,11] The innate immune response defines a set of non-specific barriers designed to prevent and/or eradicate foreign threats. Physical barriers such as the skin regulate external contact with the body, while cellular barriers such as macrophages, natural killer (NK) cells, dendritic cells, and mastocytes aid in the recruitment of additional immune cells and the identification and removal of foreign particles (**Figure 2**). The inflammatory response aids in localizing phagocytes

and macrophages to engulf foreign particles and recruit other immune cells.[12–14] MSCs have been found to directly interact with the innate immune response, for example by converting inflammatory M1 macrophages into an anti-inflammatory M2 phase.[15] MSCs have also been observed to repress dendritic cell differentiation and mastocyte function.[4,16] Since, the inflammatory response is largely induced by the innate immune system through the release of proinflammatory cytokines like tumor necrosis factor α (TNFα) and interleukin-1 (IL-1) from macrophages, mastocytes, and other immune cells, MSCs are also able to directly regulate the inflammatory response, for example through the release of IL-1 receptor antagonist and by decreasing monocyte activation.[13,14,17] In fact, MSCs express a number of chemokine receptors and adhesion molecules, allowing them to selectively localise at the site of the native inflammatory response.[8,18] Thus, MSCs are able to specifically inhibit the innate immune and inflammatory responses.

The adaptive immune response defines a set of specific defense mechanisms designed to enhance the eradication of previously encountered foreign substances. T and B lymphocytes recognize pathogen specific antigens on foreign cells, substrates, or native cells (within their major histocompatibility complex [MHC]) and facilitate their removal.[13,14] Numerous other cell types help facilitate and regulate the adaptive immune response, including regulatory T cells, helper T cells, macrophages, and follicular B helper T cells (**Figure 2**).[12–14] In particular, helper T cells can be activated to differentiate into inflammatory type 1 helper T cells (Th1) and anti-inflammatory type 2 helper T cells (Th2), which are directly involved in B cell antibody secretion, macrophage activation, and cytolytic T cell activation.[19] MSCs have been shown to repress both $CD4^+$ and $CD8^+$ T cell proliferation and activation, by inhibiting activation markers such as CD35 and CD38.[11] Moreover, MSCs have even been observed to inhibit memory T cells

from binding to their cognate peptides and impair B cell proliferation and chemotactic properties.[10,20] MSCs have also been observed to promote the generation of regulatory T cells, which inhibits the immune response.[7] Thus, MSCs are able to modulate both the adaptive and innate immune responses through a variety of immune cell types.

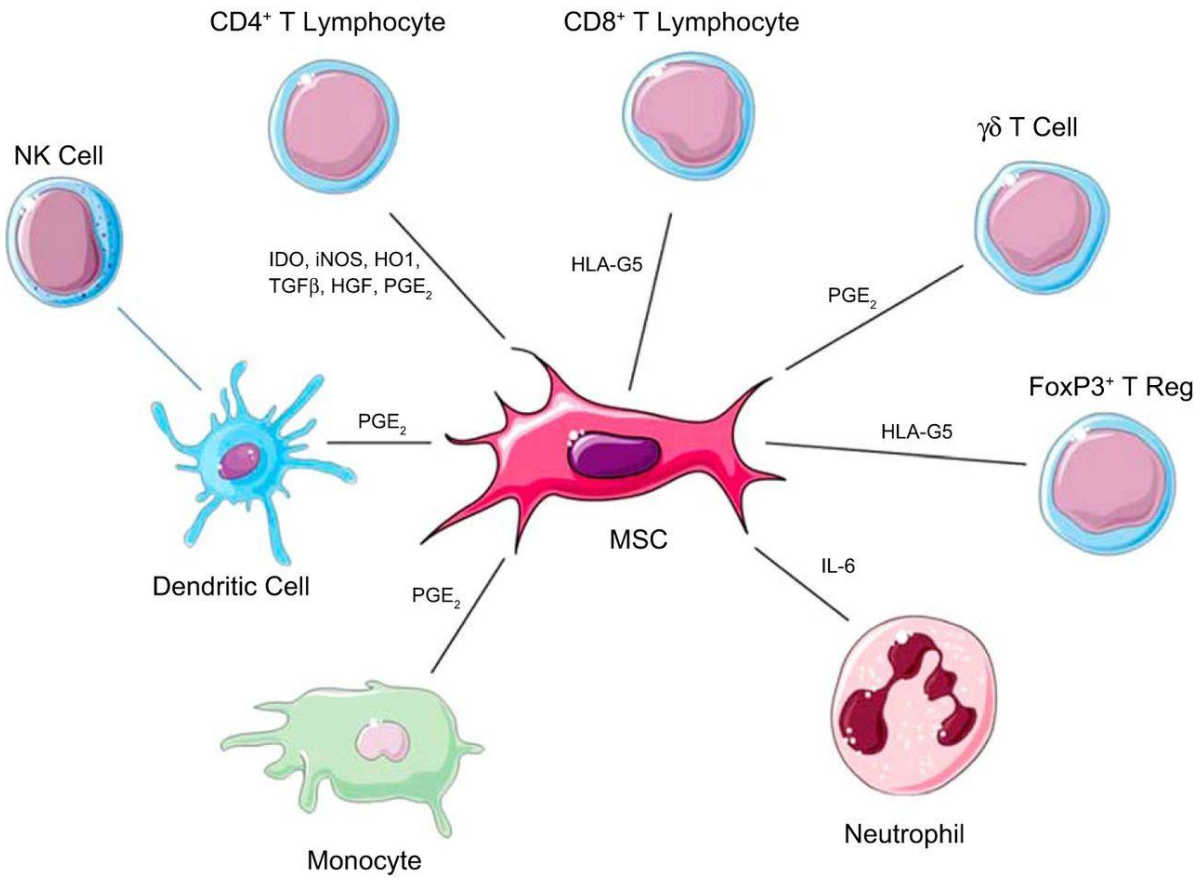

Figure 1. *Immunomodulatory properties of MSCs.*[21] Lines represent MSC interactions with immune cells as mediated by MSC secreted factors. PGE2: Prostaglandin E2, IDO: indoleamine 2,3-dioxygenase, iNOS: inducible nitric oxide synthase, HO1: heme oxygenase 1, HGF: hepatocyte growth factor, TGFβ: transforming growth factor beta, HLA-G5: human leukocyte antigen-G.

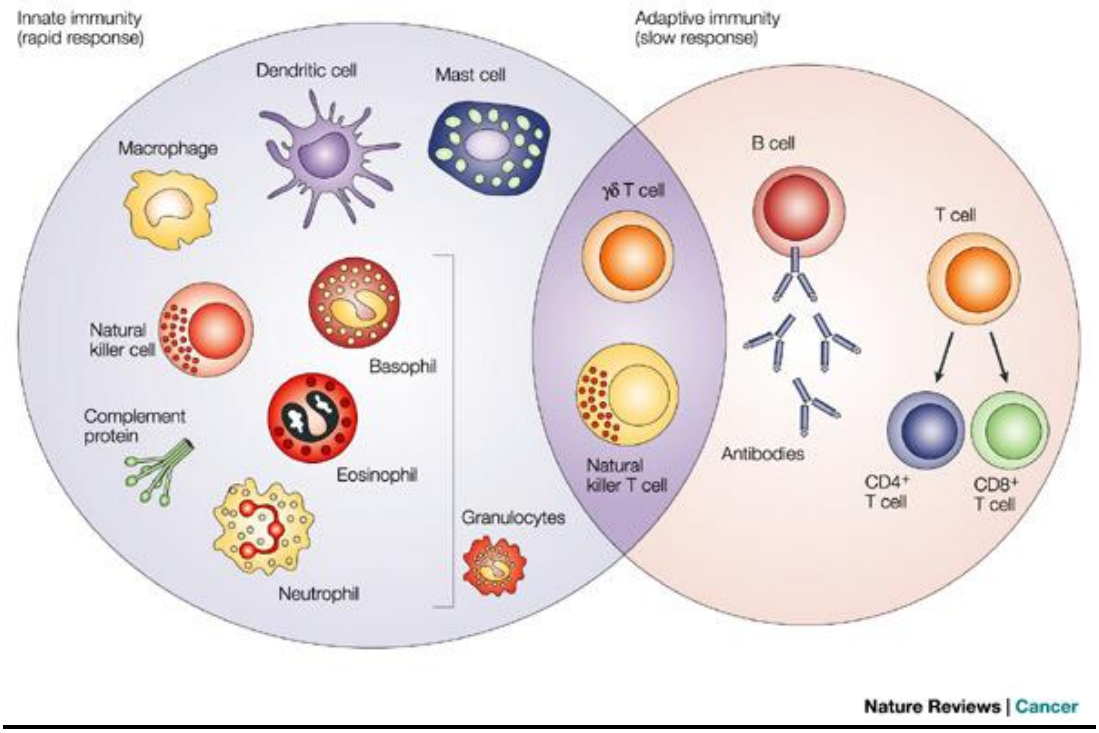

Figure 2. *Overview of important cell types in the adaptive and innate immune responses.*[22]

1.3 MSC immunomodulatory mechanisms

Several MSC immunomodulatory mechanisms have been elucidated, involving cell to cell contact and soluble factors. Studies have demonstrated MSCs secrete numerous factors that generate an immunosuppressive environment within the body.[3,23,24] These factors include prostaglandin E2 (PGE2), indoleamine-pyrrole 2,3-dioxygenase (IDO), and anti-inflammatory cytokines such as IL-10. PGE2 has been shown to inhibit T cell proliferation by inhibiting dendritic cell maturation, activated T cell proliferation and cytokine secretion.[24] IDO catalyzes the conversion of tryptophan to kynurenine, which suppresses the mTORC1 pathway, inhibits T-effector cell growth, and promotes dendritic cell, macrophage, and $CD4^+$ T cell differentiation. These cellular changes activates T regulatory cells, inhibits IL-2 signalling, and impairs $CD4^+$ T

cell survival.[25–28] Interestingly, MSC-mediated lymphocyte suppression can be recovered by the addition of exogenous IL-2, also indicating the prominent role of cytokines in MSC immunomodulation.[8,29] In addition, MSCs secrete numerous other cytokines, including IL-10, IL-6, TGFβ, CCL1, CCL5, VEGF and ICAM, which have varying effects on adaptive and innate immune cell proliferation, activation, and differentiation.[28] MSCs have also been observed to secrete microvesicles and exosomes. MSC-derived microvesicles inhibit T cell proliferation and promote the secretion of anti-inflammatory cytokines including IL-10 and TGF-β.[30] In fact, MSC exosomes have been applied to treat GVHD by promoting activated $CD4^+$ T cell differentiation into T regs.[31] Thus, the release of numerous exogenous factors and vesicles is essential for MSC immunomodulatory capacity. While MSCs have been shown to regulate their local environment via exogenous soluble facts as described above, cell to cell contact has also been shown to enhance MSC immunosuppressive capabilities.[23] For example, MSCs inhibit T cell proliferation and increase the proportion of T regs in a cell contact dependent manner.[7] One possible mechanisms is through the FAS ligand /FAS-mediated T cell apoptosis.[32] Thus, MSCs employ a wide range of soluble and cell to cell dependent mechanisms to induce immunosuppression.

However, it has been reported that MSCs can have varied immunomodulatory influences on the local environment, ranging from anti-inflammatory to proinflammatory responses. Indeed, toll like receptors 1 and 3 have been implicated in controlling the MSC immunosuppressive phenotype, highlighting the importance of environment on MSC phenotype. While both primed and unprimed MSC treatments have been shown to be therapeutically efficacious,[33,34] inducing MSCs with TNFα and INFγ has been shown to increase the secretion of exogenous factors as well as a number of cytokines.[35] Indeed, priming MSCs in a proinflammatory environment has been shown to potentiate their immunosuppressive capabilities.[36,37] In particular, INFγ and TNFα

has been used to increase the secretion of immunosuppressive exogenous factors and to increase MSC efficacy in treating GVHD.[38] TNFα stimulation activates TNFR1 and 2, which are known regulators of inflammatory cytokine production such as IL-6.[39] INFγ primed MSCs have been shown to downregulate T cell activation, enhance T cell negative signalling, interact with antigen-presenting cells and increase proliferation or induce regulatory cells.[36,40–42] Thus, while MSCs represent a promising cellular therapy to treat immune and inflammatory disorders, the precise mechanisms by which MSCs immunomodulate the innate and adaptive immune responses are not fully understood.

1.4 MSC immunoevasion

MSCs lack HLA-DR or co-stimulatory CD40, CD40L, CD80 and CD86, which are key immunogenic surface markers recognized by the human immune system.[43,44] This grants MSCs low immunogenicity, thereby making them an excellent candidate for allogeneic cellular therapeutic. In fact, MSCs express only low levels of MHC I and lack the expression of MHC II, largely protecting MSCs from natural killer cells.[43,45] These features have led to the concept that MSCs are immunoprivileged within the body. However, recent studies have observed immune rejection of allogenic MSCs in some patients.[18,46] Moreover, despite the lack of MHC molecules on MSCs, NK cells have been observed lysing MSCs.[29] These data suggest that the allogeneic effects of MSCs would be transient. Thus, MSCs are likely immunoevasive, making them an ideal candidate for allogenic cellular therapy.

1.5 Umbilical cord MSCs

Umbilical cord MSCs (UC-MSCs) have been shown to exhibit more robust immunomodulatory activity compared with other adult MSC sources such as the bone marrow, especially when primed with inflammatory cytokines such as INFγ and TNFα.[47,48] UC-MSCs are often extracted from two areas within the umbilical cord. Wharton's Jelly MSCs (WJ-MSCs) are derived from connective tissue surrounding the vessels of the umbilical cord, while human umbilical cord perivascular cells (HUCPVCs) are extracted from the perivascular tissue directly wrapping the vasculature (**Figure 3**).[47] Umbilical cord MSCs (UC-MSCs) are also significantly more abundant and readily accessible than bone marrow MSCs (BM-MSCs). While the density of MSCs found in bone marrow varies greatly between humans and is affected by the health and age of the donor, BM-MSCs on average only make up 0.001 to 0.01% of mononuclear cells isolated from bone marrow aspirates, resulting in on average 1500-3000 per mL of aspirate.[49,50] On the other hand, obtaining umbilical cord tissue is non-invasive, while the cord contains on average 1 to 5×10^4 MSCs per cm of cord.[51] Moreover, while exhibiting MSC characteristics, UC-MSCs from neonatal tissue types tend to be more proliferative and differ in their differentiation potential than MSCs of differing origins.[4] As such, UC-MSCs are ideal for the development of novel cellular therapies due to their immunomodulatory ability and ease of procurement.

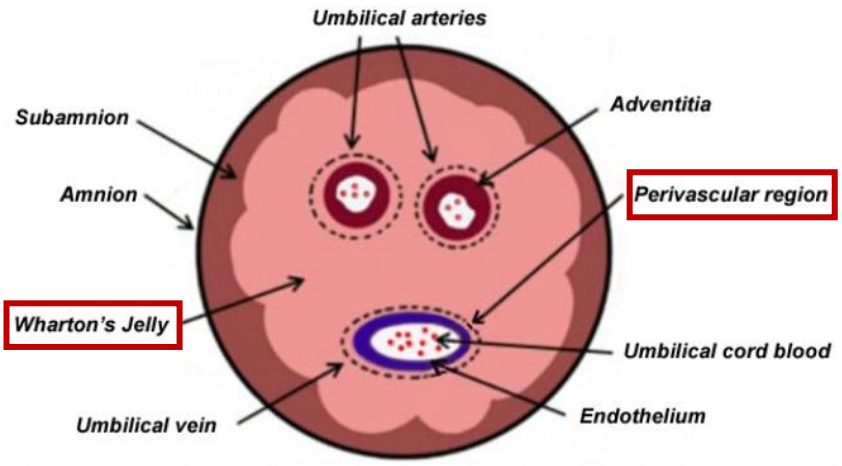

Figure 3: *Cross section of human umbilical cord*. Adapted from Kim et al.[52]

1.6 Detrimental immune and inflammatory responses

Because of their immunomodulatory abilities, MSCs have the potential to treat any number of diseases if its pathophysiology involves the immune or inflammatory response. Detrimental immune and inflammatory responses (DIIRs) are characterized by the harmful misregulation of one or both responses and contribute to the pathogenesis of various autoimmune and hyperinflammatory disorders such as Crohn's disease, type 1 diabetes, lupus, and sepsis.[9,53,54] In Canada alone, more than 500,000 Canadians live with either type 1 diabetes or Crohn's disease, while septic shock remains one the leading causes of in-hospital mortality, with an estimated mortality rate of 30%.[54,55] Autoimmune diseases are characterized by the immune system attacking self-molecules and tissues, ranging from organ specific to systemic. Resultant tissue damage often triggers an inflammatory response that exacerbates the disease my recruiting more immune cells. Similarly, severe inflammatory diseases are propagated by innate immune cells such as macrophages and monocytes. Current treatment options for DIIRs predominantly focus upon treating the inciting trauma or infection with antibiotics to control any infection and

corticoid steroids to control the inflammatory response. Unfortunately, novel treatments for DIIRs have been met with little success. Over the past 40 years, none of the over 100 clinical trials targeting the systemic inflammatory response of sepsis demonstrated therapeutic efficacy.[56] These failures have been largely attributed to the complexity and progression of the inflammatory response and disease course heterogeneity between patients.[57] Consequently, treatment methods targeting a single element of the immune response may have little or potentially detrimental therapeutic efficacy if administered. On the other hand, MSCs modulate numerous immune cell types, making them ideal to treat DIIRs.

Crohn's disease exemplifies this interplay, being a type of inflammatory bowel disease caused by autoimmune interactions.[58] Specifically, T cell autoimmune function has been largely implicated in causing the detrimental inflammatory response.[58] Moreover, current research increasingly implicates the innate immune system's regulatory role in disease pathophysiology. For example, NFκB – an important regulator of the innate immune response – has been shown to both exacerbate and suppress the Crohn's inflammatory response.[59–61] NFκB activation has been observed to upregulate protective molecules that inhibit the inflammatory response such as CARD15, cyclo-oxygenase 2 (COX 2), β defensins, PPARγ and IκBα, while stimulating the expression of inflammatory cytokines such as IL-6, and TNFα.[60,61] Consequently, considering the complexity of Crohn's pathophysiology, it is not surprising that anti-inflammatory drugs and immune suppressers that target specific cell types or cytokines do not always exhibit therapeutic efficacy. MSCs on the other hand have been shown to have greater immunosuppressive capability in the presence of inflammatory cytokines such as TNFα, promoting greater suppression of inflammatory cytokines including COX 2. In fact, pilot clinical trails employing MSCs to treat Crohn's disease showed promising results after 12 months post treatment.[33,62]

Thus, the ability of MSCs to target multiple aspects of both the immune and inflammatory response makes them an excellent candidate for novel therapeutics.

Sepsis is another example of a life-threatening organ dysfunction caused by a dysregulated host response to infection. It is elicited by a complex host response to infection causing immune-mediated systemic inflammation, aberrant coagulation, and microvascular instability.[63,64] In particular, sepsis is characterized by a hyperactivation of the inflammatory response, causing the over-production of pro and anti-inflammatory cytokines, also known as a cytokine storm. The resultant inflammatory response places great stress on the patient's body, causing body temperature fluctuations between fever and hypothermia, significant changes in white blood cell count, and increased heart and respiratory rates.[65,66] If the underlying circulatory, cellular, and metabolic abnormalities are profound enough to substantially increase mortality, the patient is deemed to be in a state of septic shock.[56,65] Those patients that do not succumb to septic shock are susceptible to potentially fatal secondary infections due to anti-inflammatory mediated immunosuppression.[67–70] Indeed, the initial inflammatory phase is often followed by an anti-inflammatory or immunosuppressive phase characterized by a marked decrease of proinflammatory cytokines and T cell exhaustion — the global downregulation in T-cell proliferation.[71–74] Furthermore, a decrease in inflammatory Th1 has been observed compared to anti-inflammatory type Th2, further muting the inflammatory response.[75,76] MSCs can address the complex nature of the sepsis immune and inflammatory response by suppressing the initial proinflammatory phase through interactions with macrophages and monocytes. Moreover, as mentioned earlier, MSCs exhibit greater immunosuppression in the presence of proinflammatory cytokines.[38] Conversely, if a patient progresses to the immunosuppressive phase, MSC immunosuppression would also decrease, reducing the chances of exacerbating the patient's

condition. In fact, a bone marrow MSC treatment for septic shock currently passed phase I safety trials and are proceeding to phase II clinical trials.[77] Thus, the ability of MSCs to modulate numerous immune cell types and be sensitive to their inflammatory environment make them an excellent potential therapy for DIIRs.

1.7 Developing MSC cellular therapies

Despite indications that MSCs would be a potential cellular therapeutic to treat inflammatory and immune disorders, clinical trials that have employed MSC cellular therapies have produced varying and sometimes conflicting results. As mentioned above, MSCs have been applied to prevent GVHD to varying success.[78] In fact, a number of studies have shown MSC efficacy to treat or delay GVHD, including a phase II trail by Le Blanc and colleagues showing a 50% response rate using MSCs to treat GVHD with a mean of 1.4 million bone marrow MSCs.[79] However, numerous MSC clinical trails have demonstrated mixed results. A meta-analysis examining MSC treatment of steroid refractory acute graft versus host disease as caused by allogeneic hematopoietic stem cell transplantation revealed only limited efficacy treating lower grade GVHD.[80] MSC trials for ulcerative colitis and ischemic stroke (Athersys), three cardiac repair studies (Miltenyi Biotec; FBC Pharmicell, Korea; and Stempeutics Research), Acute respiratory distress syndrome (China), and Multiple Sclerosis (Spain) have failed or been terminated.[33] Due to these varying results, no MSC cellular therapy has received FDA approval as of January 2018.[81] Thus, while MSCs have numerous promising characteristics, more research is required to determine what aspects are contributing to therapeutic efficacy.

A number of factors are likely impacting the efficacy of MSC therapeutics. For example, MSC treatments often exhibit little to no long term engraftment, despite MSCs homing to sites of inflammation.[82] The lack of engraftment severely impacts therapeutic efficacy by limiting the

time and level of interaction between MSCs and their therapeutic targets.[83] Indeed, as described above, some immunomodulatory interactions are dependent on cell-cell contact. Perhaps the greatest hurdle facing the development of MSC therapeutics lies in the phenotypic heterogeneity between MSCs of differing donors, tissue types, and potentially clones.[5] While each of these extracted samples are MSCs by definition, they often differ in their proliferative capacity and potency.[84] For example, MSCs harvested from the same type of tissue exhibit a large range of donor to donor variability, exhibiting differences in functional potential depending on donor age and health.[84–86] MSCs derived from the bone marrow of 17 healthy human donors exhibited varying growth rate, alkaline phosphatase levels, and osteogenic potential.[84] Surprisingly, even MSCs isolated from the same tissue and donor exhibit different differentiation and proliferation potential, often favouring a particular lineage.[87,88] This heterogeneity has been observed in therapeutic efficacy of MSC treatments for immunological diseases such as graft versus host disease (GVHD).[23,78] In another study, Jiang et al was able to induce greater MSC-mediated cartilage repair using screened MSC clonal populations with greater chondrogenic capacity than unscreened populations.[89] It should be noted that for most clonal studies, MSCs are cultured for at least some period *in vitro*, raising the possibility that the MSC clonal variation could be exacerbated by culture conditions such as hard substrates and non-dynamic environments as they select for particular clones. Consequently, since large numbers of MSCs are required for a robust cellular therapy, the selected clones may differ between MSC cultures even from the same source, introducing more heterogeneity into therapeutic efficacy.

To address MSC phenotypic heterogeneity, novel biomarkers to identify and characterize MSC subpopulations are being studied. For example, $Nestin^+$ bone marrow perivascular MSCs have been postulated to contribute to bone development.[90]. Han et al. found $CD106^+$ chorionic

villi MSCs exhibited greater immunomodulatory qualities and was found to be expressed across multiple MSC sources including umbilical cord, adipose tissue, and bone marrow.[91] However, the manner in which CD106 (VCAM1) contributes to immunomodulatory regulation within MSCs is largely unknown. These results indicate that a better characterization of MSC heterogeneity, bioprocessing of MSC lots, and an improved understanding of MSC immunomodulation would potentially allow the isolation and optimization of MSC-based cellular therapies.[92]

1.8 Disease models

Pre-clinical models that better recapitulate the human condition would also facilitate the development of better MSC immune and inflammatory therapies. Numerous therapeutics – including MSCs – that target the aberrant immune responses demonstrated promise in preclinical animal models but fail to translate in clinical trials. In fact, as many as two thirds of highly cited animal studies failed to translate to human randomized trials, mainly due to the inherent differences between mice and humans, and the inability of certain animal models to faithfully recapitulate the human condition.[57,93] To address this disconnect from bench to clinic, researchers have generated mouse models that incorporate human cells to better recapitulate human disease pathophysiology to facilitate the development of novel therapies. Patient derived xenograft (PDX) model captures human tumor biology via the transplantation of primary human tumor cells into immunocompromised mice and has significantly contributed to translational cancer research by modelling numerous human cancers and enabling the identification of therapeutic targets.[94,95] In the context of sepsis, the development of humanized mice, which are generated by transplanting the human hematopoietic system into immunodeficient mice, can also be used in the clinical translation of sepsis therapies.

Currently, the cecal ligation and puncture (CLP) mouse model is extensively used to study human sepsis whereby the cecum is ligated and punctured to extrude cecal bacteria into the abdominal cavity.[96,97] However, this technique leads to inconsistent pathogenic responses due to the variability in the amount of pathogenic species entering the peritoneum post-surgery. It is also due to the percentage of the cecum ligated, as well as the number and size of cecal punctures, which all contribute to highly variable experimental outcomes.[97] Taken together, mouse morbidity varies greatly between studies and even within experimental cohorts.[97] Moreover, recent data revealed that the murine peripheral blood transcriptional response post-CLP poorly correlates with that observed in human sepsis patients. Thus, there is a great need for robust inflammatory models that better recapitulate the human immune response to develop effective therapies.

1.9 Rationale

Clinical trials that employed MSC cellular therapies for various inflammatory diseases have produced inconsistent results. These discrepancies are mainly due to heterogeneity within MSC populations as well as the loss of immunosuppressive properties during prolonged MSC culture to generate clinically relevant cell numbers. The current lack of reliable biomarkers or standardized metrics to measure MSC immunomodulation makes identifying and isolating therapeutic MSC subpopulations extremely difficult. Thus, my project is aimed at identifying biomarkers and gaining mechanistic insights into UC-MSC immunomodulation to develop more efficacious cellular therapies. Immunomodulatory MSCs were screened to assess their immunomodulatory function using mixed lymphocyte reaction and macrophage assays. Potential biomarkers and mechanistic insights were determined via transcriptomic analysis of cytoplasmic RNA and proteomic analysis of the secretome. Furthermore, I developed a humanized mouse model for sepsis to validate the efficacy of immunomodulatory MSCs to treat inflammatory

disease. To do so, NSG immunodeficient mice were transplanted with human umbilical cord-derived hematopoietic stem and progenitor cells (HSPCs) to reconstitute the mice with human immune cells. In addition, human progenitor T (pro T) cells were co-transplanted to decrease the time required for robust mature T cell engraftment. I also developed a cecal slurry and puncture (CSP) surgical procedure and demonstrated that humanized mice that underwent CSP consistently exhibited symptoms indicative of sepsis and rapidly succumbed to the systemic infection. Analysis of a human specific sepsis gene signature demonstrated that the humanized CSP mouse model more closely recapitulates the human sepsis transcriptional response than the CLP mouse model.

Ultimately, I plan to integrate a metric for immunomodulation into a pipeline to identify, isolate, validate *in vitro*, and manufacture MSCs with the greatest immunomodulatory activity to treat immune and inflammatory diseases.

2.0 Methods

2.1 Mesenchymal Stromal Cell culture

Wharton's Jelly MSCs (WJ-MSCs) were obtained by Dr. Bernard Thébaud's lab. MSCs were cultured at 1333 cells/cm^2 in alpha MEM (Gibco) with 20% FCS (Lot #: 1739823) polypropylene culture flasks. Cells were passaged when they reached 75-80% confluency. Each WJ-MSC and HUCPVC line was harvested from separate donors. Human UC-MSCs were isolated from the umbilical cord of healthy, term pregnancies after parental consent. After delivery, the cord was dissected from the placenta, milked to remove remaining intravascular blood and placed in a storage solution containing 30% [vol/vol] citrate phosphate dextrose adenine anti-coagulant (CPDA-1) in phosphate buffered saline (PBS). After disinfection with povidone-iodine (Purdue Pharma, Stamford, CT), multiple incisions were made into the epithelium of the cord. Sterile cord tape (Ethicon, Somerville, NJ) was used to ligate the cord vessels prior to placing the tissue in Phosphate-buffered saline (PBS) supplemented with Ca_2^+, Mg_2^+, glucose and pyruvate (Thermo Fisher Scientific) as well as with 750 U/mL collagenase and 500 U/mL hyaluronidase (both from Worthington). Following digestion at 38°C for 4 hours, 2000 BAEE-U/ml trypsin and 3 mM ethylenediaminetetraacetic acid (EDTA) (both from Sigma-Aldrich) were added and allowed to incubate for another 30 min at 38°C. The dissociation process was stopped by placing the mixture on ice and adding FBS to a final concentration of 10% [vol/vol]. Remaining undigested tissue was removed by utilizing 40 µm cell strainers (BD Biosciences). Cells were rinsed in PBS and seeded in minimum essential medium Eagle, alpha modification (αMEM) containing 20% fetal bovine serum (FBS) (both from Sigma-Aldrich) and standard antibiotics (Thermo Fisher Scientific) in tissue culture treated plastic flasks (Greiner Bio-One).

Human umbilical cord perivascular cells (HUCPVCs) were obtained from Tissue regeneration therapeutics (TRT). HUCPVCs were plated on human plasma fibronectin (EMD Millipore) coated flasks (0.75ug/cm^2) at 1333 cells/cm^2 in supplemented Lonza mesenchymal stem cell growth medium (MSCBM). Lonza stopped producing the media in early 2017. Consequently, HUCPVCs were cultured in alpha MEM (Gibco) with 20% FCS (Lot #: 1739823). Both were cultured in a 5% CO_2, 5% O_2 humidified atmosphere with media changes every 3rd day. WJ-MSCs and HUCPVCs were lifted using enough TrypLE (Gibco) to cover the bottom of the flask. Lifted cells were diluted with an equal amount of growth media, centrifuged at 400g for 10 minutes, and resuspended in growth media.

2.2 Human umbilical cord blood processing

Umbilical cord blood (UCB) samples were obtained from the Canadian Blood Services after informed consent. To process, 1 mL of Pentaspan was added per 5 mL of umbilical cord blood sample. Samples were centrifuged for 50g or 10 minutes at room temperature and the top layer was isolated, then centrifuged at 400g or 10 minutes at room temperature and supernatant aspirated. The cell pellet was resuspended in 10 mL of red blood lysis buffer (Potassium bicarbonate 9.98 mM, ammonium chloride 160 mM, EDTA 0.25 M) for 5 minutes at room temperature and pelleted at 400g. The subsequent pellet was resuspended in Phosphate-Buffered Saline (PBS) without $CaCl_2$ and $MgCl_2$ (Gibco) for counting.

2.3 Mixed Lymphocyte Reaction (MLR)

$CD3^+$ T lymphocytes were isolated from umbilical cord blood samples (Canadian Blood Services) using a positive selection kit (StemCell Technologies) and stained with 1 µM CFSE (Molecular Probes) for 5 minutes. Cells were washed twice with PBS (without $CaCl_2$ and

$MgCl_2$), resuspended in OpTmizer media (Invitrogen) and 4 x 10^4 $CD3^+$ cells per well were seeded in triplicate in a 96-well plate (BD Falcon) and stimulated with CD3/28 Dynabeads (Invitrogen). MSCs were grown as described above in proinflammatory conditions with or without induction with 15 ng/mL TNFα and 10 ng/mL IFNγ, 48 h prior to harvesting. MSCs were resuspended in OpTimizer media and 4 x 10^3 cells were added to the stimulated $CD3^+$ T cells. Co-cultures were placed at 37ºC in a humidified incubator, at 5% CO_2 and 5% O_2 for 5 days. To analyze T lymphocyte proliferation, cells were stained with anti-CD45 antibodies (clone 2D1) conjugated to AlexaFluor700 (eBioscience) and 10ng µL -1 propidium iodide (Sigma) and analyzed using a BD Fortessa flow cytometer. Carboxyfluorescein succinimidyl ester (CFSE) fluorescence of stimulated $CD3^+$ $CD45^+$ cells, in the absence or presence of MSCs, were compared to determine T cell proliferation. Most MLR experiments were conducted by Chandarong Choey.

2.4 M1/M2 Macrophage assay

On day 0, $CD14^+$ (Stem cell technologies) cells were isolated from processed human umbilical chord blood cells. $CD14^+$ cells were seeded on a flat bottom 96-well plate at 50,000 cells/well in 100 µL of RPMI 1640 (Gibco) with 10% FBS (Gibco). 25 ng/mL of MCSF (Peprotech) was added to M2 control cultures and 25ng/ml of GMCSF (Peprotech) was added to M1 cultures. On Day 3, 100 µL of RPMI was added to each well. Additionally, 25 ng/mL of GMCSF and 500 ng/mL of LPS (Peprotech), and 20 ng/mL of IFNγ (Peprotech) were added to M1 cultures and 25 ng/mL of MCSF and 30 ng/mL of IL-4 (Peprotech) were added to the control M2 cultures. IFNγ 10 ng/mL and TNFa 15 ng/mL were added to induce MSCs for 48 hours. On day 5, 100 µL of media was removed and MSCs were added at a 1:5 or 1:10 ratio (10,000 or 5,000 cells) in 100µL of RPMI 1640 with 10% FBS and 25 ng/mL GMCSF to co-cultures,

25ng/mL GMCSF was added to M1 cultures and 25 ng/mL MCSF to M2 cultures. On day 7, cells were washed in PBS (without $CaCl_2$ and $MgCl_2$), lifted with TrypLE, stained for CD80, CD45, CD163, and CD206 and analysed via flow cytometry.

2.5 IL-10 ELISA

The BioLegend human IL-10 ELISA MAX deluxe was used to determine IL-10 concentration in the conditioned media from MSC-M1/M2 macrophage cocultures. 100 µL of capture antibody was added to each well and incubated overnight at 4˚C. The plate was washed with PBS and standards and 1/4 diluted samples were added and incubated for 2 hours with shaking. The plate was washed and detection 100 µL of antibody was added and incubated for 1 hour. The plate was again washed and 100 µL of Avidin-HRP solution was added to each well and incubated for 30 minutes. The plate was washed and 100 µL of freshly mixed TMB solution and incubated in the dark for 30 minutes. 100 µL of stop solution was then added to each well and absorbance was read at 450 nm and 570 nm on a Beckman Coulter DU 800 spectrophotometer. Angela Raymond assisted me with the completion of ELISAs.

2.6 Western blotting

Following protein determination by Bradford assay (Protein Assay Dye Reagent Concentrate, BioR), 5-10 µg of protein extracts were prepared in LDS sample buffer (Novex, life technologies) supplemented with dithiothreitol and the lysates were then electrophoresed on a 4-12% precast gradient gel (NuPAGE) using the XCell SureLock® Mini-cell (Invitrogen) and transferred onto a polyvinylidene fluoride (PVDF) or nitrocellulose membrane (Invitrogen). The membranes were blocked with 5% BSA or 5% non-fat dry milk (BD) in 0.1% TBS-Tween-20 for at least 1h at RT and probed with rabbit or mouse antibodies overnight at 4°C. The

membranes were then washed and probed with alexa-fluor 680 or 700 conjugated goat anti-rabbit (Thermo scientific) or goat anti-mouse (Thermo scientific) secondary antibodies for 1h at RT. Blots were washed and bands were visualized using the LI-COR Odyssey Infrared Imager.

Manufacturer	Antibody	Catalogue #	Dilution
Cell Signalling	Calnexin	2433	1:1000
Cell Signalling	AKT	2920	1:1000
Cell Signalling	P-AKT	4060	1:1000
Abcam	GAPDH	8245	1:2000

2.7 Endoplasmic Reticulum and Golgi apparatus isolation

Endoplasmic reticulum and Golgi apparatus extraction were adapted from Rao et al. 2012.[100] MSCs were washed twice with ice cold PBS, lifted with TripLE and counted in TBS. Cells were centrifuged and resuspended in a sucrose buffer (250 mM sucrose, 25 mM KCl, 5mM MgCl, 10mM triethanolamine, 10mM acetic acid, with protease and phosphatase inhibiters) PH 7.6 and lysed using a 25 gauge needle. The samples were centrifuged at 3000g of 10 min at 4°C and the supernatant was collected. Mitochondria elements were removed using Miltenyi mitochondrial isolation kit. Supernatant was centrifuged at 15,000g for 30 min at 4°C and the pellet containing the organelles was solubilized in 10 µL of 8M urea and 50mM ammonium bicarbonate.

2.8 Surface protein biotinylation

I adapted our protocol was adapted from Thermo Scientific's Pierce Cell Surface Protein Isolation Kit protocol. MSCs in culture flasks were washed with ice cold PBS (without $CaCl_2$ and $MgCl_2$) twice. 0.5 mg/mL of Sulfo-DHS-SS-Biotin in PBS with $CaCl_2$ and $MgCl_2$ was added

to each flask to cover the bottom and incubated at 4°C for 30 minutes. 250µL-1mL of 50mM glycine solution in PBS + was added to quench biotinylation. Cells were scraped and washed. Cells were lysed using a 1% triton based lysis buffer, sonicated, and centrifuged to remove cell debris. The supernatant was incubated with streptavidin magnetic beads overnight at 4°C with gentle shaking. Beads were eluted with 25µL of 50 mM DTT.

2.9 Silver staining

Proteins were run on 4-12% precast gradient gel (Invitrogen, Burlington, Ontario) using the XCell SureLock® Mini-cell (Invitrogen, Burlington, Ontario). Gels were then fixed in 50% ethanol and 5% acetic acid for 30 minutes with gentle agitation. Gel was washed twice in wash solution (50% ethanol) and sensitized with fresh 0.8 mM Sodium thiosulfate for 2 minutes. Three more washes were conducted before 6 mM silver nitrate was added for 30 minutes to stain. Gels were developed in 0.04% formaldehyde and 0.19 M sodium carbonate until bands were clearly visible. To stop development, 5% acetic acid was added. Gels were stored in 1% acetic acid.

2.10 Mass Spectrometry Digestion

All tools, surfaces, and tubes were cleaned with 70% ethanol and all work was conducted in a positive pressure clean hood. Proteins were isolated, electrophoresed, and silver stained using the above described methods. Bands with similar protein levels as determined by stain darkness were separated, chopped into 1 mm cubes and were washed in water for 60 minutes in a shaker. 250 µL of acetonitrile was added to each tube and incubated at room temperature for at least 10 minutes to dehydrate the gel. Supernatant was removed and 9.7 µM DTT in 50mM ammonium bicarbonate and 50% acetonitrile was added to gel pieces and incubated at 56°C for 30 minutes. 500 µL of acetonitrile was added and incubated for addition 10 minutes. Gel pieces

were incubated in iodoacetamide for 20 minutes to prevent the formation of disulfide bonds. Gel pieces were then trypsinized in 13.3 µg/mL trypsin in 10% acetonitril and 10 mM ammonium bicarbonate on ice for 2 hours. Proteins were extracted with 5% formic acid in acetonitrile and vacuum dried to isolate proteins. Proteins were resuspended in 1% formic acid.

2.11 Mass Spectrometry

Mass spectrometry was conducted by the OHRI Mass spectrometry core facility. The Dionex Ultimate 3000 RSLC nano (Thermo Scientific) HPLC in tandem with the Orbitrap Fusion Lumos (Thermo Scientific) spectrometer were used. Dr. Lawrence Puente conducted analysis using Xcalibur (Thermo Scientific), Mascot and Scaffold, which controlled the mass spectrometer and conducted analysis. High Performance Liquid Chromatography was used to separate proteins at a flow rate of 300 nanolitres per minute. Gradient was 5%-36% of increasing acetonitrile. Scanning speed was 100ms on the first pass. Peak picking was based largely on isotopic patterns. Counts were excluded if 2 counts were measured in 10 seconds, resulting in exclusion for 60 seconds.

2.12 RNA extraction

Pelleted cells were harvest using 500 µL of TRIzol® reagent and frozen for later processing (Thermo Scientific). To thawed samples, 5 µL of 1M MgCl and 100 µL of chloroform was added. Samples were shaken for 5 seconds and incubated on ice for 5 minutes. Samples were centrifuged at 4˚C for 15 minutes at 10000g After centrifugation, the top aqueous portion was extracted and the precise volume removed recorded. 250 µL of isopropanol was added to each sample, inverted, and incubated for 10 minutes on ice. Samples were centrifuged for 10 minutes at 4˚C at 10,000g. Supernatant was decanted and tubes were dapped with

Kimwipes. Pellet was ethanol washed with 500 µL of 75% ethanol and centrifuged for 5 minutes at 4˚C at 10 000g. Ethanol wash was conducted 4 more times. Pellet was left to dry at 40˚C for 5 minutes, followed by 5 minutes at room temperature before being resuspended in RNAase and DNAase free water. RNA was also extracted using Direct-zol RNA miniprep kit (Zymo).

2.13 RNA quality control

RNA fragment analysis and quantification was conducted by the OHRI StemCore facility using the Advanced Analytical High sensitivity RNA analysis kit (Agilent) and the Qubit RNA HS assay kit (Invitrogen).

2.14 RNA sequencing

WJ-MSC RNA sequencing was conducted at the SickKids Centre for Applied Genomics (Toronto). Libraries were generated using TruSeq Stranded TL RNA LT Ribo-Zero Gold (Illumina, P/N RS-122-2301). Single end sequencing as conducted on the Hiseq 4000 (Illumina). HUCPVC RNA sequencing was conducted at Donnelly Sequencing centre at the University of Toronto. Libraries were generated using TruSeq Stranded mRNA kit (Illumina). Single end sequencing was conducted on NextSeq500, High Output v2 for 75 cycles (Illumina). Both library preparation and sequencing was conducted by the sequencing facilities.

2.15 Mice

NOD-*scid* IL2Rγ^{null} (NSG) (Jackson Laboratories) were housed in sterile ventilated cages of up to 5 mice per cage; fighting males were separated and housed separately. Mice were kept on a 12:12 light:dark cycle and given irradiated chow and autoclaved acidified water ad libitum. Animal protocols were approved by the University of Ottawa Animal Care Committee, in

accordance with the Canadian Council on Animal Care Standards and the Province of Ontario's Animals for Research Act.

2.16 Transplantation of human hematopoietic stem and progenitor cells into NSG mice

Umbilical cord blood (UCB) samples were collected following informed consent by the Canadian Blood Services (Ottawa, Canada) and the Mount Sinai Hospital Research Centre for Women's and Infants' Health BioBank, (Toronto, Canada). Use of donated UCB samples for research was approved by the respective Research Ethics Boards and the Ottawa Hospital Research Institute Research Ethics Board.

Lineage negative (Lin^-) cells were isolated from UCB samples using the Easy Sep Human Progenitor Cell Enrichment kit with Platelet Depletion (Stem Cell Technologies). Purified Lin^- cells were stained with anti-human CD34 APC (CLONE:4H11) and CD38 PE-Cy7 (CLONE:HIT2) and purified by FACS to obtain $CD34^+38^-$ hematopoietic stem and progenitor cells.

$CD34^+$ cells were isolated from fresh UCB samples using the Easy Sep CD34 Isolation kit (Stem Cell Technologies) and purified $CD34^+$ cells were differentiated on OP9-DL1 stromal cells to generate progenitor T cells (pro T) cells.[101] Human pro T cells and $CD34^+CD38^-$ cells were transplanted into 1-5 day old NSG pups as previously described.[101] Briefly, neonatal pups were irradiated with 125 Rads. 2h-6h post radiation, each pup received 2 x 10^5 human pro T cells, 2 x10^4 $CD34^+CD38^-$ HSPCs plus 0.5 µg rh-IL-7 (Peprotech) and 2.5 µg anti-IL-7 antibody (clone M25) via 30 µL intrahepatic injection. Pups were administered 30 µL of rhIL-7 (0.5 µg) and M25 (2.5 µg) via intraperitoneal injection every 3-4 days for two weeks post-transplant. Transplantation was conducted by Dr. Caryn Ito and Priya Chandran.

2.17 Cecal Slurry Puncture (CSP) model

Cecal slurry (CS) was prepared by harvesting cecal contents from C57BL/6 mice as described by Starr et al.[102] Bacterial quantification for each cecal slurry preparation was determined by performing serial dilution of the CS stock – 1:5000 and 1:10000 for aerobic bacteria and 1:20000 and 1:30000 for anaerobic bacteria using Luria broth (LB) –. CS dilutions were plated onto either CDC-Blood agar plates (REMEL) or Tryptone Soya Agar with 5% sheep blood (Oxoid) to culture anaerobic or aerobic bacterial growth, respectively. The agar plates were incubated at 37ºC for 24h and 48h in aerobic or anaerobic conditions (Anaeropack, Oxoid) and colonies were counted to determine the colony forming unit (CFU) per µL.

At 12-35 weeks post-transplantation, humanized NSG mice were randomized to either undergo the cecal slurry and puncture (CSP) surgical procedure to induce sepsis or a sham surgical procedure. Both groups of mice were anesthetized with 3% isofluorane/O_2, a 1cm midline abdominal incision was made and the cecum exposed. For the treatment group, cecal slurry was injected through the cecum, using an 18-gauge needle, into the peritoneum to induce sepsis, but the cecum was not ligated. The amount of cecal slurry was titrated between $5.0 \times 10^4 – 2.2 \times 10^5$ bacterial CFU/g. The incision was sutured with 5-0 silk and the skin closed with metallic clips. For the sham procedure, the cecum was exposed, but not punctured and an equal volume of saline was injected into the peritoneum, then the incision was closed as above.

All mice received 1ml of Lactated Ringer's 0 and 12 hours post-surgery and 0.03 mg/kg of buprenorphine via sub-cutaneous injection 0, 6, 12 and 24 hours post-surgery. Mice were monitored every hour for wellness traits including attitude, grip strength, piloerection. Humane moribund endpoint was determined by monitoring internal body temperature and traits such as alertness, hunched posture, piloerection and weak grip strength. Rectal temperatures were recorded

to detect changes in internal body temperature. Moribund mice were sacrificed and sham control mice were sacrificed 24-96 hours post-surgery. Surgeries were performed by Dr. Caryn Ito.

A total of n=12 independent CSP experiments were performed for this study. The total number of mice used in this study was n=44; n=24 females (n=13 CSP; n=9 sham; 2 unmanipulated) and n=20 males (n=12 CSP; n=7 sham; 1 unmanipulated).

2.18 Collection of blood samples for analysis

Cardiac puncture was performed to collect peripheral blood (PB) using EDTA coated syringes. Mononuclear cells were isolated by centrifugation and the collected blood was diluted in buffer containing PBS (without $CaCl_2$ and $MgCl_2$) /2% FBS (Gibco) and mixed thoroughly. Samples were centrifuged at 400g for 5 minutes and incubated at room temperature with red blood cell (RBC) lysis buffer (155mM of Ammonium Chloride, 10mM of Potassium Bicarbonate, 0.1mM EDTA) for 5 minutes to lyse the RBCs. Mononuclear cells in the PB were then washed, resuspended in PBS (without $CaCl_2$ and $MgCl_2$) /2%FBS/1mM EDTA and filtered using 40 μm nylon cell strainer (Thermo Fisher Scientific). Cells were analyzed by flow cytometry to assess engraftment levels and apoptosis.

Bone marrow cells were obtained from femurs and tibiae by flushing them with 1 mL PBS (without $CaCl_2$ and $MgCl_2$). Spleen cells were harvested by straining the spleen through a 40 μm nylon cell strainer in 1 mL of PBS using the plunger of a 3 ml syringe (Becton Dickinson). Bone marrow and spleen cells were then pelleted at 3,500g in a microcentrifuge for 3 minutes to collect the cells. The cell pellet was then resuspended in RBC lysis buffer for 5 minutes at room temperature followed by a wash with PBS/2%FBS. Mononuclear cells obtained from bone marrow and spleen were resuspended in PBS/2%FBS/1mM EDTA and filtered using 40 μm nylon cell

strainer. Cells were analyzed by flow cytometry to assess engraftment levels and apoptosis of immune cells by Priya Chandran.

PB collected in EDTA coated syringes was transferred to capillary tubes (Fisher, Thermo Fisher Scientific) sealed and centrifuged for 5 minutes to separate the plasma. Blood plasma was collected and stored at -80ºC until further analysis.

2.19 MALDI-TOF Mass Spectrometry Bacterial Speciation

To determine the species of bacteria present in the blood, PB was collected by cardiac puncture and coded for blinded analysis. PB samples were serially diluted 1:10 from 10^{-2} to 10^{-4} in thiol broth, plated on CDC-Blood agar plates (REMEL) or Tryptone Soya Agar with 5% sheep blood (Oxoid), and grown for 48 hours in at 37°C in aerobic or anaerobic conditions (Anaeropack, Oxoid), respectively. Morphologically distinct colonies grown under aerobic or anaerobic conditions were spotted on a reusable MSP 96 polished steel BC target plate (Bruker) and were overlaid with 70% formic acid, and α-Cyano-4-hydroxycinnamic acid (Bruker Daitonik). reconstituted in 50% acetonitrile (Thermo Fisher Scientific), 47.5% HPLC/MS Grade H_2O (Thermo Fisher Scientific) and 2.5% trifluoroacetic acid (Sigma-Aldrich). Target plate was analyzed using a MALDI-TOF tandem mass spectrometer.

2.20 Flow Cytometry Analysis

Peripheral blood, bone marrow and spleen cells collected from CSP and sham treated mice were analyzed by flow cytometry by Priya Chandran. To determine the engraftment levels of human immune cells, the cells were stained with following human specific antibodies: CD45 AF-700 (Clone:2D1) to assess overall human immune cell engraftment; CD33 eFLUOR 450 (Clone:P67.6), CD14 PE-Cy7 (Clone:61D3), CD15 FITC (Clone:HI98) to detect human myeloid

engraftment; and CD19 APC (Clone:HIB19), CD8 FITC (Clone:HIT8a), CD3 eFLUOR 450 (Clone:OKT3) and CD4 APC (Clone:OKT4) to determine human lymphoid engraftment. Human immune cell apoptosis was determined using Annexin-V eFluor 450 and 7AAD. Isotypes corresponding to the fluorochrome conjugated antibodies were used as controls. Flow cytometry was performed using BD LSR Fortessa (BD Bioscience) and the data were analyzed using BD FACSDiva (BD Bioscience).

2.21 Organ Function and Histology

Blood plasma was harvested and coded for blinded analysis. Blood chemistry was analyzed by the Beckman Coulter AU480 to measure levels of AST and ALT. Lung and liver tissues were fixed in 10% formaldehyde (Thermo Fisher Scientific), embedded with paraffin, and probed using CD68 monoclonal (Clone:KP1) (1:50) (Thermo Fischer scientific) or myeloperoxidase (1:100) (Thermo Fischer scientific) polyclonal antibody overnight at 4°C and counter-stained with hematoxylin. Goat HRP polyclonal secondary antibody was incubated for 1 hour and visualized in 2% 3,3'-Diaminobenzidine (DAB) and 0.1% hydrogen peroxide.

2.22 Cytokine Analysis

Blood plasma was harvested and coded for blinded analysis. 25 µL of plasma was analyzed in duplicate using a customized Millipore human cytokine/chemokine magnetic bead panel (interleukin [IL]-1R α, IL-10, tumor necrosis factor [TNF]- α, IL-12 p40, IL-12 p70, gamma interferon [IFNγ], IL-8, IL-6, GM-CSF, and IL-1α). Mean fluorescent intensity was measured using the Luminex xMAP MAGPIX® system and analyzed using Milliplex Analyst software (Luminex). Plasma from C57BL/6 mice was used as a negative control.

2.23 Human Sepsis Gene Signature Generation

Significant fold changes (false discovery rate [$q<0.01$], $\log_2$ fold change > 2) were determined between human (GSE13904)[103] and mouse (GSE5663)[104] sepsis PB microarray datasets. Genes with significant fold changes in opposing directions between mouse and human were selected. Genes were further filtered to include only genes that are biologically relevant to sepsis (**Table 7**). Gene signature fold changes were extracted from other publicly available human sepsis patient and mouse CLP PB microarray datasets. Human sepsis gene signature expression from humanized mice was determined by RT-qPCR on PB RNA from CSP and sham mice. Gene signature fold changes were then correlated with a human sepsis patient fold changes to determine similarity.

2.24 Quantitative PCR

Human specific primers were designed to determine the gene expression of our human sepsis gene signature in humanized mice by reverse transcriptase quantitative PCR (RT-qPCR). PB was harvested from humanized NSG mice that underwent CSP or sham surgery. PB was also harvested from unmanipulated humanized NSG mice and C57BL/6 mice as controls. mRNA was extracted using the ARCTURUS® PicoPure® RNA Isolation Kit (Thermo Fisher Scientific). The RNA was converted to cDNA using SuperScript® II Reverse Transcriptase (Thermo Fisher Scientific). RT-qPCR was conducted using SYBR® Green PCR Master Mix's protocol (Thermo Fisher Scientific) and a Roche LightCycler 480 Real-Time PCR system. 5 ng of cDNA from the PB of humanized NSG mice was used for the RT-qPCR analysis. Primer sequences can be found in **Supplementary Primer Sequences**.

2.25 Bioinformatic Analysis

RNA sequencing analysis was conducted from raw FASTQ files obtained from either Donnelly or the SickKids Centre for Applied Genomics sequencing facilities and quality control was conducted using FASTQC. Read alignment was conducted using HISAT2[105] to the Genome Reference Consortium Human Build 38 (GRCH38) using GENCODE 23 annotations. Reads were counted using featureCounts.[106] Differential gene expression was calculated using DESeq2.[107] A p-value cutoff of 0.05 and fold change of two was applied to Bonferroni corrected values. Functional analysis was conducted using the Gene Ontology Consortiums web tool, KEGG pathway analysis, and STRING protein interaction analysis.[108–110] REViGO was used to visualize significant gene ontology results.

Proteomic analysis was conducted using Scaffold to calculate spectral counts by Dr. Lawrence Puente. Differentially expressed proteins were determined by comparing cell number normalized spectral counts between samples. Rankings were determined by magnitude of spectral count difference and difference in ranking within each dataset.

Data have been expressed as mean or mean ± standard error mean (mean ± s.e.m). Statistical calculations were done using Graphpad Prism 7.0 software or embedded R functions. Survival curves analyzed with Kaplan Meier log rank test. For other results, comparison of means performed using unpaired two-tailed Student's t test with Welch's correction using a level of significance of $p \leq 0.05$.

3.0 Results

3.1 Early passage UC-MSCs have greater immunomodulatory ability than late passage UC-MSCs *in vitro*

Contributions

- Mixed lymphocyte reactions were conducted in large by Dr. Caryn Ito and Chandarong Choey. I completed late passage replicates for HUCPVC6.
- IL-10 ELISAs were completed by both Angela Raymond and me.
- I completed all macrophage assays and proliferation assays.

Previously published data has demonstrated that UC-MSCs exhibit immunosuppressive qualities. However, the numerous conflicting clinical trails testing MSC therapeutics evidence the lack of understanding pertaining to MSC immunomodulatory ability and its regulation.[33,62] Moreover, MSC heterogeneity has often confounded results, making identifying immunomodulatory mechanisms difficult. Therefore, to properly interrogate MSC immunomodulatory ability, I needed to identify UC-MSCs with greater and lesser immunomodulatory ability for comparison. We performed mixed lymphocyte reactions and macrophage assays using different lots of UC-MSC primary cells that were co-cultured with stimulated $CD3^+$ T cells derived from umbilical cord blood to determine the ability of UC-MSCs to suppress activated T cell proliferation. Using this method, it was found that immunomodulatory capacity varies greatly across different UC-MSC lines (**Figure 4**). As a result, HUCPVC6 and WJ-MSC1 were chosen due to their greater immunomodulatory capacities in comparison to other MSC lots we tested. Interestingly, phenotypic differences have been observed between MSCs of differing passage numbers. Le Blanc et al. demonstrate a significant difference in MSC treatment of GVHD using passage 1-2 cells versus 3 to 4.[79] Furthermore,

Klinker et al. demonstrated BM-MSC immunosuppression of T cells decreased over longer passage *in vitro*. Since our objective was to interrogate the immunomodulatory phenotype, comparing MSC with varying immunomodulatory ability from the same MSC extraction would greatly reduce confounding variables. However, due to the number of cells required for downstream transcriptomics and proteomic analyses, passage 1 cells could not be feasibly used. Therefore, to confirm if immunomodulatory ability decays significantly over *in vitro* passaging, we co-cultured early passage 3 and late passage 6 UC-MSCs with immune cells to determine their immunosuppressive phenotype. A severe drop in proliferative capacity was observed in late passage MSCs versus early passage MSCs (**Figure 5A**). Moreover, as expected, when co-cultured with stimulated $CD3^+$ T cells, early passage UC-MSC suppressed T cell proliferation in a more significant manner compared to late passage UC-MSCs (**Figure 5B**). To ensure that the immunosuppressive abilities of UC-MSCs is not limited to T cell suppression, MSCs and control 293T cells were co-cultured with M1 inflammatory $CD14^+$ macrophages to determine whether the macrophages adopt an immunosuppressive M2 phenotype in the presence of MSCs (**Figure 6**). As with the MLRs, while all MSCs exhibited greater immunosuppression than 293T cell controls, I found that early passage UC-MSCs significantly decreased the proportion of $CD80^+$ inflammatory macrophages (M1) compared to 293T cell controls than late passage MSCs (**Figure 6**). Early passage UC-MSCs had a far more significant reduction of M1 macrophages than late passage cells. Moreover, as mentioned earlier, IL-10 secretion is a robust immunosuppressive cytokine and likely extracellular mediator of MSC immunomodulation. Consequently, I conducted ELISAs on the conditioned media harvested from macrophage-MSC cocultures, which revealed elevated levels of IL-10 in early versus late passage MSCs, further indicating that the MSCs were exerting their immunomodulatory activity on proinflammatory

macrophages (**Figure 7**). Thus, I validated a significant loss of immunomodulatory capacity between early and late passage UC-MSCs for downstream interrogation of MSC immunomodulatory mechanism.

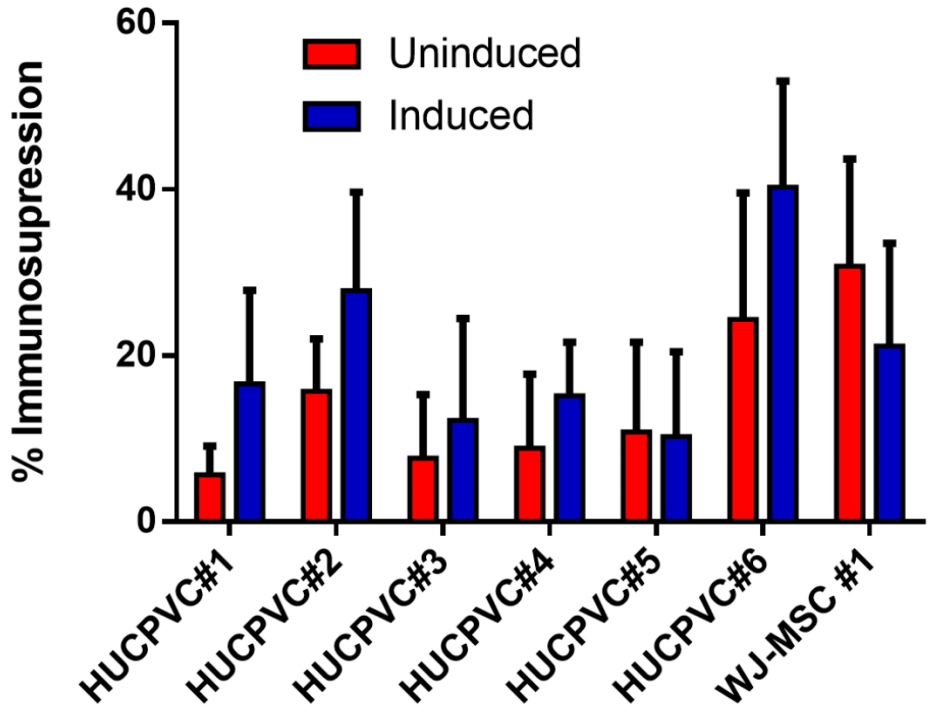

Figure 4. *Mixed Lymphocyte reactions of native and primed UC-MSCs with T cells.* WJ-MSCs and HUCPVCs were cocultured with stimulated $CD3^+$ T cells at a 1:5 ratio under normoxic conditions. T cell proliferation was measured via carboxyfluorescein succinimidyl ester staining. MSCs were primed with interferon gamma (IFNγ) and tumor necrosis factor alpha (TNFα) 48 hours before detection. n=3. Experiments were conducted by Dr. Caryn Ito and Chandarong Choey.

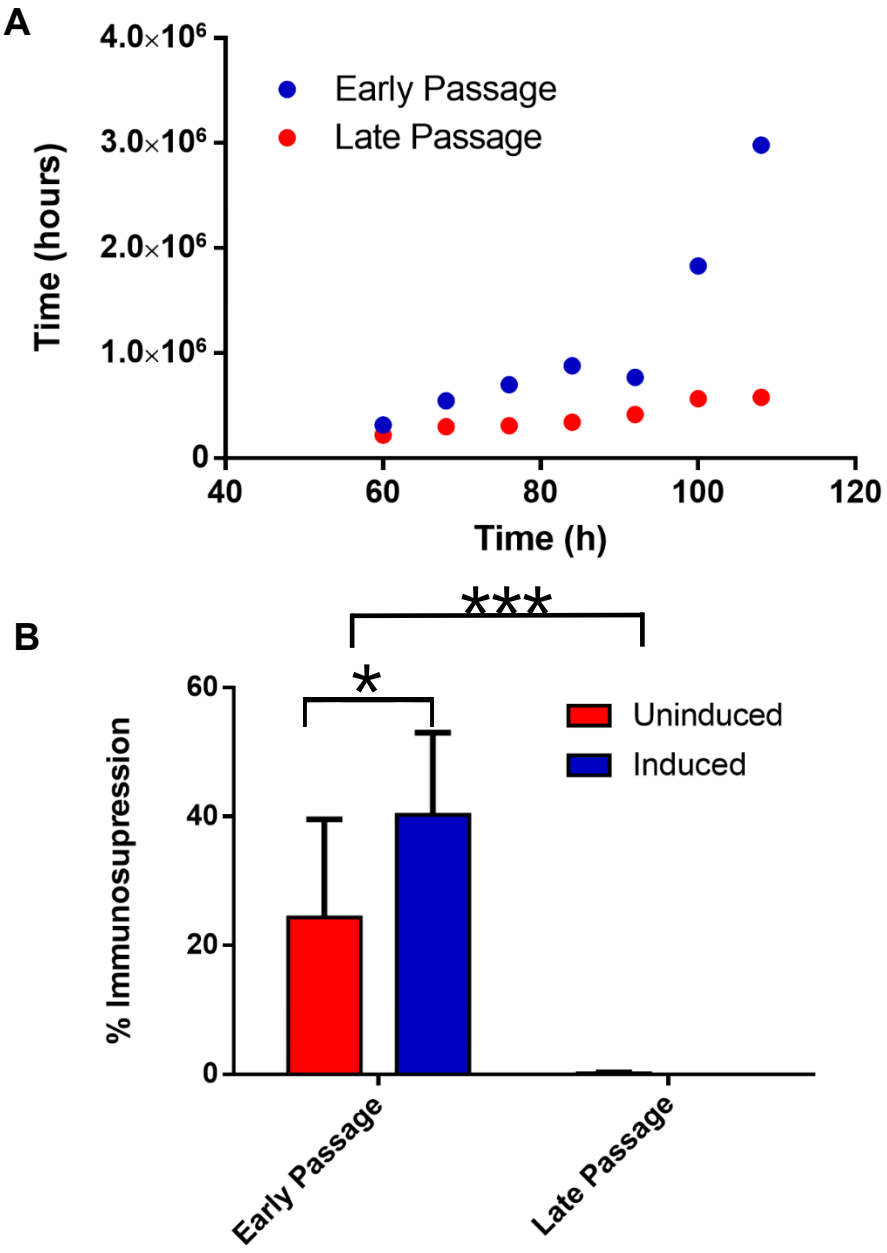

Figure 5. *Phenotypic differences between early and late passage UC-MSCs.* (**A**) Early passage 3 HUCPVC6 exhibit greater proliferation than late passage 6. (**B**) Early passage and not late passage UC-MSCs suppress T cell proliferation. Early passage 3 and late passage 6 HUCPVC6 was cocultured with $CD3^+$ T cells at a 1:5 ratio under normoxic conditions. T cell proliferation was measured via carboxyfluorescein succinimidyl ester staining. MSCs were primed with interferon gamma (IFNγ) and tumor necrosis factor alpha (TNFα) 48 hours before detection. Statistics were calculated between uninduced early and late passage cells and induced early and late passage cells respectively. n=3. * P≤0.05, ** P≤0.005, *** P≤0.0005. Experiments were conducted by Dylan Siriwardena, Dr. Caryn Ito and Chandarong Choey.

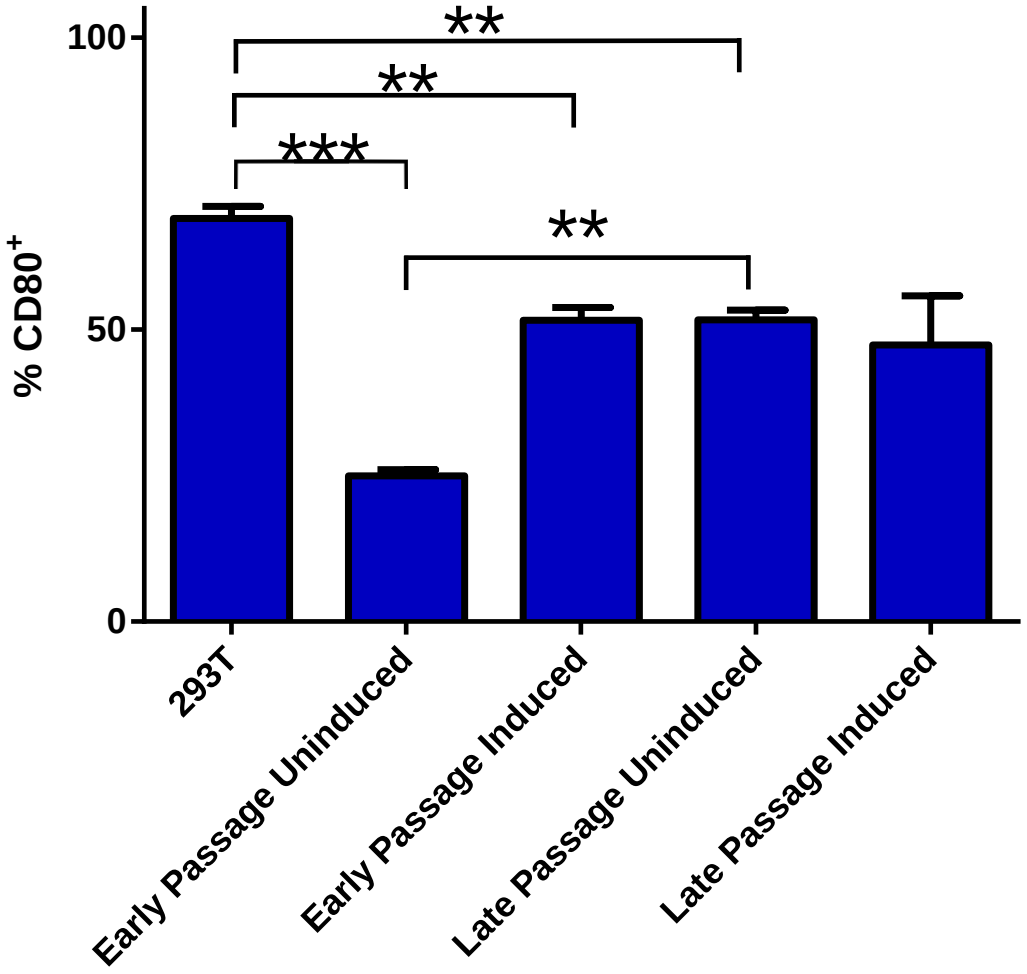

Figure 6. *Early Passage HUCPVCs suppress the M1 inflammatory macrophage phenotype.* Early passage 3 and late passage 6 HUCPVC6 cells were co-cultured with M1 $CD14^+$ macrophages at a 1:5 ratio under hypoxic conditions. Macrophage phenotype was measured via CD80 staining. MSCs were primed with interferon gamma (IFNγ) and tumor necrosis factor alpha (TNFα) 48 hours before detection. * $P \leq 0.05$, ** $P \leq 0.005$, *** $P \leq 0.0005$.

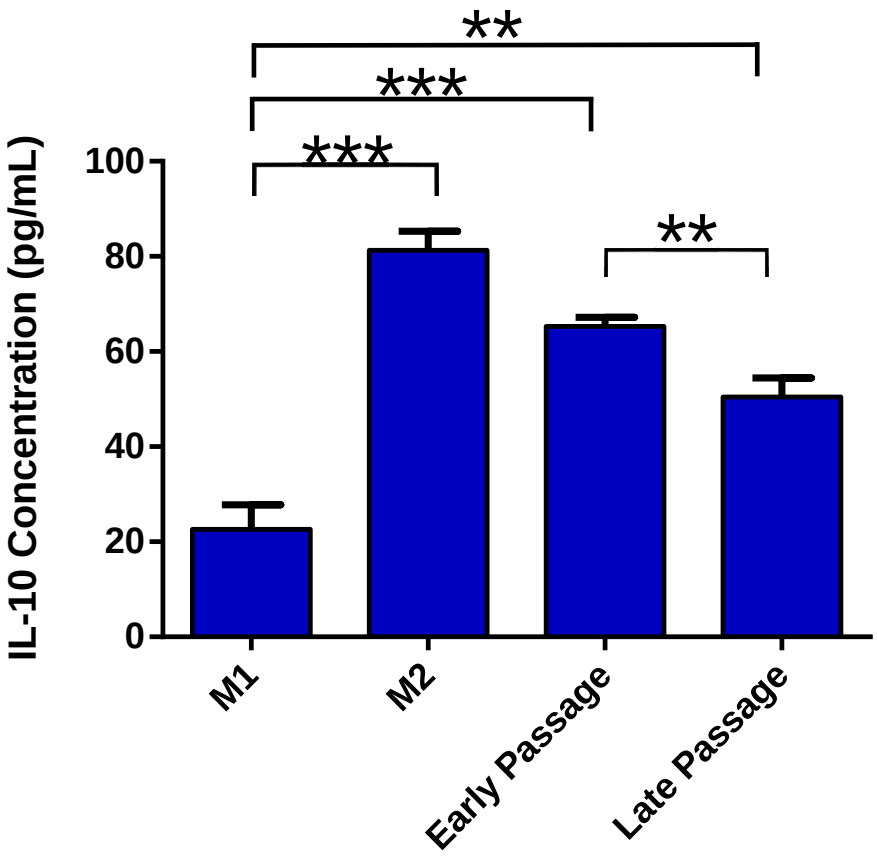

Figure 7. *Macrophage coculture with Early Passage HUCPVCs secretes more extracellular IL-10 than with late passage HUCPVCs*. IL10 concentration was detected in conditioned media from HUCPVC6 and M1 $CD14^+$ cocultures by ELISA. Early passage 3 and late passage 6 HUCPVCs were cocultured with $CD14^+$ macrophages at a 1:5 ratio under hypoxic conditions. Concentrations were determined via ELISA. Experiments were completed with the aid of Angela Raymond. n=4. * $P \leq 0.05$, ** $P \leq 0.005$, *** $P \leq 0.0005$.

3.2 Inducing UC-MSCs with IFNγ and TNFα has heterogenous effects on immunomodulatory ability *in vitro*

Contributions

- IL-10 ELISAs were completed by both Angela Raymond and me.
- I completed all macrophage assays.

As discussed above, while uninduced MSCs have shown therapeutic promise, inducing MSCs with IFNγ and TNFα has been shown to increase their immunomodulatory abilities.[36,38] To characterize the effect of inflammatory priming on immunomodulatory UC-MSCs, MLRs, M1/2, and IL-10 assays were conducted on early passage UC-MSC. Interestingly, inflammatory induction had a donor dependent effect on UC-MSC suppression of T cell proliferation (**Figure 4**). However, UC-MSC inflammatory induction promoted significantly greater inhibition of T cell proliferation (**Figure 5B**). Interestingly, UC-MSC inflammatory induction decreased M1 macrophage inhibition in early passage cells (**Figure 6**). In fact, uninduced early passage HUCPVCs produced significantly more IL-10 than induced early passage MSCs (**Figure 8**). This discrepancy did not persist in late passage HUCPVCs (**Figure 8)**. Since induction influences UC-MSC immunomodulation in an immune cell dependent manner, I chose to examine both induced and uninduced UC-MSCs.

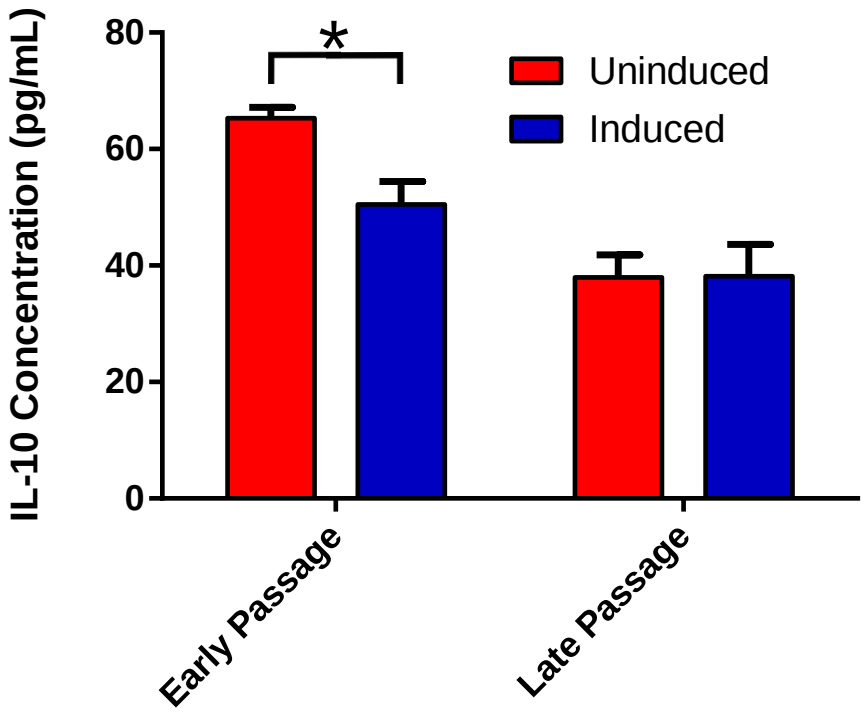

Figure 8. *Macrophage coculture with uninduced HUCPVCs secretes significantly more IL-10 than coculture with induced HUCPVCs.* IL-10 concentration was detected in conditioned media from HUCPVC and M1 $CD14^+$ cocultures. Early passage 3 and late passage 6 HUCPVC6 cells were cocultured with M1 $CD14^+$ macrophages at a 1:5 ratio under hypoxic conditions. IL-10 concentrations were determined via ELISA. Experiments were completed with the aid of Angela Raymond. n=4. * $P \leq 0.05$.

3.3 Development of UC-MSC Secretome Isolation Protocols

Contributions

- Endoplasmic reticulum and Golgi apparatus extractions were developed with the aid of Dr. Julien Yockell-Lelievre. I conducted all extractions and blots.
- I completed all in-gel digestions for mass spectrometry. Protein identification and quantification via mass spectrometry was conducted by Dr. Lawrence Puente.
- I completed all statistical and functional analysis.

Particular UC-MSC lines such as WJ-MSC1 and HUCPVC6 exhibit greater immunomodulatory potential than other UC-MSCs (**Figure 4**). Moreover, I demonstrated that *in vitro* culture of UC-MSC results in a loss of immunomodulatory ability (**Figure 5B, 6-7**). Finally, I found that induction of UC-MSCs with IFNγ and TNFα has varying immunomodulatory consequences, depending on UC-MSC line and passage (**Figures 6 and 8**). Consequently, due to the significant contrasts in immunomodulatory ability by varying passage number and induction, I chose to compare early and late passage UC-MSCs with and without induction to gain the most insight into immunomodulatory mechanisms. As discussed earlier, MSC immunomodulation occurs through a plethora of extracellular interactions involving surface and cytokine interactions that can be exploited to identify potential biomarkers and extracellular mechanisms for immunomodulation. Thus, to determine potential control mechanisms and biomarkers, I examined differences in the UC-MSC secretome between early and late passage MSCs. To do so, I isolated the secretory organelles: endoplasmic reticulum (ER), Golgi apparatus, and other secretory vesicles via centrifugation as adapted from Rao et al's published protocol.[100] I was able to greatly enrich for both the ER and Golgi apparatus (ER/G) as validated using Western Blotting for calnexin, a known ER marker (**Figure 9**). Surface proteins were isolated via biotinylation with sulfo-NHS-SS biotin followed by isolation with magnetic

microbeads from both early and late passage MSCs. Silver staining was then conducted on each protein fraction, and proteins of similar molecular weight were collected, digested, and sent for liquid chromatography-tandem mass spectrometry (LC-MS) analysis (**Figure 10**). LC-MS was used to determine the compliment of secreted proteins and their differential abundance in our samples. Differential abundance was determined by comparing spectral counts between high and low passage proteins. For immunomodulatory WJ-MSCs, 1209 proteins were found in the ER/G fraction along with 570 proteins in the surface fraction across 2 technical replicates. For the HUCPVCs, 1043 proteins were found in the ER/G with 523 proteins in the surface fraction. Since the surface protein fraction should be largely recapitulated by the ER/G fraction (as part of the secretory system), I examined the overlap between the two fractions to reduce noise and generate a robust list of surface proteins. 447 were found to overlap between the two HUCPVC lists (**Figure 11**). Moreover, cellular localization ontology showed significant enrichment of secretory and ER/G related terms (**Figure 12**). 64% of detected WJ-MSC proteins and 74% of detected HUCPVC proteins were from secreted cellular fractions while HUCPVC proteins enriched for 74%. Indeed, significant mitochondrial contamination was detected. While mitochondrial proteins are not secretory, they were still incorporated into our analysis as they give insights into role of metabolism in immunomodulation. In fact, amino acid metabolism has been reported to be linked with immunomodulatory activity in MSCs. For example, as mentioned earlier, indoleamine-pyrrole 2,3-dioxygenase (IDO) and the tryptophan catabolism pathway, which are linked to T-effector cell and CD4 T cell proliferation inhibition,[24] were upregulated in our early passage proteomic data set, further validating our comparison of early and late passage. To narrow down a list of meaningful secreted proteins, all secreted proteins were ranked based differences in spectral count between early and late passage across the ER/G

and surface fractions. Due to the large overlap between the ER/G and surface fractions, both lists were merged for differential analysis. If a protein appeared in both, the ER/G spectral count was used as its extraction was not dependent on bead affinity and elution. To further narrow our list, a fold change cut-off of 2 was applied and only proteins found across both HUCPVCs and WJ-MSCs were initially used, narrowing the list down to 552 proteins. Functional analysis on the 552 proteins revealed significant enrichment of immune related terms such as *neutrophil degranulation* and *leukocyte mediated immunity* (**Figure 13**). Moreover, other MSC functions such as *wound healing* and *coagulation* related terms were also enriched (**Figure 13**). I performed KEGG Pathway analysis to determine upregulated signalling pathways and cellular functions and found a significant enrichment of metabolic and cytoskeletal processes as well as the PI3K-AKT and IL-12 signalling pathway. While it is likely the metabolic and cytoskeletal pathways are in large upregulated by the faster proliferation observed in early passage umbilical cord cells (**Figure 5A**), both may still play a role in immunomodulation. This is consistent with a study done by Klinker at al., which demonstrated that IFN-γ stimulated bone marrow MSC morphology can predict immunomodulatory ability.[111] Thus, the UC-MSC secretome is enriched for proteins involved in immunomodulation and may provide insight into extracellular regulatory mechanisms of MSCs.

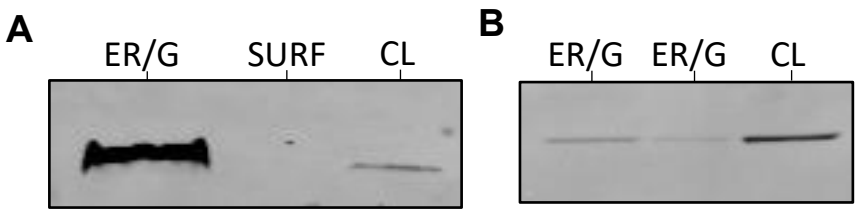

Figure 9. *Validation of Endoplasmic Reticulum and Golgi apparatus protein extraction from WJ-MSCs.* Western blot probing **(A)** calnexin, and **(B)** GAPDH, in the Endoplasmic reticulum and Golgi apparatus (ER/G) fraction, surface protein fraction (SURF), and total cell lysate (CL).

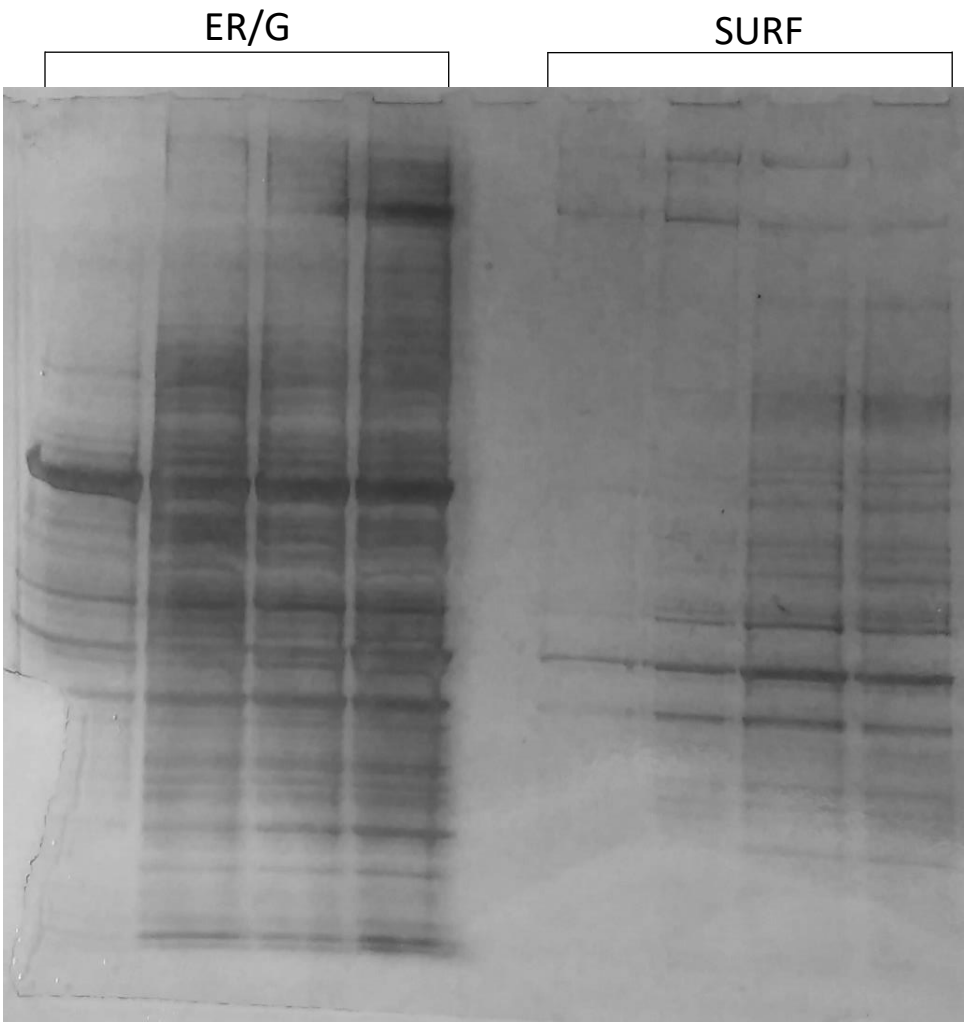

Figure 10. *Total isolated proteins from ER/Golgi apparatus fraction (ER/G) and biotinylation of surface proteins (SURF) in WJ-MSCs.* Silver staining was conducted on bolt-well gradient gels. Lanes were fractioned into 3 sections for mass spectrometry analysis.

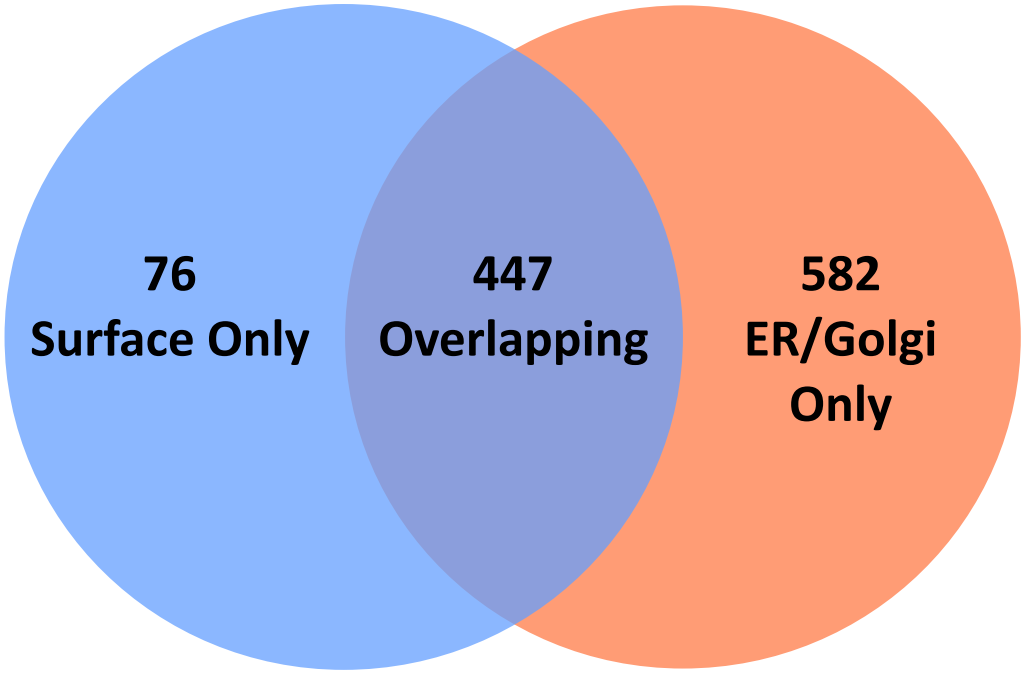

Figure 11. *Overlapping proteins between surface and ER/Golgi fractions in HUCPVC secretome.* Proteins were obtained via LC-MS.

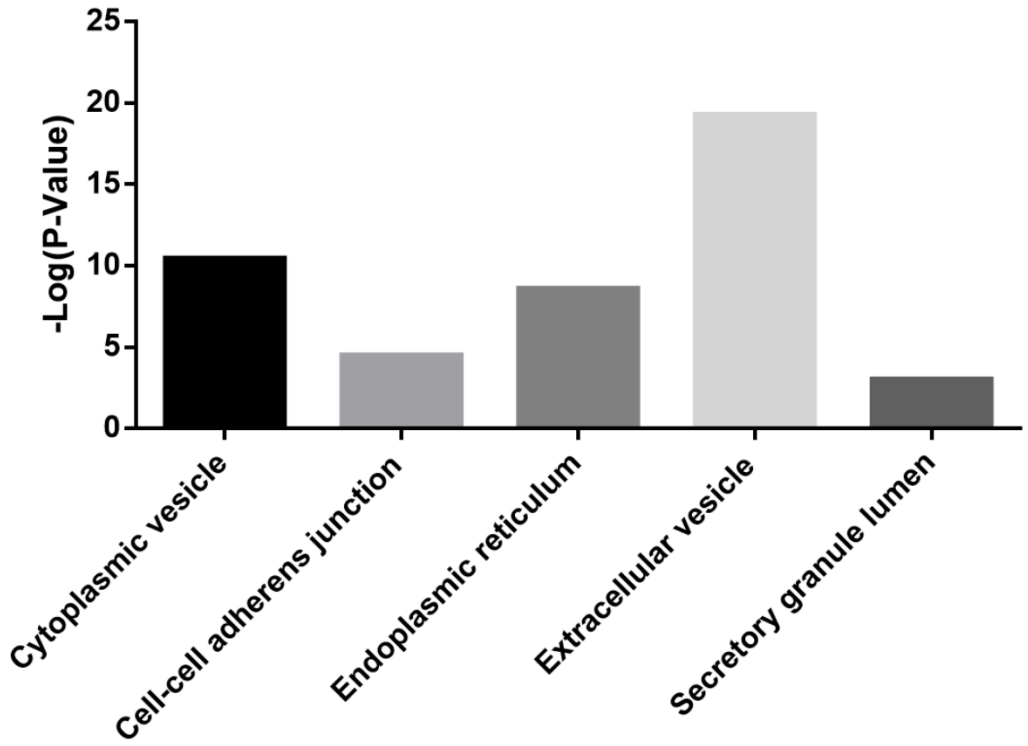

Figure 12. *Enrichment of ER/Golgi cellular component terms from WJ-MSC secretome.* Term specifications and analysis were completed using Gene Ontology. P-values represent the GO term FDR.

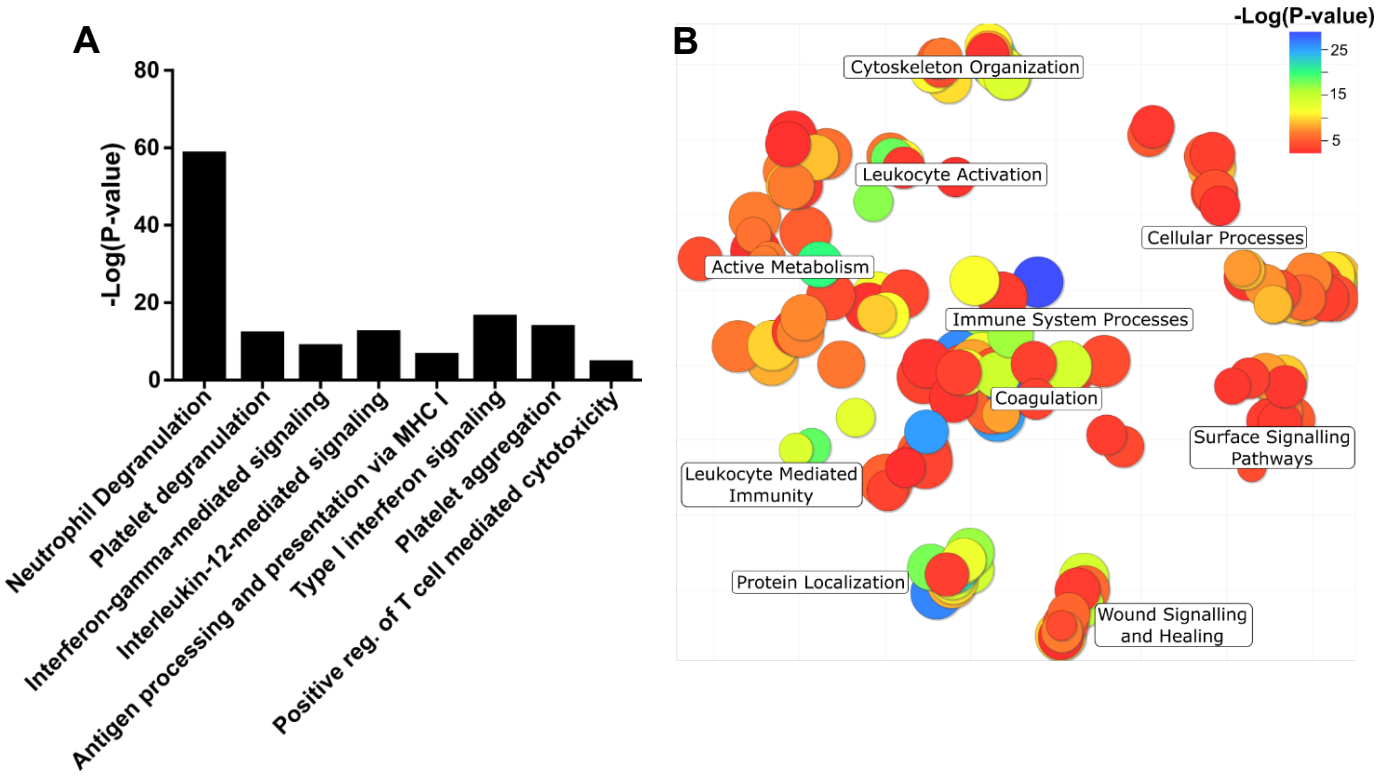

Figure 13. *Functional enrichment of immune terms in secreted proteins from WJ-MSCs.* **(A)** Significantly enriched immune-modulatory or healing response GO terms. P-values represent the false discovery rate (FDR) that a given GO term was randomly enriched. (**B)** Clustering of significant gene ontology (GO) terms generated from immunomodulatory UC-MSCs. Each node represents a single GO term. Node colour indicates the FDR of each node. Distance between nodes represents semantic similarity between respective GO terms.

3.4 Intracellular WJ-MSC transcriptomics enriches for immunomodulatory terms

Contributions

- I conducted all culture, RNA extraction, RNA sequencing analysis, and functional analysis.

While providing information on extracellular interactions of MSCs, the ER/G and surface fractions only represent a portion of the proteins in the cell and provides limited insight into intracellular regulation of immunomodulatory phenotype. Moreover, due to the largely qualitative nature of mass spectrometry, increasing stringency of a fold change cut-off would be inappropriate to eliminate noise. Preliminary analysis of publicly available microarray data between early and late passage WJ-MSCs demonstrates significant differences between the transcriptomes of WJ-MSC lines (**Figure 14**).[112] Therefore, I conducted intracellular RNA sequencing on WJ-MSCs. Due to issues with sequencing and media, I was only able to send a limited number of samples for sequencing. However, for the remaining samples, I obtained sequencing depths of over 45 million reads along with low ribosomal RNA rates in depleted samples, suggesting the sequencing and ribosomal depletion step were performed successfully (**Table 1**).

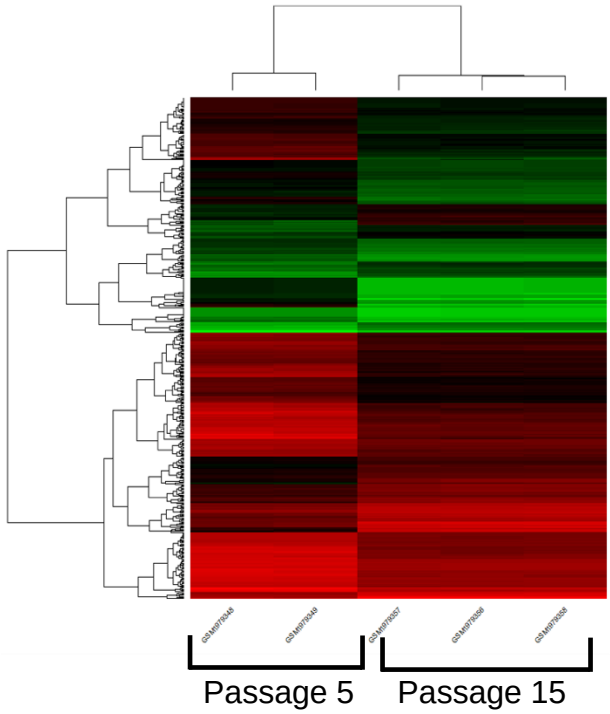

Figure 14. *Gene expression profiling and hierarchical clustering of WJ-MSC of differing passage.* Genes with very significant fold changes are shown (p = 0.0005). Red represents lower expression while green higher expression.[113]

Table 1: *Summary of WJ-MSC RNA sequencing results.* Technical replicates were collected from the same primary cell line on different days.

Sample	Reads	Unmapped	Ribosomal Rate
WJMSC1_P2_1	49,241,813	730,694	0.55%
WJMSC1_P2_2	42,591,255	1,001,626	0.62%
WJMSC1_P9_1	48,602,614	731,581	1.06%
WJMSC1_P9_2	47,160,804	737,095	0.82%

A total of 1040 differentially expressed genes were identified in WJ-MSCs using a 0.05 p-value cut-off after Benjamini multiple testing correction. Initial functional analysis using gene ontology yielded immune-related terms such as immune system process. However, there is a considerable amount of noise still present, which could be a consequence of the varied proliferation rates between WJ-MSC lines (**Figure 5A**). KEGG analysis revealed the enrichment of numerous signalling pathways including the PI3K/AKT, mTOR, canonical WNT, NFκB, and MAPK signalling pathways. Similarly, some pathways, in particular mTOR signalling, may be upregulated in early passage MSCs due to increased cell division. Nonetheless, genes that are upregulated may still play vital role in MSC immunomodulation. Moreover, the PI3K/AKT pathway in MSCs has been shown to be activated by IFNγ induction.[29] Since both early and late passage cells were induced with IFNγ, the differential protein and gene expression observed could be due to a greater response of early passage cells to cytokine induction.

3.5 Integration of WJ-MSC differential transcriptomic and proteomic analysis reveals enrichment for genes involved in MSC immunomodulation

Contributions

- I completed all dataset analysis and functional analysis.

To further refine our list of candidate biomarkers for MSC immunomodulation and reduce noise, I integrated our transcriptomics data with our proteomic data. Our initial functional analysis of differentially expressed genes (DEGs) from WJ-MSC total RNA sequencing analysis yielded immunomodulatory term enrichment (**Figures 15A**). Moreover, WJ-MSC total RNA sequencing showed an upregulation of IDO between early and late passages, providing further validation of our comparison. However, the increased proliferation observed in early passage WJ-MSCs appears to dominate the variance between early and late WJ-MSC gene expression, since mitochondrial and proliferation-related pathways were predominantly enriched. Decreasing our p-value cut-off and focusing on only positive fold changes resulted in a greater enrichment of immune related terms, but this cut-off still produced a total of 531 genes (**Figure 15B**). Downregulated genes were compared separately, as functional analyses such as gene ontology do not differentiate between up and down regulated DEGs. To further trim the list of candidates and focus on extracellular biomarkers and mechanisms, WJ-MSC upregulated transcriptomic and proteomic data was merged by selecting genes/proteins that were significantly different in our transcriptomic data and highly ranked in our proteomic data (rankings were determined by normalized spectral counts and a cut off of the top 200 proteins was applied). This intersection resulted in a list down of 89 potential targets. Functional analysis of the trimmed targets still produced multiple immune terms, while greatly reducing the number of cellular processes, cell division, and metabolic related (**Figure 15C**). KEGG analysis again yielded a number of

metabolic, cytoskeletal, and cell adhesion terms, along with PI3K/AKT, WNT, and G-protein related signalling, further validating our trimming strategy.

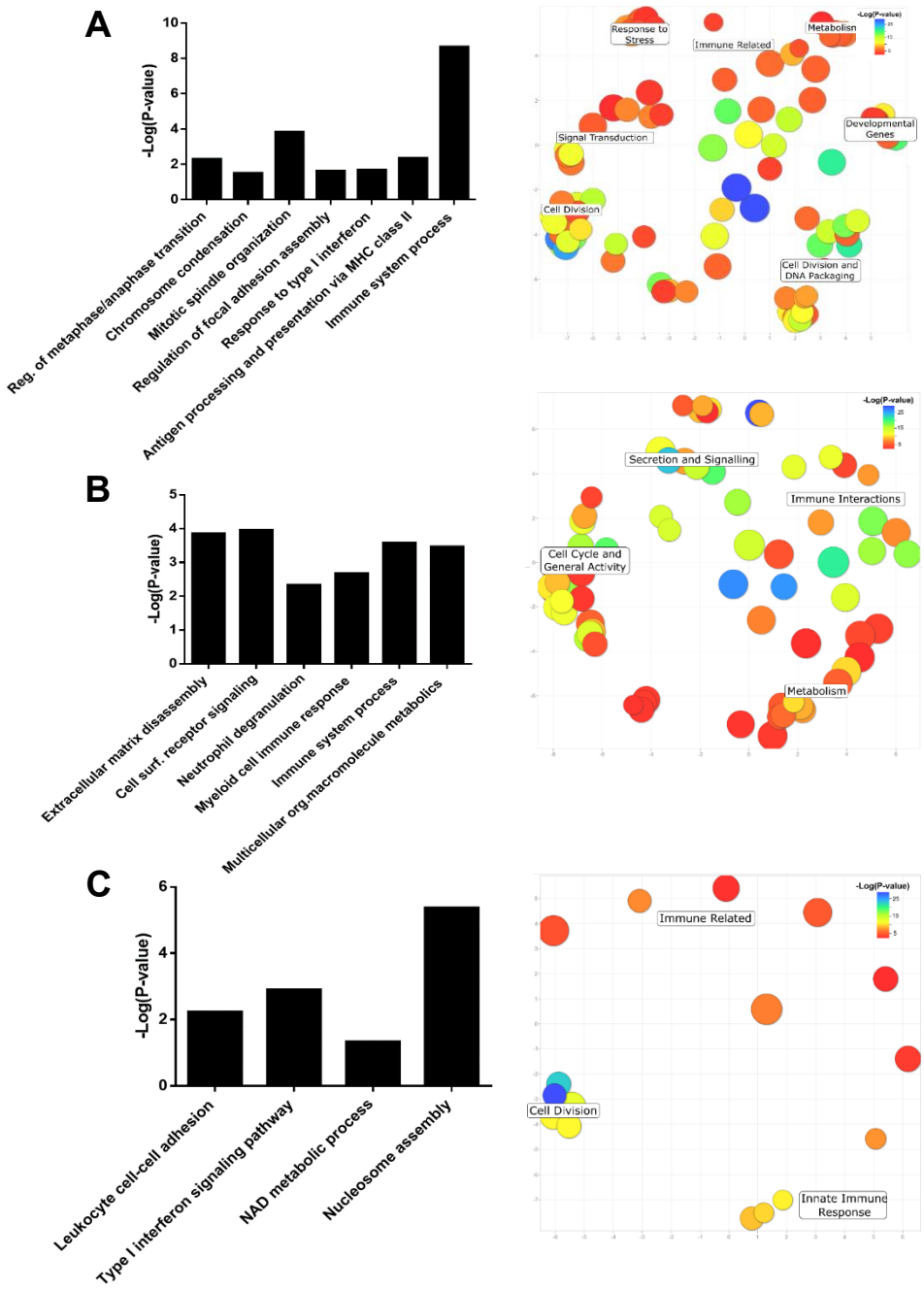

Figure 15. *Comparative analysis of WJ-MSC total RNA results in immunomodulatory functional enrichment.* Functional enrichment analysis was conducted on **(A)** all DEGs, **(B)** significantly upregulated genes, **(C)** genes found in both the secretome and total RNA. **(Left)** Selection of significantly enriched GO terms. P-values represent the GO term FDR that a given GO term was randomly enriched. **(Right)** Clustering of significant gene ontology (GO) terms generated from immunomodulatory WJ-MSCs. Each node represents a single GO term. Node colour indicates the FDR of each node. Distance between nodes represents semantic similarity between respective GO terms.

3.6 Intracellular HUCPVC transcriptomics enrich for immunomodulatory phenotypes

Contributions

- I conducted all culture, RNA extraction, RNA sequencing analysis, and functional analysis.

To gain a better understanding of immunomodulatory regulation and to eliminate cell line specific noise, I conducted RNA sequencing analysis of another UC-MSC line: early and late passage HUCPVC6. Unfortunately, there were several differences between the HUCPVC and WJ-MSC RNA sequencing experiments that may contribute to differences between the two datasets. First, while total RNA sequencing with ribosomal depletion was conducted on WJ-MSCs, HUCPVCs employed a stranded library preparation, due to issues in ribosomal depletion in the second set. Consequently, HUCPVC libraries do not contain any information on other non-mRNA RNA species such as long non-coding RNAs (lncRNAs) but were able to be robustly sequenced (**Table 2**). HUCPVC culture was unfortunately conducted in a different serum free media due to company supply issues. Moreover, HUCPVC samples were not induced, as subsequent immunomodulatory tests of the cells in the new media revealed a diminished immunomodulatory capacity in induced early cells (**Figures 6-7**). Interestingly, the new culture conditions appeared to reduce the disparity in proliferation between early and late passages. By mitigating the proliferation disparity between passages and removing proinflammatory induction, I was able to reduce the extraneous phenotypic differences between early and late passage MSCs, resulting in only 160 differentially expressed genes from our RNA sequencing analysis. Despite the low number of genes, DEGs between uninduced early and late passage HUCPVC similarly revealed enrichment for MSC therapeutic and immunomodulatory terms, including *leukocyte migration*, *extracellular matrix organization,* and *wound healing* (**Figure 16**). KEGG

analysis on the DEGs between early and late HUCPVCs also demonstrate an enrichment for PI3K-AKT, MAPK, and P53 signalling pathways. Filtering HUCPVC DEGS on those that are significantly differentially expressed in the WJ-MSC data set revealed only 19 overlapping genes (**Table 3**). Gene ontology analysis of those 19 genes resulted in similar immune related results to the HUCPVC dataset alone, indicating an enrichment of immune related genes. Only 12 targets were found in both proteomic and transcriptomic data, likely a result of differences in culture and induction between the two sets of MSCs (**Table 3**). However, those 12 targets still enriched for immune terms as *immune system process*, *positive regulation of chemotaxis*, and *wound healing*. Moreover, KEGG analysis again enriched for PI3K-AKT and MAPK signalling pathways. Several of the 12 targets were also surface proteins, such as SERPING1^{+} and PDGFRB^{-}, which potentially could be used as biomarkers for therapeutic UC-MSCs. Future experiments will validate these two promising lists of targets by correlating surface expression with immunomodulatory ability.

Table 2: *Summary of HUCPVC RNA sequencing results.* Technical replicates were collected from the same primary cell line on different days.

Sample	Reads	Unmapped
HUCPVC#6_P3_1	44,730,066	988,540
HUCPVC#6_P3_2	33,818,535	5,1831,39
HUCPVC#6_P6_1	45,703,457	1,047,985
HUCPVC#6_P6_2	36,977,926	7,384,072

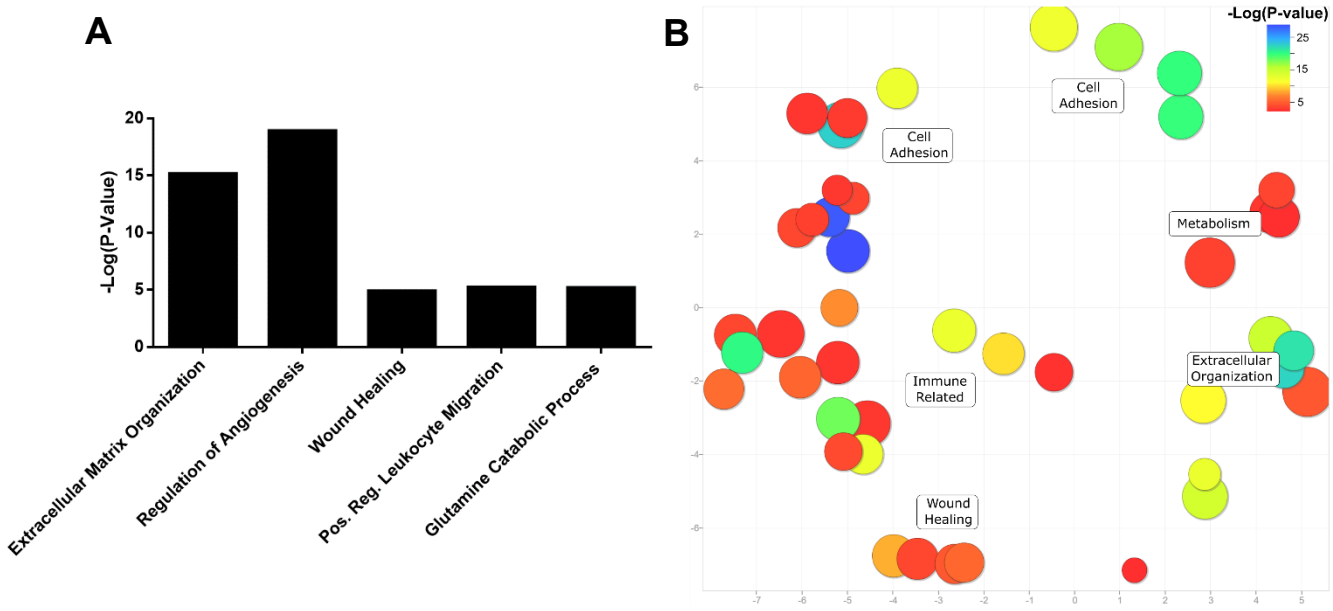

Figure 16. *Comparative analysis of HUCPVC mRNA from early and later passages results in immunomodulatory functional enrichment.* **(A)** Significantly enriched immune-modulatory or healing response GO terms. P-values represent the FDR that a given GO term was randomly enriched. (**B)** Clustering of significant GO terms generated from immunomodulatory UC-MSCs. Each node represents a single GO term. Node colour indicates the false discover rate (FDR) of each node. Distance between nodes represents semantic similarity between respective GO terms.

Table 3: *UC-MSC immunomodulatory gene candidates.* HUCPVC vs WJ-MSC genes were determined from overlaps in RNA sequencing DEGs while HUCPVC proteomics vs transcriptomics was determined via overlaps between RNA sequencing and mass spectrometry.

HUCPVC vs WJ-MSCs	HUCPVC Proteomics vs Transcriptomics
SERPINB7	CPA4
ANGPTL4	PDGFRB
GREM1	THBS1
FGF5	CTGF
GPNMB	SERPINE1
ANKRD1	DCN
DUSP6	DSP
LPXN	SERPING1
THBS1	CFH
IL6	GFPT2
CCND1	HMGA2
WNT5B	
IL13RA2	
GALNT6	
ADAMTS1	
HMGA2	
CCBE1	
SRGN	
FMN2	

3.7 Proinflammatory induction enhances immunomodulatory ability through unique control mechanisms

Contributions

- I completed all qPCRs.

As demonstrated above, induction with inflammatory cytokines has varied effects on UC-MSC immunomodulatory ability. To interrogate the effects of induction on immunomodulation regulation, I conducted functional analysis of DEGs that were exclusively found in our induced WJ-MSC RNA sequencing analysis and not in our uninduced HUCPVC analysis. Functional terms such as *macrophage cytokine production*, *extracellular matrix organization*, and *antigen processing* were upregulated, indicating that induction had a profound effect on the extracellular activity of WJ-MSCs.

To investigate the role of IFNγ and TNFα induction in immunomodulation, I examined general immunomodulatory markers such as VCAM1, and WARS (associated with tryptophan catabolic pathway and protein synthesis) as well as interferon pathway-related genes (IFIH1 and IFIT3). VCAM1 and WARS were found to be upregulated in both induced WJ-MSCs and HUCPVCs via qPCR validation, though HUCPVCs appeared to exhibit greater induction (**Figure 17**). Moreover, VCAM1 was elevated in uninduced HUCPVCs versus induced HUCPVCs, indicating induction with proinflammatory cytokines may have varying effects on immunomodulatory function (**Figure 18**). On the other hand, IFIH1 and IFIT3 were upregulated in the UC-MSC data set in induced UC-MSCs rather than uninduced (**Figure 18**). Interestingly, IDO levels were found to be significantly lower in uninduced cells, which could suggest that IDO is only transiently expressed when induced. Thus, inflammatory cytokines adjust the intracellular regulation of immunomodulatory mechanisms, potentially modifying how MSCs

immunosuppress. We will continue to examine the differences between induced and uninduced samples by including RNA sequencing data on induced HUCPVC samples into our analysis.

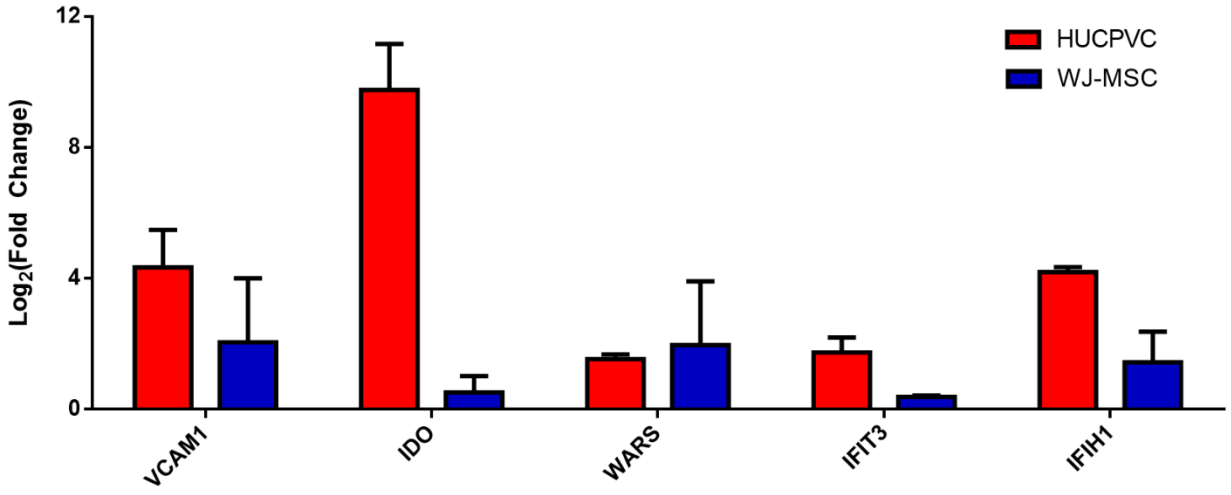

Figure 17. *qPCR validation of UC-MSC immunomodulatory candidate genes.* Genes were selected from candidate genes if they exhibited large fold changes in RNA sequencing data while being related interferon signalling and tryptophan catabolism. cDNA was generated from the total RNA stock that was originally RNA sequenced.

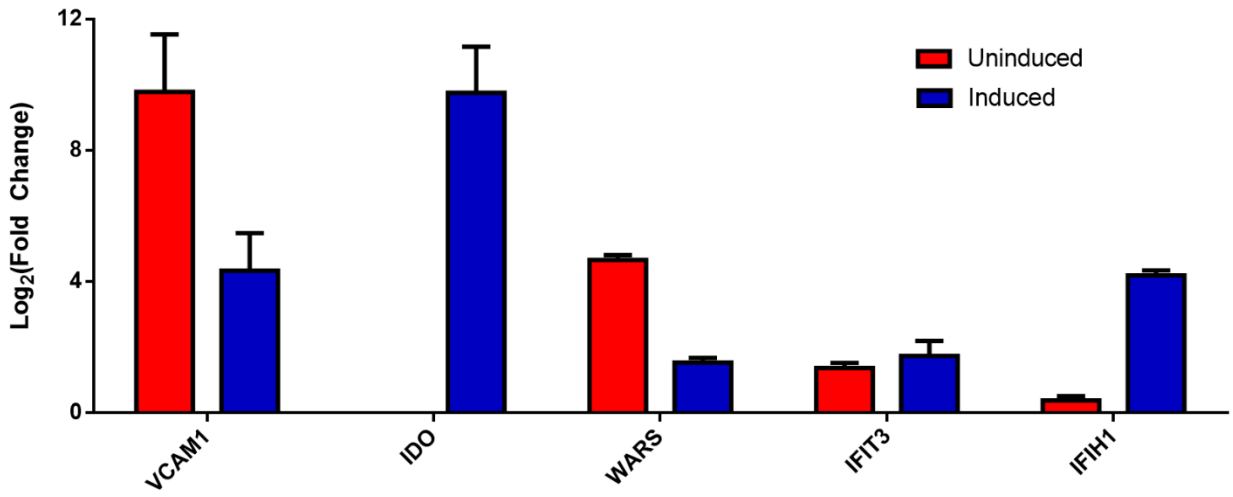

Figure 18. *Induction of UC-MSC activates differing immunomodulatory transcriptional mechanisms.* Genes were selected from candidate genes if they exhibited large fold changes in RNA sequencing data while being related interferon signalling and tryptophan catabolism. cDNA was generated from the total RNA stock that was originally RNA sequenced.

3.8 PI3K-AKT Pathway plays a role in immunomodulatory regulation

Contributions

- I completed all Western Blots.

One of the most upregulated pathways between early and late passage WJ-MSCs and HUCPVCs was the PI3K-AKT pathway: proteins involved in this pathway were identified in the ER/G and surface proteomics and genes in the RNA sequencing experiments. While no significant transcriptional differences were detected in AKT between early and late passage, a pronounced increase in AKT phosphorylation was detected via Western blotting in early passage MSCs (**Figure 19**). Uninduced HUCPVCs exhibited far less difference between early and late passage p-AKT. Since this phosphorylation does not occur in the late passage despite interferon stimulation at both time points, differences in AKT phosphorylation appears to be a cell intrinsic process rather than dependent on IFN-signaling. Therefore, UC-MSC immunomodulatory capability could be directly regulated by the PI3K/AKT signalling pathway.

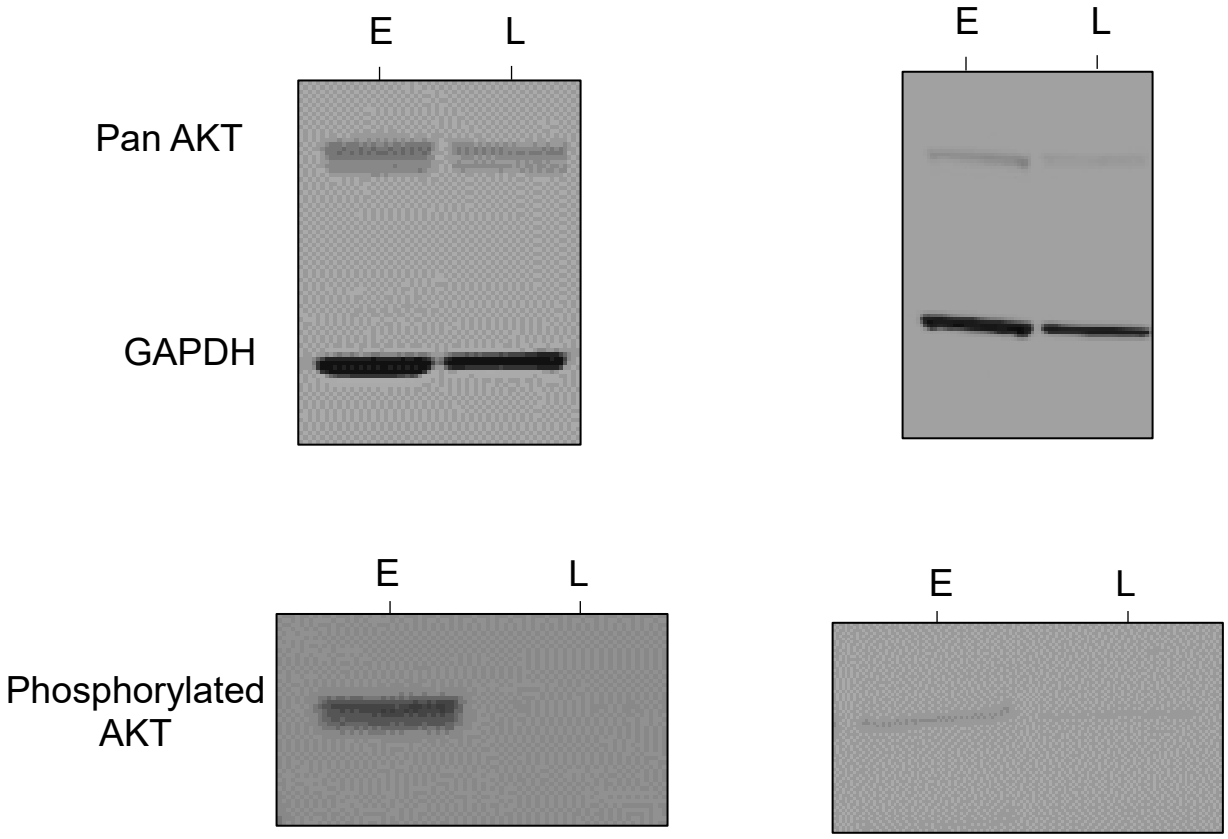

Figure 19. *Greater phosphorylation of AKT in early versus late passage UC-MSCs.* Whole cell lysate was isolated from IFNγ and TNFα induced early and late UC-MSCs. **(Left)** Induced UC-MSCs, **(Right)** Uninduced UC-MSCs. E, early and L, late passage MSCs.

3.9 Cecal Slurry Puncture model consistently elicits sepsis in humanized mice.

Contributions

- All direct mouse work was completed by Dr. Caryn Ito and Priya Chandran.
- I completed all bacterial speciation and quantification.
- Flow cytometry for immune cell engraftment was predominantly completed by Priya Chandran with my technical assistance.

Concurrently, I developed a humanized mouse model to validate immunomodulatory UC-MSC subpopulations based on our transcriptomic and proteomic analysis. As mentioned previously, numerous MSC therapeutics that have shown pre-clinical promise *in vitro* and *in vivo* exhibited little to no therapeutic efficacy. This disparity is likely exacerbated by discrepancies in the immune and inflammatory responses between the *in vivo* models used and human patients. By developing accurate and feasible *in vivo* models, proper validation of novel therapeutics such as MSC cellular therapies can be promptly conducted, saving time and resources that could be wasted on clinical trials. I developed a reproducible preclinical animal model that dependably recapitulates the human sepsis response. Additionally, a cecal slurry and puncture (CSP) procedure was developed to consistently induce sepsis whereby a defined bacterial dose was injected into the abdominal cavity through the surgically exposed cecum. Specifically, the CSP procedure was performed on humanized mice, which were generated by co-transplanting human progenitor T cells with human $CD34^{+}38^{-}$ hematopoietic stem and progenitor cells into NOD-*scid* $IL2R\gamma^{null}$ (NSG) pups to ensure robust multilineage human cell engraftment and to decrease the time required for mature T cell engraftment.

The CLP mouse model, which is currently considered the gold standard animal model for sepsis, does not dependably induce a reproducible sepsis response.[114,115] Different techniques in

ligating and puncturing the cecum significantly contribute to the variability in the severity of the sepsis response and experimental outcome.[116,117] Moreover, abscess formation at the site of ligation and puncture has been observed in CLP mice, often limiting and possibly eliminating systemic bacterial infection by localizing the infection.[96,97] Thus, the development of an *in vivo* model that consistently simulates the sepsis response observed in human patients is critical to understand the complex molecular and cellular dysfunction associated with this condition and ultimately to develop effective therapies. Since inconsistencies in the murine sepsis response following the cecal ligation and puncture (CLP) procedure stem from variability in the systemic bacterial load,[118,119] I developed the cecal slurry and puncture (CSP) procedure whereby the cecum is surgically exposed and a defined bacteria dose is injected into the abdominal cavity through the cecum. Furthermore, since there are also inconsistencies between the murine and human patient sepsis responses,[99] I hypothesized that performing the CSP procedure on humanized mice would better mimic the human sepsis response.

At ≥12 weeks post-transplantation with human HSPCs and pro T cells, NSG mice were randomized into groups to either undergo CSP or sham surgeries. Two lots of cecal slurry (CS-1 and CS-2) were prepared from the cecum of C57BL/6 mice[102] and the concentration of aerobic and anaerobic bacteria present in each cecal slurry (CS) was quantified and speciated (**Tables 4-5**). The effective dose of CS to consistently elicit a reproducible sepsis response was determined by titrating the CS administered. CS doses lower than 1.0×10^5 bacterial CFU/g body weight resulted in variable morbidity. Surviving mice that received less than 1.0×10^5 CFU/g exhibited sepsis symptoms such as cytokine dysregulation and elevated AST and ALT levels, but no bacteria was detected in the peripheral blood (PB) and they fully recovered from the procedure when monitored for 96 hours post-surgery (data not shown). Thus, an effective CS dose of $\geq 1 \times 10^5$ CFU/g

was utilized in subsequent experiments that consistently elicited a lethal sepsis response in 87% of CSP treated humanized mice (n=23) within 24 hours in contrast to 100% survival of sham control mice (n=16) (**Figure 20A**). To determine whether a systemic bacterial infection was associated with morbidity post-CSP, PB was collected at time of sacrifice and cultured under anaerobic and aerobic conditions, then speciated using matrix assisted laser desorption ionization-time of flight mass spectrometry (MALDI-TOF MS) (**Figure 20B**). Aerobic bacteria, facultative anaerobic bacteria, and anaerobic bacteria, predominantly of gut origin, were found in the PB of all CSP treated mice, while no bacteria were detected in the PB of sham controls. Despite the 4-fold difference in anaerobic bacteria content between CS-1 and CS-2 lots, the total bacteria CFU/g determined the CS effective dose rather than the bacteria species.

Table 4. *Bacterial concentration in cecal slurry preparations***.** Cecal slurry (CS) was prepared by harvesting cecal contents from C57BL/6 mice (n=5-6/lot).[120] Bacterial colony forming unit (CFU) quantification for each cecal slurry preparation was determined by performing serial dilutions of the CS stock that were plated onto either CDC-Blood agar plates or Tryptone Soya Agar with 5% sheep blood to assess anaerobic and aerobic bacterial growth, respectively.

Type of Bacteria	Cecal Slurry Lot#1 Bacterial Concentration (CFU/µL)	Cecal Slurry Lot#2 Bacterial Concentration (CFU/µL)
Aerobic	$9.0x10^3$	$6.2x10^3$
Anaerobic	$23.8x10^3$	$6.0x10^3$

Table 5. *Major bacterial species in cecal slurry preparations.* Bacterial speciation for each cecal slurry lot was determined by plating serial dilutions of the CS stock onto either CDC-Blood agar plates or Tryptone Soya Agar with 5% sheep blood to support anaerobic or aerobic bacterial growth, respectively. Morphologically unique colonies were speciated by MALDI-TOF tandem mass spectrometer.

Cecal Slurry #1	**Cecal Slurry #2**
Lactobacillus johnsonii	Lactobacillus johnsonii
Lactobacillus murinus	Lactobacillus murinus
Enterococcus casseliflavus	Staphylococcus sciuri
Entercoccus faecalis	Staphylococcus xylosus
Streptococcus mitis	Enterococcus casseliflavus
Propinionbacterium acness	Entercoccus faecalis

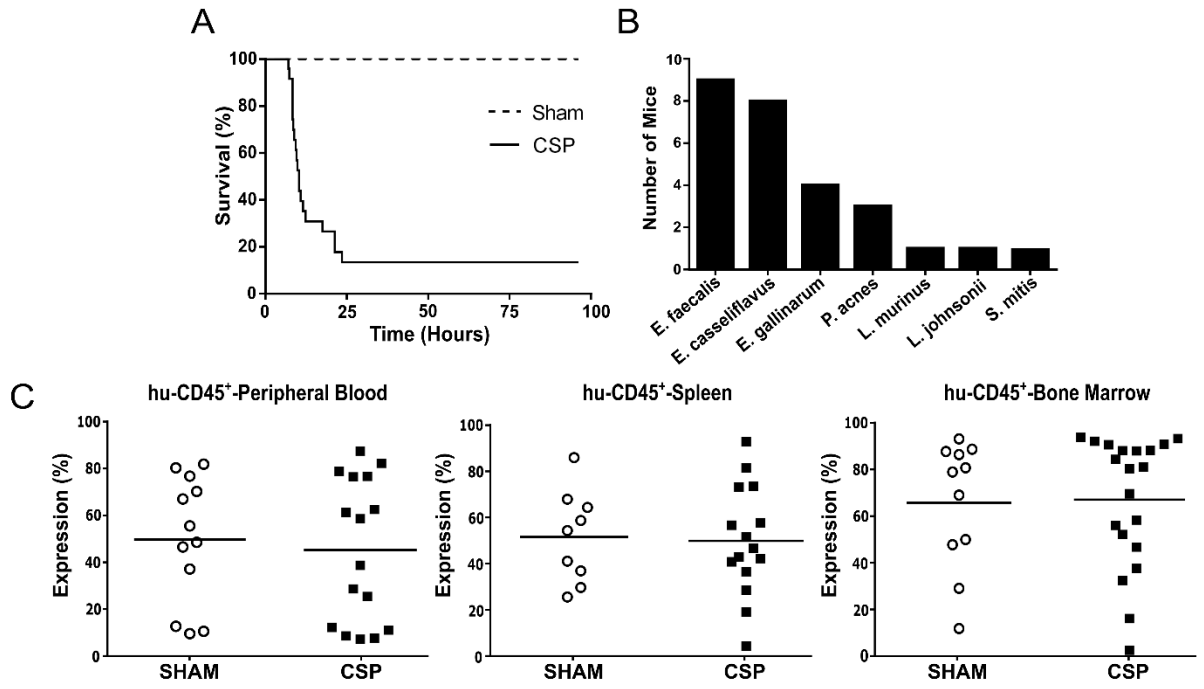

Fig 20. *Cecal Slurry Puncture model consistently induces a sepsis response in multilineage human immune cell engrafted mice.* (**A**) Kaplan-Meier survival curve of CSP treated humanized mice (n=23) compared with sham mice (n=16). (**B**) Bacteria present in peripheral blood of CSP treated mice as determined by MALDI-TOF tandem mass spectrometry. (**C**) Engraftment levels of human $CD45^+$ cells in the PB, spleen and bone marrow of repopulated NSG mice. Each data point represents one mouse from 10 independent experiments. *P≤0.05.

3.10 Humanized Mice Exhibit Multilineage Human Immune Cell Engraftment

Contributions

- Flow cytometry for immune cell engraftment was predominantly completed by Priya Chandran with my technical assistance.

Phenotypic analysis showed comparable engraftment levels of $CD45^+$ human cells in PB (51.43 ± 27.47% versus 41.98 ± 30.11%), spleen (54.88 ± 20.47% versus 57.07 ± 24.17%) and bone marrow (66.79 ± 27.68% versus 63.50 ± 29.45%) of sham and CSP treated mice, respectively (**Figure 20C**). Analysis of specific immune cell lineages revealed similar levels of innate immune cells $CD14^+$ monocytes and $CD15^+$ granulocytes, as well as adaptive immune cells $CD19^+$ B lymphocytes and $CD4^+$, $CD8^+$ and $CD3^+$ T lymphocytes in PB, spleen and bone marrow of both sham and CSP mice (**Figures 21A-B**). Furthermore, the composition of human immune cells present in the NSG mice was similar to that present in human umbilical cord blood, from which the human HSPCs were derived (**Figure 22**). Thus, I generated a robust human immune system within our NSG mice.

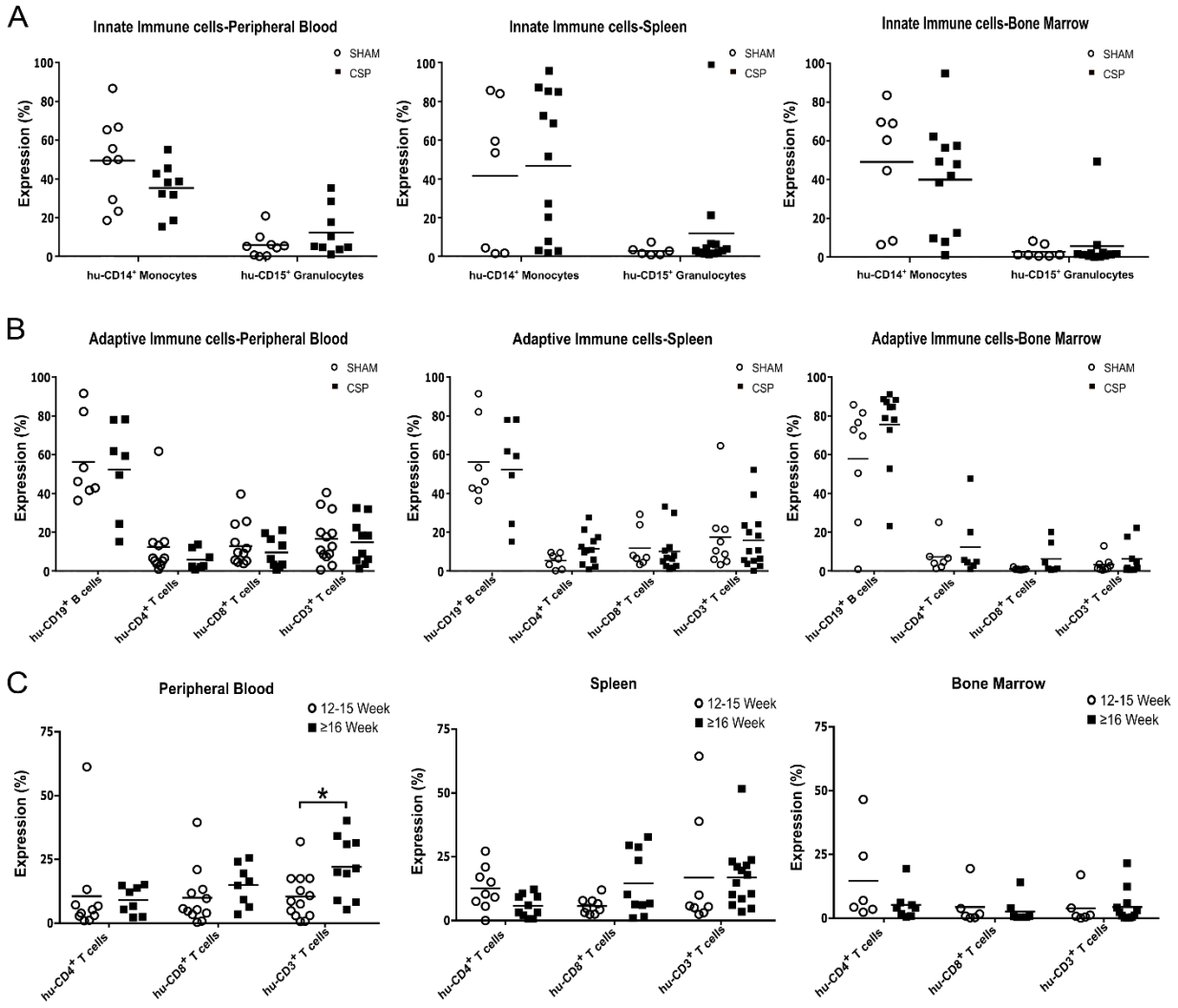

Figure 21. *Multilineage human immune cell engraftment in mice post-transplant.* Engraftment levels of (**A**) innate immune cells and (**B**) adaptive immune cells in repopulated NSG mice ≥12.5 weeks post-transplantation. (**C**) Human T cell engraftment in the peripheral blood, spleen, and bone marrow in NSG mice at 12.5-15 weeks and ≥16 weeks post-transplantation. Each data point represents a mouse from n=10 independent experiments. *P≤0.05. Flow cytometry completed by Priya Chandran and Dr. Caryn Ito.

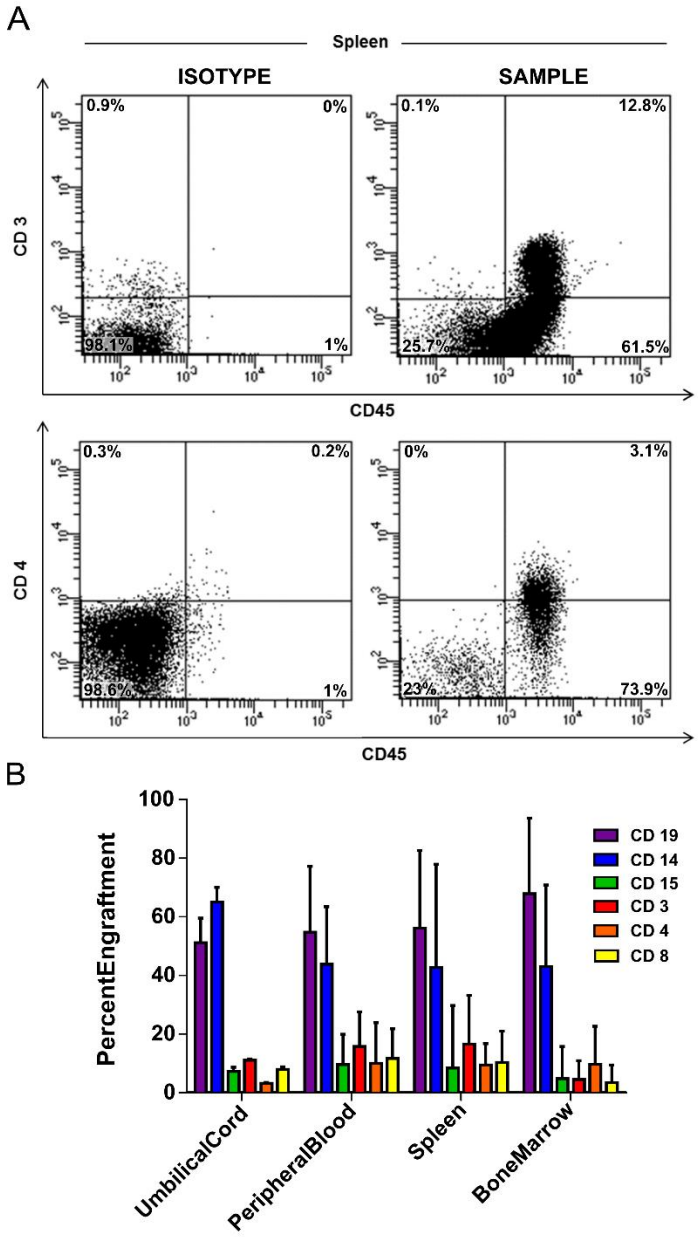

Figure 22. *Composition of multilineage human cell engraftment in NSG mice is comparable to human umbilical cord blood. (***A**) Representative flow cytometry plots of $CD3^+$ and $CD4^+$ T cells versus $CD45^+$ cells identifying human immune cells subpopulations in NSG mice. Percentages of each population are indicated on the graph. (**B**) Composition of innate and adaptive immune cells present in human umbilical cord blood (UCB) (n=5) and NSG mice peripheral blood (PB), spleen and bone marrow (BM) (n=14). Error bars represent mean ± s.e.m.

The presence of T lymphocytes is critical in the initial sepsis response as they are recruited and amplified by the initial immune response.[121] Moreover, T cell apoptosis and exhaustion has often led to prolonged immunosuppression causing reduced immunity in sepsis patients while the remaining T cells are functionally impaired inducing dysregulated cytokine production. In a previously reported CLP humanized mouse model of sepsis, the time to robust mature T cell engraftment was found to be 20 weeks.[120] Therefore, to decrease the time required for mature T cell engraftment, immature progenitor T (pro T) cells were co-transplanted with $CD34^+CD38^-$ HSPCs into NSG pups.[101] Flow cytometry analysis determined that mice engrafted at 12.5-15 weeks or greater than 16 weeks post-transplantation had comparable engraftment of $CD3^+$, $CD4^+$ and $CD8^+$ T cells in the PB, spleen and bone marrow. Higher levels of T cell engraftment were observed in the PB and spleen, while the level of bone marrow T cell subpopulations was lower, as expected (**Figure 21C**). Peripheral blood engraftment of $CD3^+$ T cells was significantly higher in mice at ≥16 weeks (n=13) versus 12.5-15 weeks (n=10) post-transplantation, however, engraftment levels of $CD4^+$ and $CD8^+$ T cell subpopulations were comparable in both cohorts. Since robust T cell engraftment was observed in mice as early as 12.5 weeks post-transplant, the time required for relevant levels of T cell engraftment in this mouse model has been greatly reduced.

3.11 Cecal Slurry Puncture model consistently elicits a human sepsis response in humanized mice

Contributions

- I completed all cytokine ELISAs, AST and ALT determination, and immunohistochemistry.
- Flow cytometry for T-cell apoptosis was predominantly completed by Priya Chandran with my technical assistance.

To further characterize the efficacy of CSP to induce sepsis, mice were monitored post-CSP surgery for sepsis related symptoms. Mice that underwent the CSP procedure were markedly less active and weaker than their sham counterparts. Since hypothermia is a known symptom as well as an important objective prognostic indicator of sepsis,[122] temperatures of the mice were measured pre- and post-surgery. A significant decrease in body temperature was observed in CSP mice, but not in sham mice post-surgery (**Figure 23A**).

I next determined if CSP humanized mice recapitulated human sepsis pathophysiology. Septic patients consistently have elevated plasma levels of pro-inflammatory and anti-inflammatory cytokines.[123,124] Likewise, both pro- and anti-inflammatory human cytokines were significantly increased in the blood plasma of CSP treated mice compared to sham controls and no human cytokines were detected in the plasma from unmanipulated controls, indicating the presence of functional human immune cells in the humanized CSP treated mice that recapitulated human cytokine dysregulation observed in human sepsis patients (**Figure 23B**).

Because organ failure is a contributing cause of death due to septic shock, I also evaluated liver function by monitoring biochemical markers in the peripheral blood. Since aspartate transaminase (AST) and alanine transaminase (ALT) are concentrated in the liver and enter the

capillaries post liver damage, I analyzed AST and ALT levels in the blood plasma of mice that underwent either sham or CSP procedures. I found CSP mice exhibited significantly increased levels of AST and ALT compared with sham controls (**Figure 23C-D**). Interestingly, CSP treated mice segregated into groups based on high or low AST or ALT concentrations, which did not significantly correlate with gender, body weight, age, immune cell engraftment, CS dose or experimental cohort. Moreover, ALT/AST concentration did not directly correlate with the severity of liver damage,[125] indicating our high and low responders may had similar levels of liver damage. Previous studies have correlated tissue damage and organ failure with macrophage and neutrophil infiltration during sepsis.[126–128] Moreover, excessive extracellular myeloperoxidase (MPO) activity during inflammation has been shown to cause oxidative damage in the surrounding tissue.[129,130] Consistent with elevated AST and ALT indicators of liver damage, increased macrophage ($CD68^+$) and neutrophil (MPO^+) infiltration was also observed in the liver and lungs of CSP mice compared to sham mice (**Figure 23E-F**).

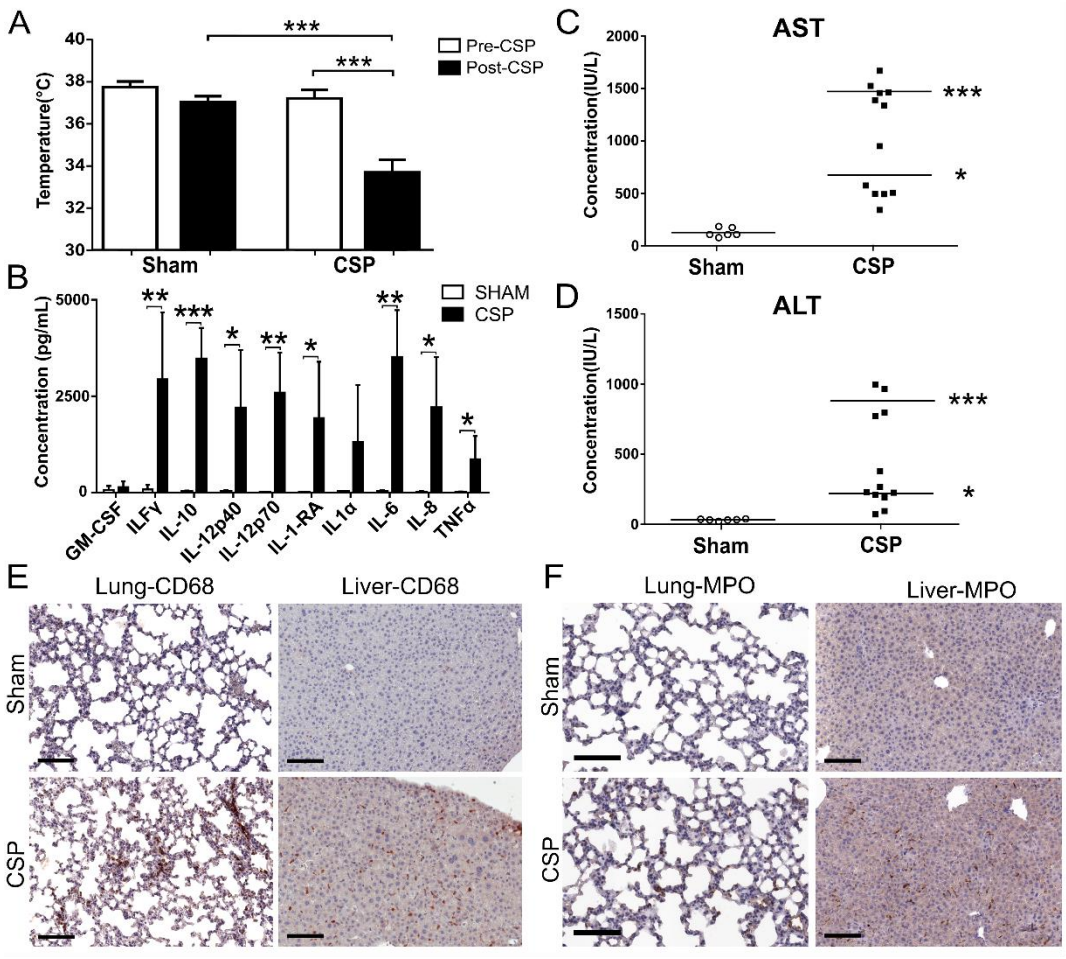

Figure 23. *The humanized CSP model recapitulates the human sepsis response.* (**A**) Comparison of body temperature pre- and post-surgery between CSP (n=20) and sham (n=16) mice. (**B**) Human cytokine response in peripheral blood post-CSP. All sham mice had cytokine concentrations lower than 100pg/mL. (**C,D**) Blood chemistry analysis of (**C**) aspartate transaminase (AST) and (**D**) alanine transaminase (ALT) levels in plasma of sham (n=5) or CSP mice (n=10). Sham mice were compared to either high or low CSP responders. (**E,F**) Representative immunohistochemistry staining of (**E**) $CD68^+$ macrophage and (**F**) MPO^+ neutrophil infiltration in paraffin embedded liver and lung tissue from sham (n=4) and CSP (n=4) treated mice. Bar = 100uM. Significance was determined using an unpaired two tailed student's t-test. Error bars represent mean ± s.e.m. * $P \leq 0.05$ ** $P \leq 0.005$ *** $P \leq 0.0005$

Another hallmark of human sepsis pathophysiology is lymphocyte apoptosis, which has been shown to exacerbate the condition in sepsis patients and render them more susceptible to secondary infections.[67,131] Hence, we analyzed the level of lymphocyte apoptosis in humanized mice following CSP surgery by flow cytometry using apoptosis specific markers Annexin-V and 7AAD to determine the percentage of apoptotic cells in the spleen and peripheral blood (PB). We found that mice that underwent CSP procedure exhibited significantly increased splenic $CD8^+$ and $CD4^+$ T cell apoptosis compared with sham controls **(Figure 24A-B)**. Similar trends were observed for splenic $CD19^+$ B cells, however it was not significant **(Figure 24B)**. In PB, we also observed an increase in early apoptotic $CD8^+$ T cells in CSP mice vs sham mice, but not in $CD19^+$ B cells (**Figure 24C**).

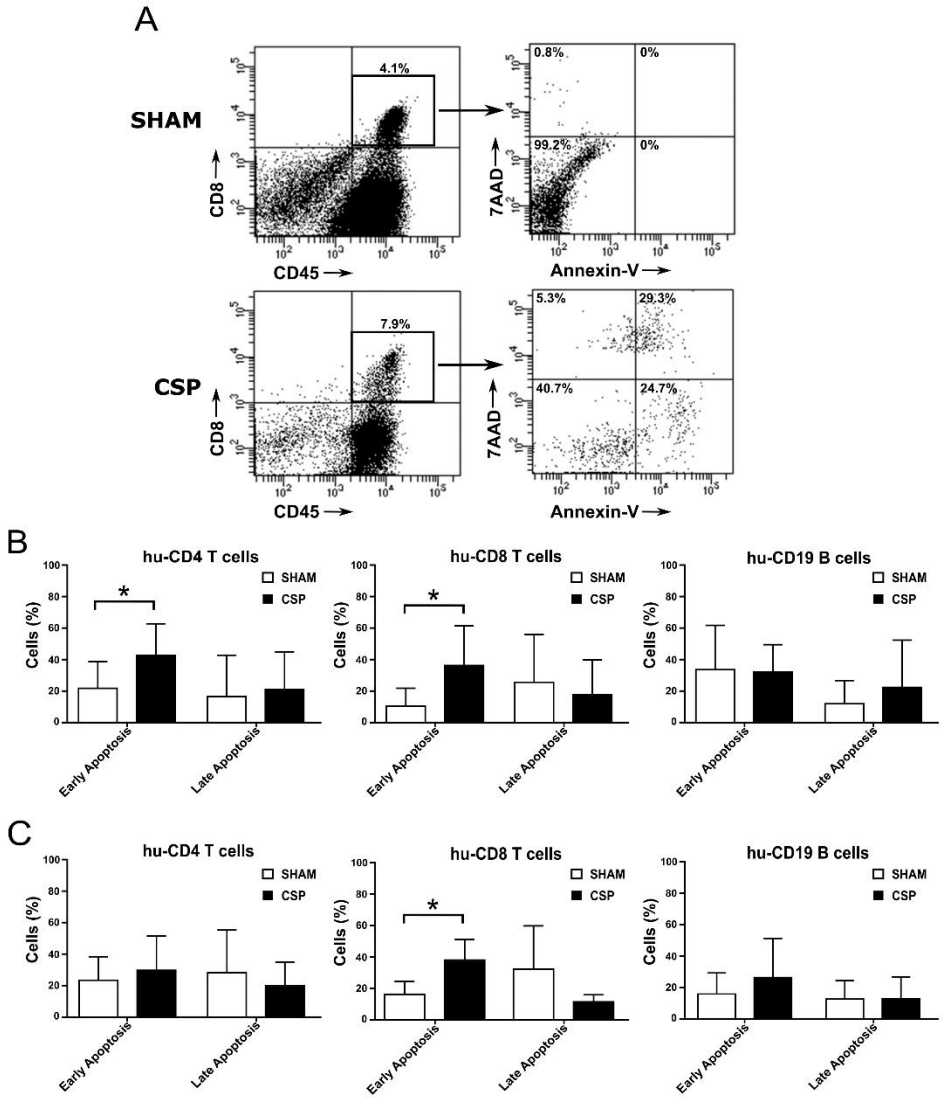

Figure 24. *Humanized CSP model demonstrates increased immune cell apoptosis.* (**A**) Representative flow cytometry analysis of human $CD45^{+}CD8^{+}$ T lymphocytes obtained from the spleens of CSP and sham treated mice. (**B,C**) Analysis of early ($AnnexinV^{+}7AAD^{-}$) and late ($AnnexinV^{+}7AAD^{+}$) apoptotic human lymphocytes obtained from (**B**) spleen and (**C**) peripheral blood of sham (n=7) or CSP (n=9) treated mice from at least 3 independent experiments. *P≤0.05. Flow cytometry conducted by Priya Chandran.

3.12 Improved Humanized CSP mouse model recapitulates human sepsis genomic response

Contributions

- I completed a majority of the qPCRs and all the analysis.
- Dr. Harinad Maganti and I developed the human sepsis gene signature.
- Winston Cheung and Chandarong Choey assisted with initial primer validation and testing.

Seok et al. found that the CLP sepsis model does not correlate with the human leukocyte transcriptomic response.[99] Thus, to determine whether our model recapitulated the human sepsis gene response, I generated a human sepsis gene signature based upon PB mononuclear cell gene expression using publicly available microarray datasets. Since studies using differing sepsis gene signatures reported contradicting results regarding the correlation between the transcriptional response of human sepsis patients and mice sepsis models following CLP,[99,132] I generated an unbiased gene signature based on significant gene expression levels, relevance to leukocyte biology, and differential directionality of gene expression (**Table 6**). PB gene fold change directionality and correlation analysis was conducted between human sepsis patients (GSE13904), other human and murine datasets and our humanized mouse model. I found that gene expression from the CSP treated humanized mice correlated significantly with human sepsis patient responses rather than with the murine sepsis response induced by CLP (**Figure 25**). Thus, our CSP humanized mouse model mimics the human sepsis response significantly better than the standard murine CLP sepsis model.

Table 6. *Human sepsis gene signature.* Human sepsis gene signature was generated by comparing publicly available human sepsis patient (GSE13904) and mouse (GSE5663) peripheral blood microarray data. Significant gene expression (false discovery rate [$q<0.01$]) was determined between healthy and septic humans and mice respectively. Genes with significant fold changes (log_2 fold change > 2) in both human and mouse PB but with fold changes in opposing directions were selected. The list was further filtered to include only genes that are biologically relevant to sepsis.

Gene	Function
ADM	Vasodilation, regulation of hormone secretion, promotion of angiogenesis, and antimicrobial activity
CD28	T cell proliferation and survival, cytokine production, and T-helper type-2 development
CD55	Regulation of the complement cascade
CD96	Activated T and NK cell interactions and antigen presentation.
CD160	Cytolytic effector activity in CD8 T cells and NK cells
GATA3	T cell development
IL7R	V(D)J recombination during lymphocyte development
IL18R1	Interleukin 1 receptor family
ITK	T cell kinase
LAT	T cell receptor activation response
LTF	Secondary granules of neutrophils
NCF4	Myeloid lineage cytosolic regulatory component
PRF1	Cytolytic protein in T cells and NK cells
TNFAIP6	Extracellular matrix stability and cell migration associated with inflammation

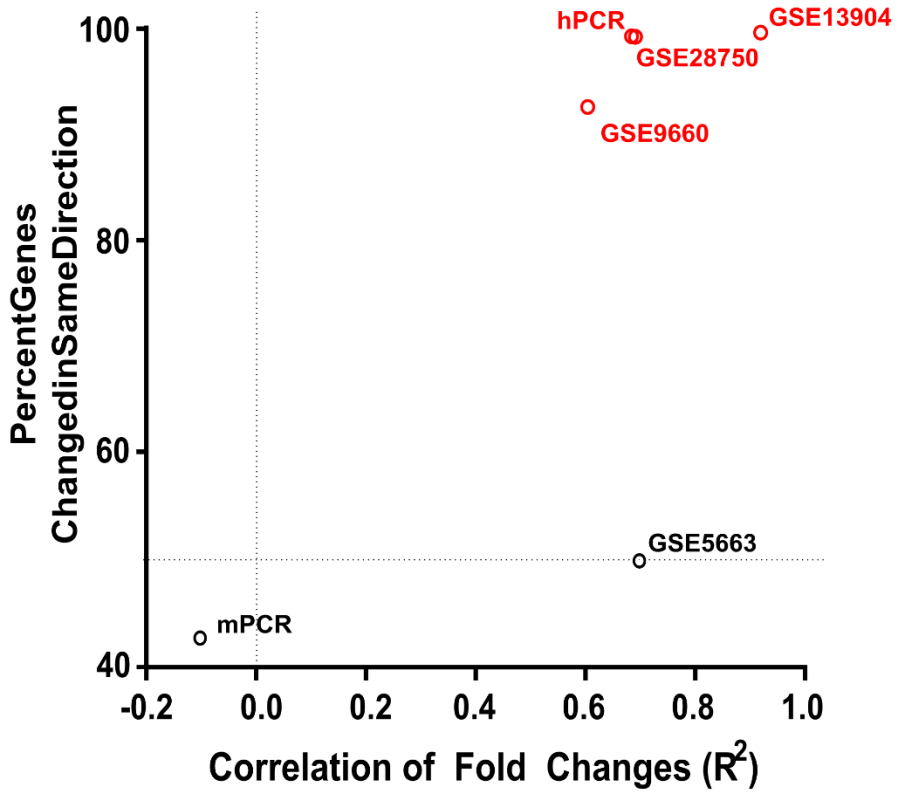

Figure 25. *Humanized mouse model recapitulates human genomic sepsis response.* Gene expression of the human specific sepsis gene signature (**Table 6**) was analyzed in blood samples collected from sham (n=6) and CSP (n=5) humanized NSG mice from n=5 independent experiments as well as from C57BL/6 mice (n=3). Pearson correlation and directionality was calculated in reference to the human sepsis patient data set, GSE13904, using the 14 gene signature, which is differentially expressed between mice and humans during sepsis. hPCR = CSP treated humanized mice, mPCR = unmanipulated C57BL/6 mice, and GSE codes represent publicly available peripheral blood microarray data sets obtained from human sepsis patients and CLP mice (GSE5663). Red and black text in the plot represent human and mouse data sets, respectively.

4.0 Discussion

In this study, I aimed to elucidate novel immunomodulatory biomarkers and gain mechanistic insights into UC-MSC immunomodulatory to isolate therapeutic subpopulations and develop efficacious MSC cellular therapeutics. To do so, I identified UC-MSCs with greater immunomodulatory ability (**Figure 4**). I found that immunomodulatory ability was partially lost if cultured *in vitro*, which I used as the base comparison of our study. To determine potential extracellular and surface proteins essential to the immunomodulatory phenotype, I conducted proteomic analysis of the UC-MSC secretome to determine upregulated biomarkers and extracellular regulators in early passage UC-MSCs versus late passage. On top of validating known immunomodulatory biomarkers such as VCAM1 and known immunomodulatory regulators such as IDO, I identified several potential immunomodulatory biomarkers such as SERPING1^{+}, SERPINB7^{+}, and PDGFRB^{-} (**Table 3**). To gain a better understanding of the intracellular mechanisms of immunomodulation, I conducted RNA sequencing on early and late passage UC-MSCs. I identified numerous signaling pathways including the PI3K-AKT signaling pathway, which potentially regulates immunomodulatory ability. Finally, I developed a humanized mouse model for sepsis that can be used to test the therapeutic efficacy of identified immunomodulatory UC-MSCs for the development of cellular therapies.

4.1 UC-MSC Immunomodulatory ability negatively correlates with differentiation

Despite the profound impact *in vitro* culture has on MSC function, very little is known of how culture influences the molecular mechanisms that govern MSC immunomodulation.[111] Previous studies have shown that *in vitro* culture influences MSC potency, metabolism, growth rate and immunomodulatory ability.[34,111,133] I also found *in vitro* culture of UC-MSCs results in the significant reduction of immunomodulatory ability and growth rate (**Figures 5-6**). Therefore,

I hypothesized that the regulation of UC-MSC differentiation, metabolism, proliferation, and immunomodulation are intrinsically linked in some manner. To explore the role of MSC potency and differentiation on immunomodulation, I examined our proteomic transcriptomic datasets for evidence of differentiation in late passage MSCs. While key adipogenic, chondrogenic, and osteogenic lineage markers were not upregulated in later passage UC-MSCs, functional enrichment analysis of early versus late passage HUCPVC6 revealed the *mesenchymal cell differentiation* ontological term was up regulated in late passage HUCPVCs. Moreover, early passage UC-MSCs exhibited a downregulation of regulators of MSC differentiation. For example, PDGFRB, which was downregulated in both our transcriptomic and proteomic HUCPVC datasets (**Table 3**), has been shown to promote differentiation in MSCs.[134] SOX11, a transcriptional factor that has been shown to suppress MSC self-renewal and promote MSC differentiation, was also upregulated in late passage UC-MSCs.[135,136] Thus, immunomodulatory ability and differentiation activation appear to be negatively correlated.

Jones et al. and Nasef et al. demonstrated a positive correlation between the tryptophan catabolic pathway and MSC immunomodulatory ability in 2007.[137,138] Our data is consistent with these findings as the tryptophan catabolic pathway was upregulated within the HUCPVC secretome. Moreover, the relationship between MSC metabolism and immunomodulation has long been explored through the optimization of MSC cell culture conditions.[139,140] Our proteomic and transcriptomic analysis yielded a number of enriched metabolic processes, the most upregulated in earlier passage UC-MSCs enrichment glycolysis. Increased glycolysis has been observed in MSCs grown in hypoxic conditions, which have significant effects on MSC viability, proliferation, and differentiation.[141–143] I found that UC-MSCs cultured in hypoxic conditions marginally suppressed T cell proliferation. Since both early and late passage cells were cultured in hypoxic

culture conditions, and others have reported that MSCs exhibit similar immunomodulatory abilities under normoxic and hypoxic conditions,[141,144] other factors beyond hypoxia must be upregulating glycolysis in early passage UC-MSCs. Interestingly, decreases in glycolysis and increases in oxidative phosphorylation are indicative of MSC differentiation.[141,145] Moreover, Dr. Mario Joliceur, our collaborator, examined intracellular and extracellular metabolites between early and late passage UC-MSCs to correlate metabolomic differences with immunomodulatory ability.[146] They also found a significant upregulation of glycolysis in immunomodulatory early passage WJ-MSCs.[146] These findings are consistent with a downregulation of differentiation and explains the difference between early and late passage UC-MSCs. Therefore, I hypothesize that *in vitro* culture of UC-MSCs causes them to enter a "poised" state, wherein they have not differentiated but are more likely to differentiate and are consequently less able to immunomodulate. This state is likely the result of culture conditions pushing MSCs towards differentiation. To ascertain if the two phenotypes (poised and immunomodulatory) are negatively correlated, future experiments will be conducted to determine decreases in immunomodulatory ability in differentiating MSCs via induction in differentiation media. Early and late passage MSCs will be collected, induced to differentiate, and co-cultured with immune cells at various time points to determine when the loss of immunomodulatory ability occurs. Conversely, regulators that govern self-renewal such as SOX11 and PDGFR can be selectively overexpressed then immunomodulatory ability tested, and RNA sequencing and ChIP experiments conducted to identify potential small molecule targets. Ultimately, these findings would help optimize therapeutic MSC culture and expansion for clinical trials.

4.2 Role of cytokine competency in UC-MSC immunomodulatory ability

Cytokines are important mediators of the human innate and adaptive immune response. Consequently, one of the greatest potential assets of a MSC based cellular therapy is their sensitivity to cytokines, since their ability to modulate their immunosuppressive function is highly dependent on the presence of proinflammatory cytokines (**Figure 6**).[36] However, when I investigated the effect of proinflammatory cytokines on the immunomodulation of UC-MSCs, I observed that IFNγ and TNFα induction of UC-MSCs from different MSC donors produced variable effects on their immunomodulatory abilities (**Figure 4**). These results suggest that MSC immunomodulatory ability has varying levels of potency or multiple independent control mechanisms that are influenced by extrinsic cellular factors. This variability between UC-MSC donors is likely caused by differences in UC-MSC immunomodulatory capacity if both the primed and unprimed UC-MSCs are consistent. However, it is possible that the variability observed is due to differences in UC-MSC sensitivity to cytokine activation. Interestingly, when I examined the effect of cytokine induction on immunomodulation in MSCs between early and late passages from the same donor, I found that the effect of cytokine induction appears more muted in later passage cells from the same donor (**Figures 6**-7). In fact, the term *cellular response to cytokine stimulus* was functionally enriched in early versus late passage UC-MSCs. Thus, a potential explanation for the observed reduction in immunomodulatory capacity after *in vitro* passage could be a reduction in cytokine competency. While the classical IFNγ and TNFα receptors (IFNAR and CD120) were not downregulated in late passage UC-MSCs, other associated TNF receptors such as TNFRSF10A and CD40 were downregulated in late passage UC-MSCs. Furthermore, a loss in competency could have a multiplicative effect on immunomodulatory inactivation, as MSCs also secrete cytokines that influence neighboring MSCs. For example, IL-6, a cytokine commonly

secreted by MSCs, has been shown to regulate MSC stemness in the bone marrow.[147] Therefore, later passage MSCs may have a diminished capacity to become induced into a more immunomodulatory state. Future experiments can interrogate immunomodulatory regulation by selectively inhibiting pathways that are activated by inflammatory cytokines in early versus late passage UC-MSCs and examining its impact on immunomodulation between the two passages. Moreover, it is possible that while cytokine binding is occurring, downstream signal translation is being blocked or entirely absent. I observed a reduction in AKT phosphorylation between induced early and late passage UC-MSCs (**Figure 20**). It is possible that the lack of PI3K-AKT phosphorylation in late passage MSCs could be evident of a block in the cytokine signal cascade, since IFNγ directly activates the pathway. I also found that MAPK and NFκB signaling pathways were upregulated in early passage UC-MSCs through our RNA-sequencing analysis, where both pathways are essential for Toll-like receptor mediated cytokine secretion.[148–150] Future experiments could artificially activate downstream pathways such as the PI3K-AKT, MAPK, and NFκB signaling pathway in late passage UC-MSCs to examine whether immunomodulatory phenotype can be rescued.

4.3 Serpin protease inhibitors as markers for therapeutic MSC subpopulations

One particular group of genes that consistently appeared as highly upregulated in both early passage WJ-MSC and HUCPVC transcriptomic DEGs were Serpin protease inhibitors (SERPINs). As the name suggests, SERPINs inhibit extracellular serine proteases.[151,152] SERPINs have also been observed to have catalytic activity of other proteases such as cysteine proteases.[151] Serine proteases are essential in the regulation of blood clotting and in the immune and inflammatory response. Massber et al. demonstrated blood neutrophils regulated coagulation through SERPIN activity (neutrophil elastase and cathepsin).[153] Interestingly, Massberg et al. asserted that the

SERPIN mediated coagulation would compartmentalize infection and participate in the innate immune response. Moreover, C1-inhibitors inhibit the complement system via cleavage of C1 and prevention of C1 binding to antigen-antibody complexes. SERPING1, a C1-inhibtor, was in fact upregulated in early passage HUCPVCs. Thus, MSC expression of SERPINs may play similar roles in regulating the immune response and coagulation. SERPINB2 was also upregulated in both WJ-MSCs and HUCPVCs and has been shown to inhibit human bone marrow stromal cell differentiation, supporting our previous hypothesis of a downregulation of differentiation.[151] Additionally, SERPINs have been found to aid in MSC immune privileged state in mice, through SERPIN9 cleavage of granzyme B (grB).[154] In fact, SERPIN9 is expressed in a number of immune privileged tissues such as the placenta and brain.[155] Therefore, the identification of SERPINs could represent an important set of biomarkers that identify undifferentiated, immunomodulatory, immunoevasive, and anti-coagulant MSCs: all characteristics that are ideal for application as a cellular therapy.

4.4 Inflammatory phase of CSP model

The development of an *in vivo* model that consistently simulates DIIRs observed in human patients is critical to understand the complex molecular and cellular dysfunction associated with various DIIRs and ultimately to develop effective therapies. In our humanized CSP mouse model of sepsis, a human sepsis response were reliably recapitulated, in contrast to the commonly used CLP model.[118,119] This reproducibility and consistency is vital to the development of MSC cellular therapies, as any variability in the model system will exacerbate any heterogeneity associated with the therapy. Along the same lines, understanding precisely what aspects of a human disease the model system represents is important to understanding and applying the results of *in vivo* experiments to improve potential therapeutics. Therefore, due to the dynamic nature of the sepsis

response, I examined the extent our humanized CSP mouse model recapitulated sepsis pathophysiology. During sepsis, the initial pro-inflammatory response to the infection is often paralleled by a strong anti-inflammatory response.[120,156,157] As sepsis progresses, immune cells exhibit a decreased responsiveness to inflammatory stimuli or immunoparalysis,[157,158] ultimately inducing an immunosuppressive state, which can be potentially lethal since patients are vulnerable to secondary infections.[67,157,158] Significantly elevated levels of both pro- and anti-inflammatory cytokines, which are currently being studied as potential clinical biomarkers for sepsis,[159] were indeed observed in CSP treated humanized mice, indicative of the initial pro-inflammatory phase. Moreover, immune cell organ infiltration, organ dysfunction and the speed at which the CSP treated mice succumbed to the infection indicates that this CSP humanized mouse model recapitulates the initial pro-inflammatory phase of sepsis. Interestingly, the increased lymphocyte apoptosis observed in the spleen and PB of CSP treated mice may represent the transitioning to the early stages of the immunosuppressive phase of sepsis.

4.5 Role of Humanized mouse model on sepsis response

Humanized mice have been used to model various medical conditions including infectious diseases, cancer and immune disorders to enable significant advances in preclinical studies in the development of therapies to treat these conditions.[94,95,159–162] The efficacy of humanized mice to recapitulate the human immune system depends on the ability of the immunodeficient mouse background to support human immune cell development. While the NSG model greatly improved the engraftment of human tissues, the NSG background does not fully facilitate human immune development. Other immunodeficient mouse strains have since been developed that provide potential backgrounds for the application of our CSP sepsis model. The NOD-Rag1^{null} IL2rγ^{null} (NRG) background introduced a Rag1 mutation that blocks T and B cell differentiation earlier and

more robustly than the SCID defect.[156,163] NSG mice also are unable to effectively reconstitute myeloid cells, largely due to the lack of niche factors essential for early hematopoietic differentiation.[163,164] MISTRG knock-in genes for human cytokines M-CSF, human IL-3, GM-CSF and TPO, on top of bearing a BAC-transgene encoding human SIRPα to facilitate myeloid development, enabled unprecedented levels and diversity of human myelomonocytic cell engraftment.[165] Thus, the application of our CSP model in other immunodeficient backgrounds may allow better recapitulation of the human response and a deeper understanding of how the different immune cell populations contribute to the sepsis response.

4.6 Impact of pathogen induction on sepsis

While any bacterium can induce sepsis, the type and severity of the septic state is dependent on the type of infecting bacterium. Common sepsis-inducing pathogens include *Staphylococcus aureus, Escherichia coli, Streptococcus pyogenes,* and *Pseudomonas aeruginosa*.[166] While both gram-negative and gram-positive bacteria appear to induce sepsis, the initial inflammatory response triggered is sensitive to different stimuli mechanisms.[68,167] For example, gram-negative bacteria have been observed to induce sepsis through the release of excess amounts of endotoxins such as Lipopolysaccharides (LPS).[68] Endotoxins are recognized by Toll like receptors and activate the release of proinflammatory cytokines, which can induce an immune reaction.[168] On the other hand, gram-positive bacterium such as *Staphylococcus aureus* can secrete super antigens that are capable of activating T helper cells through directly binding to MHC-II sites and T cell receptors.[166] Sepsis can even be induced by fungi and other foreign organisms.[68] Moreover, while sepsis is most commonly caused by a single infection, multiple pathogens have been observed in some patients.[169] The mechanisms by which sepsis is induced may be dependent on the inducing pathogens. Our CSP procedure induced sepsis using a large variety of bacterium found within the

cecal contents of black 6 mice, including numerous anaerobes and aerobes (**Table 4-5**). As a result, our CSP model may not recapitulate the exact sepsis response induced by other common pathogens. However, the same method of bacterial tittering and dosing employed by our CSP model can be applied to any bacterial source to determine the proper lethal dose. Furthermore, the same downstream experiments may be employed to characterize and compare the sepsis response of various inducing pathogens. In fact, we are currently testing the ability of *Staphylococcus aureus* to induced sepsis within our humanized mice. Ultimately, we hope to develop a cellular therapy using immunomodulatory MSCs to treat sepsis as induced by any pathogen.

4.7 Conclusion

MSC cellular therapy is a promising therapeutic for the treatment of DIIRs, however there remain numerous hurdles that must be overcome to improve therapeutic efficacy. In particular, MSC immunomodulatory heterogeneity has hampered clinical trials by introducing variability into treatment. In this study, I discovered potential biomarkers for the isolation of robust immunomodulatory MSCs. Moreover, I have gained insights into the mechanisms that regulate MSC immunomodulation, which may be applied to developing culture conditions and small molecules to optimize MSC therapeutic efficacy. Finally, I developed a humanized mouse model for sepsis to robustly test MSC therapeutic efficacy, facilitating clinical translation. Altogether, the findings of this study can be applied to the development of robust MSC cellular therapies for the treatment of DIIRs.

Works Cited

1. Matthay, M. A., Pati, S. & Lee, J.-W. Concise Review: Mesenchymal Stem (Stromal) Cells: Biology and Preclinical Evidence for Therapeutic Potential for Organ Dysfunction Following Trauma or Sepsis. *Stem Cells Dayt. Ohio* **35,** 316–324 (2017).
2. Soleimani, M. & Nadri, S. A protocol for isolation and culture of mesenchymal stem cells from mouse bone marrow. *Nat. Protoc.* **4,** 102–106 (2009).
3. Siegel, G., Schäfer, R. & Dazzi, F. The immunosuppressive properties of mesenchymal stem cells. *Transplantation* **87,** S45-49 (2009).
4. Pittenger, M. F. *et al.* Multilineage potential of adult human mesenchymal stem cells. *Science* **284,** 143–147 (1999).
5. Crisan, M. *et al.* A perivascular origin for mesenchymal stem cells in multiple human organs. *Cell Stem Cell* **3,** 301–313 (2008).
6. Le Blanc, K., Tammik, L., Sundberg, B., Haynesworth, S. E. & Ringdén, O. Mesenchymal stem cells inhibit and stimulate mixed lymphocyte cultures and mitogenic responses independently of the major histocompatibility complex. *Scand. J. Immunol.* **57,** 11–20 (2003).
7. Krampera, M. *et al.* Bone marrow mesenchymal stem cells inhibit the response of naive and memory antigen-specific T cells to their cognate peptide. *Blood* **101,** 3722–3729 (2003).
8. Horwitz, E. M. *et al.* Isolated allogeneic bone marrow-derived mesenchymal cells engraft and stimulate growth in children with osteogenesis imperfecta: Implications for cell therapy of bone. *Proc. Natl. Acad. Sci. U. S. A.* **99,** 8932–8937 (2002).
9. Klinker, M. W. & Wei, C.-H. Mesenchymal stem cells in the treatment of inflammatory and autoimmune diseases in experimental animal models. *World J. Stem Cells* **7,** 556–567 (2015).
10. Corcione, A. *et al.* Human mesenchymal stem cells modulate B-cell functions. *Blood* **107,** 367–372 (2006).
11. Bartholomew, A. *et al.* Mesenchymal stem cells suppress lymphocyte proliferation in vitro and prolong skin graft survival in vivo. *Exp. Hematol.* **30,** 42–48 (2002).
12. Sherwood, E. R. & Toliver-Kinsky, T. Mechanisms of the inflammatory response. *Best Pract. Res. Clin. Anaesthesiol.* **18,** 385–405 (2004).
13. Jr, C. A. J. *et al. Immunobiology*. (Garland Science, 2001).
14. Paul, W. E. Bridging Innate and Adaptive Immunity. *Cell* **147,** 1212–1215 (2011).
15. English, K. Mechanisms of mesenchymal stromal cell immunomodulation. *Immunol. Cell Biol.* **91,** 19–26 (2013).
16. Brown, J. M., Nemeth, K., Kushnir-Sukhov, N. M., Metcalfe, D. D. & Mezey, E. Bone marrow stromal cells inhibit mast cell function via a COX2-dependent mechanism. *Clin. Exp. Allergy J. Br. Soc. Allergy Clin. Immunol.* **41,** 526–534 (2011).
17. Pers, Y.-M., Ruiz, M., Noël, D. & Jorgensen, C. Mesenchymal stem cells for the management of inflammation in osteoarthritis: state of the art and perspectives. *Osteoarthritis Cartilage* **23,** 2027–2035 (2015).
18. Zhang, J. *et al.* The challenges and promises of allogeneic mesenchymal stem cells for use as a cell-based therapy. *Stem Cell Res. Ther.* **6,** (2015).
19. Alberts, B. *et al.* Helper T Cells and Lymphocyte Activation. *Mol. Biol. Cell 4th Ed.* (2002).
20. Fox, J. M., Chamberlain, G., Ashton, B. A. & Middleton, J. Recent advances into the understanding of mesenchymal stem cell trafficking. *Br. J. Haematol.* **137,** 491–502 (2007).
21. Owen, A. & Newsome, P. N. Mesenchymal stromal cell therapy in liver disease: opportunities and lessons to be learnt? *Am. J. Physiol. Gastrointest. Liver Physiol.* **309,** G791-800 (2015).
22. Dranoff, G. Cytokines in cancer pathogenesis and cancer therapy. *Nat. Rev. Cancer* **4,** 11–22 (2004).
23. Gao, F. *et al.* Mesenchymal stem cells and immunomodulation: current status and future prospects. *Cell Death Dis.* **7,** e2062 (2016).

24. Jarvinen, L. *et al.* Lung resident mesenchymal stem cells isolated from human lung allografts inhibit T cell proliferation via a soluble mediator. *J. Immunol. Baltim. Md 1950* **181,** 4389–4396 (2008).
25. Terness, P. *et al.* Inhibition of allogeneic T cell proliferation by indoleamine 2,3-dioxygenase-expressing dendritic cells: mediation of suppression by tryptophan metabolites. *J. Exp. Med.* **196,** 447–457 (2002).
26. Schmidt, S. V., Nino-Castro, A. C. & Schultze, J. L. Regulatory dendritic cells: there is more than just immune activation. *Front. Immunol.* **3,** (2012).
27. Hwu, P. *et al.* Indoleamine 2,3-dioxygenase production by human dendritic cells results in the inhibition of T cell proliferation. *J. Immunol. Baltim. Md 1950* **164,** 3596–3599 (2000).
28. Yagi, H. *et al.* Mesenchymal Stem Cells: Mechanisms of Immunomodulation and Homing. *Cell Transplant.* **19,** 667–679 (2010).
29. Spaggiari, G. M., Capobianco, A., Becchetti, S., Mingari, M. C. & Moretta, L. Mesenchymal stem cell-natural killer cell interactions: evidence that activated NK cells are capable of killing MSCs, whereas MSCs can inhibit IL-2-induced NK-cell proliferation. *Blood* **107,** 1484–1490 (2006).
30. Mokarizadeh, A. *et al.* Microvesicles derived from mesenchymal stem cells: potent organelles for induction of tolerogenic signaling. *Immunol. Lett.* **147,** 47–54 (2012).
31. Zhang, B. *et al.* Mesenchymal stem cells secrete immunologically active exosomes. *Stem Cells Dev.* **23,** 1233–1244 (2014).
32. Akiyama, K. *et al.* Mesenchymal-stem-cell-induced immunoregulation involves FAS-ligand-/FAS-mediated T cell apoptosis. *Cell Stem Cell* **10,** 544–555 (2012).
33. Stem Cell Therapies in Clinical Trials: Progress and Challenges: Cell Stem Cell. Available at: https://www.cell.com/cell-stem-cell/abstract/S1934-5909(15)00267-2. (Accessed: 5th July 2018)
34. Prasad, V. K. *et al.* Efficacy and Safety of Ex Vivo Cultured Adult Human Mesenchymal Stem Cells (Prochymal™) in Pediatric Patients with Severe Refractory Acute Graft-Versus-Host Disease in a Compassionate Use Study. *Biol. Blood Marrow Transplant.* **17,** 534–541 (2011).
35. Bernardo, M. E. & Fibbe, W. E. Mesenchymal stromal cells: sensors and switchers of inflammation. *Cell Stem Cell* **13,** 392–402 (2013).
36. English, K., Barry, F. P., Field-Corbett, C. P. & Mahon, B. P. IFN-gamma and TNF-alpha differentially regulate immunomodulation by murine mesenchymal stem cells. *Immunol. Lett.* **110,** 91–100 (2007).
37. Prasanna, S. J., Gopalakrishnan, D., Shankar, S. R. & Vasandan, A. B. Pro-Inflammatory Cytokines, IFNγ and TNFα, Influence Immune Properties of Human Bone Marrow and Wharton Jelly Mesenchymal Stem Cells Differentially. *PLOS ONE* **5,** e9016 (2010).
38. Polchert, D. *et al.* IFN-gamma activation of mesenchymal stem cells for treatment and prevention of graft versus host disease. *Eur. J. Immunol.* **38,** 1745–1755 (2008).
39. Kelly, M. L. *et al.* TNF receptor 2, not TNF receptor 1 enhances mesenchymal stem cell-mediated cardiac protection following acute ischemia. *Shock Augusta Ga* **33,** 602–607 (2010).
40. Keating, A. How Do Mesenchymal Stromal Cells Suppress T Cells? *Cell Stem Cell* **2,** 106–108 (2008).
41. Nauta, A. J. & Fibbe, W. E. Immunomodulatory properties of mesenchymal stromal cells. *Blood* **110,** 3499–3506 (2007).
42. Ryan, J. M., Barry, F., Murphy, J. M. & Mahon, B. P. Interferon-gamma does not break, but promotes the immunosuppressive capacity of adult human mesenchymal stem cells. *Clin. Exp. Immunol.* **149,** 353–363 (2007).
43. Ankrum, J. A., Ong, J. F. & Karp, J. M. Mesenchymal stem cells: immune evasive, not immune privileged. *Nat. Biotechnol.* **32,** 252–260 (2014).
44. Machado, C. de V., Telles, P. D. da S. & Nascimento, I. L. O. Immunological characteristics of mesenchymal stem cells. *Rev. Bras. Hematol. E Hemoter.* **35,** 62–67 (2013).
45. Ryan, J. M., Barry, F. P., Murphy, J. M. & Mahon, B. P. Mesenchymal stem cells avoid allogeneic rejection. *J. Inflamm. Lond. Engl.* **2,** 8 (2005).

46. Sbano, P. *et al.* Use of donor bone marrow mesenchymal stem cells for treatment of skin allograft rejection in a preclinical rat model. *Arch. Dermatol. Res.* **300,** 115–124 (2008).
47. Batsali, A. K., Kastrinaki, M.-C., Papadaki, H. A. & Pontikoglou, C. Mesenchymal stem cells derived from Wharton's Jelly of the umbilical cord: biological properties and emerging clinical applications. *Curr. Stem Cell Res. Ther.* **8,** 144–155 (2013).
48. Weiss, M. L. *et al.* Human umbilical cord matrix stem cells: preliminary characterization and effect of transplantation in a rodent model of Parkinson's disease. *Stem Cells Dayt. Ohio* **24,** 781–792 (2006).
49. Calió, M. L. *et al.* Transplantation of bone marrow mesenchymal stem cells decreases oxidative stress, apoptosis, and hippocampal damage in brain of a spontaneous stroke model. *Free Radic. Biol. Med.* **70,** 141–154 (2014).
50. Fennema, E. M., Renard, A. J. S., Leusink, A., van Blitterswijk, C. A. & de Boer, J. The effect of bone marrow aspiration strategy on the yield and quality of human mesenchymal stem cells. *Acta Orthop.* **80,** 618–621 (2009).
51. Kalaszczynska, I. & Ferdyn, K. Wharton's Jelly Derived Mesenchymal Stem Cells: Future of Regenerative Medicine? Recent Findings and Clinical Significance. *BioMed Research International* (2015). doi:10.1155/2015/430847
52. Kim, D.-W. *et al.* Wharton's Jelly-Derived Mesenchymal Stem Cells: Phenotypic Characterization and Optimizing Their Therapeutic Potential for Clinical Applications. *Int. J. Mol. Sci.* **14,** 11692–11712 (2013).
53. Chen, X., Yin, Y. & Zhang, J. Sepsis and immune response. *World J. Emerg. Med.* **2,** 88–92 (2011).
54. Karlsson, S. *et al.* Incidence, treatment, and outcome of severe sepsis in ICU-treated adults in Finland: The Finnsepsis study. *Intensive Care Med.* **33,** 435–43 (2007).
55. Bluestone, J. A., Herold, K. & Eisenbarth, G. Genetics, pathogenesis and clinical interventions in type 1 diabetes. *Nature* **464,** 1293–1300 (2010).
56. Marshall, J. C. Why have clinical trials in sepsis failed? *Trends Mol. Med.* **20,** 195–203 (2014).
57. Brehm, M. A., Shultz, L. D., Luban, J. & Greiner, D. L. Overcoming current limitations in humanized mouse research. *J. Infect. Dis.* **208 Suppl 2,** S125-130 (2013).
58. Marks, D. J. B. & Segal, A. W. Innate immunity in inflammatory bowel disease: a disease hypothesis. *J. Pathol.* **214,** 260–266 (2008).
59. Boomer, J. S. *et al.* Immunosuppression in patients who die of sepsis and multiple organ failure. *JAMA* **306,** 2594–2605 (2011).
60. Sartor, R. B. Mechanisms of disease: pathogenesis of Crohn's disease and ulcerative colitis. *Nat. Clin. Pract. Gastroenterol. Hepatol.* **3,** 390–407 (2006).
61. Atreya, I., Atreya, R. & Neurath, M. F. NF-kappaB in inflammatory bowel disease. *J. Intern. Med.* **263,** 591–596 (2008).
62. Squillaro, T., Peluso, G. & Galderisi, U. Clinical Trials with Mesenchymal Stem Cells: An Update. *Cell Transplant.* **25,** 829–848 (2016).
63. Rhodes, A. *et al.* Surviving Sepsis Campaign: International Guidelines for Management of Sepsis and Septic Shock: 2016. *Intensive Care Med.* **43,** 304–377 (2017).
64. Minasyan, H. Sepsis and septic shock: Pathogenesis and treatment perspectives. *J. Crit. Care* **40,** 229–242 (2017).
65. Park, S.-K. *et al.* The effect of early goal-directed therapy for treatment of severe sepsis or septic shock: A systemic review and meta-analysis. *J. Crit. Care* **38,** 115–122 (2017).
66. Fink, M. P. & Warren, H. S. Strategies to improve drug development for sepsis. *Nat. Rev. Drug Discov.* **13,** 741–758 (2014).
67. Sundar, K. M. & Sires, M. Sepsis induced immunosuppression: Implications for secondary infections and complications. *Indian J. Crit. Care Med. Peer-Rev. Off. Publ. Indian Soc. Crit. Care Med.* **17,** 162–169 (2013).

68. Martin, G. S. Sepsis, severe sepsis and septic shock: changes in incidence, pathogens and outcomes. *Expert Rev. Anti Infect. Ther.* **10,** 701–706 (2012).
69. Gotts, J. E. & Matthay, M. A. Sepsis: pathophysiology and clinical management. *BMJ* **353,** i1585 (2016).
70. Chang, K. *et al.* Targeting the programmed cell death 1: programmed cell death ligand 1 pathway reverses T cell exhaustion in patients with sepsis. *Crit. Care Lond. Engl.* **18,** R3 (2014).
71. Bosmann, M. & Ward, P. A. The Inflammatory Response in Sepsis. *Trends Immunol.* **34,** 129–136 (2013).
72. Shubin, N. J., Monaghan, S. F. & Ayala, A. Anti-inflammatory mechanisms of sepsis. *Contrib. Microbiol.* **17,** 108–124 (2011).
73. Heidecke, C. D. *et al.* Selective defects of T lymphocyte function in patients with lethal intraabdominal infection. *Am. J. Surg.* **178,** 288–292 (1999).
74. Ward, N. S., Casserly, B. & Ayala, A. The Compensatory Anti-inflammatory Response syndrome (CARS) in Critically ill patients. *Clin. Chest Med.* **29,** 617–viii (2008).
75. O'Sullivan, S. T. *et al.* Major injury leads to predominance of the T helper-2 lymphocyte phenotype and diminished interleukin-12 production associated with decreased resistance to infection. *Ann. Surg.* **222,** 482–490; discussion 490-492 (1995).
76. Rodrick, M. L. *et al.* Defective IL-2 production in patients with severe burns and sepsis. *Lymphokine Res.* **5 Suppl 1,** S75-80 (1986).
77. McIntyre, L. A. *et al.* Cellular Immunotherapy for Septic Shock. A Phase I Clinical Trial. *Am. J. Respir. Crit. Care Med.* **197,** 337–347 (2018).
78. Rizk, M. *et al.* Heterogeneity in Studies of Mesenchymal Stromal Cells to Treat or Prevent Graft-versus-Host Disease: A Scoping Review of the Evidence. *Biol. Blood Marrow Transplant.* **22,** 1416–1423 (2016).
79. Le Blanc, K. *et al.* Treatment of severe acute graft-versus-host disease with third party haploidentical mesenchymal stem cells. *Lancet Lond. Engl.* **363,** 1439–1441 (2004).
80. Hashmi, S. *et al.* Survival after mesenchymal stromal cell therapy in steroid-refractory acute graft-versus-host disease: systematic review and meta-analysis. *Lancet Haematol.* **3,** e45-52 (2016).
81. Galipeau, J. & Sensébé, L. Mesenchymal Stromal Cells: Clinical Challenges and Therapeutic Opportunities. *Cell Stem Cell* **22,** 824–833 (2018).
82. Ezquer, F. E., Ezquer, M. E., Vicencio, J. M. & Calligaris, S. D. Two complementary strategies to improve cell engraftment in mesenchymal stem cell-based therapy: Increasing transplanted cell resistance and increasing tissue receptivity. *Cell Adhes. Migr.* **11,** 110–119 (2016).
83. Wei, X. *et al.* Mesenchymal stem cells: a new trend for cell therapy. *Acta Pharmacol. Sin.* **34,** 747–754 (2013).
84. Phinney, D. G. *et al.* Donor variation in the growth properties and osteogenic potential of human marrow stromal cells. *J. Cell. Biochem.* **75,** 424–436 (1999).
85. Wang, X. *et al.* Myogenic differentiation and reparative activity of stromal cells derived from pericardial adipose in comparison to subcutaneous origin. *Stem Cell Res. Ther.* **5,** 92 (2014).
86. Schimke, M. M., Marozin, S. & Lepperdinger, G. Patient-Specific Age: The Other Side of the Coin in Advanced Mesenchymal Stem Cell Therapy. *Front. Physiol.* **6,** (2015).
87. O'Connor, K. C. *et al.* High-capacity assay to quantify the clonal heterogeneity in potency of mesenchymal stem cells. *BMC Proc.* **5,** O14 (2011).
88. Phinney, D. G., Kopen, G., Isaacson, R. L. & Prockop, D. J. Plastic adherent stromal cells from the bone marrow of commonly used strains of inbred mice: variations in yield, growth, and differentiation. *J. Cell. Biochem.* **72,** 570–585 (1999).
89. Jiang, L. *et al.* Cartilage regeneration by selected chondrogenic clonal mesenchymal stem cells in the collagenase-induced monkey osteoarthritis model. *J. Tissue Eng. Regen. Med.* **8,** 896–905 (2014).
90. Xie, L., Zeng, X., Hu, J. & Chen, Q. Characterization of Nestin, a Selective Marker for Bone Marrow Derived Mesenchymal Stem Cells. *Stem Cells International* (2015). doi:10.1155/2015/762098

91. Yang, Z. X. *et al.* CD106 Identifies a Subpopulation of Mesenchymal Stem Cells with Unique Immunomodulatory Properties. *PLOS ONE* **8,** e59354 (2013).
92. McLeod, C. M. & Mauck, R. L. On the origin and impact of mesenchymal stem cell heterogeneity: new insights and emerging tools for single cell analysis. *Eur. Cell. Mater.* **34,** 217–231 (2017).
93. Translation of Research Evidence From Animals to Humans | JAMA | JAMA Network. Available at: https://jamanetwork.com/journals/jama/article-abstract/203577. (Accessed: 5th July 2018)
94. Hoffman, R. M. Patient-derived orthotopic xenografts: better mimic of metastasis than subcutaneous xenografts. *Nature Reviews Cancer* (2015). doi:10.1038/nrc3972
95. Lai, Y. *et al.* Current status and perspectives of patient-derived xenograft models in cancer research. *J. Hematol. Oncol.J Hematol Oncol* **10,** 106 (2017).
96. Dejager, L., Pinheiro, I., Dejonckheere, E. & Libert, C. Cecal ligation and puncture: the gold standard model for polymicrobial sepsis? *Trends Microbiol.* **19,** 198–208 (2011).
97. Schabbauer, G. Polymicrobial sepsis models: CLP versus CASP. *Drug Discov. Today Dis. Models* **9,** e17–e21 (2012).
98. Rittirsch, D., Hoesel, L. M. & Ward, P. A. The disconnect between animal models of sepsis and human sepsis. *J. Leukoc. Biol.* **81,** 137–143 (2007).
99. Seok, J. *et al.* Genomic responses in mouse models poorly mimic human inflammatory diseases. *Proc. Natl. Acad. Sci.* **110,** 3507–3512 (2013).
100. Sarkar, P., Randall, S. M., Muddiman, D. C. & Rao, B. M. Targeted Proteomics of the Secretory Pathway Reveals the Secretome of Mouse Embryonic Fibroblasts and Human Embryonic Stem Cells. *Mol. Cell. Proteomics MCP* **11,** 1829–1839 (2012).
101. Awong, G. *et al.* Human proT-cells generated in vitro facilitate hematopoietic stem cell-derived T-lymphopoiesis in vivo and restore thymic architecture. *Blood* **122,** 4210–4219 (2013).
102. Starr, M. E. *et al.* A new cecal slurry preparation protocol with improved long-term reproducibility for animal models of sepsis. *PloS One* **9,** e115705 (2014).
103. Wong, H. R. *et al.* Genomic expression profiling across the pediatric systemic inflammatory response syndrome, sepsis, and septic shock spectrum. *Crit. Care Med.* **37,** 1558–1566 (2009).
104. Chung, T. P. *et al.* Molecular diagnostics in sepsis: from bedside to bench. *J. Am. Coll. Surg.* **203,** 585–598 (2006).
105. Kim, D., Langmead, B. & Salzberg, S. L. HISAT: a fast spliced aligner with low memory requirements. *Nat. Methods* **12,** 357–360 (2015).
106. Liao, Y., Smyth, G. K. & Shi, W. featureCounts: an efficient general purpose program for assigning sequence reads to genomic features. *Bioinforma. Oxf. Engl.* **30,** 923–930 (2014).
107. Love, M. I., Huber, W. & Anders, S. Moderated estimation of fold change and dispersion for RNA-seq data with DESeq2. *Genome Biol.* **15,** 550 (2014).
108. Ashburner, M. *et al.* Gene ontology: tool for the unification of biology. The Gene Ontology Consortium. *Nat. Genet.* **25,** 25–29 (2000).
109. REVIGO Summarizes and Visualizes Long Lists of Gene Ontology Terms. Available at: https://journals.plos.org/plosone/article?id=10.1371/journal.pone.0021800. (Accessed: 9th September 2018)
110. Szklarczyk, D. *et al.* The STRING database in 2017: quality-controlled protein-protein association networks, made broadly accessible. *Nucleic Acids Res.* **45,** D362–D368 (2017).
111. Klinker, M. W., Marklein, R. A., Surdo, J. L. L., Wei, C.-H. & Bauer, S. R. Morphological features of IFN-γ–stimulated mesenchymal stromal cells predict overall immunosuppressive capacity. *Proc. Natl. Acad. Sci.* **114,** E2598–E2607 (2017).
112. Beeravolu, N. *et al.* Isolation and comparative analysis of potential stem/progenitor cells from different regions of human umbilical cord. *Stem Cell Res.* **16,** 696–711 (2016).
113. Beeravolu, N. *et al.* Isolation and comparative analysis of potential stem/progenitor cells from different regions of human umbilical cord. *Stem Cell Res.* **16,** 696–711 (2016).

114. Toscano, M. G., Ganea, D. & Gamero, A. M. Cecal ligation puncture procedure. *J. Vis. Exp. JoVE* (2011). doi:10.3791/2860
115. Buras, J. A., Holzmann, B. & Sitkovsky, M. Animal models of sepsis: setting the stage. *Nat. Rev. Drug Discov.* **4,** 854–865 (2005).
116. Cuenca, A. G., Delano, M. J., Kelly-Scumpia, K. M., Moldawer, L. L. & Efron, P. A. Cecal ligation and puncture. *Curr. Protoc. Immunol.* **Chapter 19,** Unit 19.13 (2010).
117. Ruiz, S. *et al.* Sepsis modeling in mice: ligation length is a major severity factor in cecal ligation and puncture. *Intensive Care Med. Exp.* **4,** (2016).
118. Wichterman, K. A., Baue, A. E. & Chaudry, I. H. Sepsis and septic shock--a review of laboratory models and a proposal. *J. Surg. Res.* **29,** 189–201 (1980).
119. Maier, S. *et al.* Cecal ligation and puncture versus colon ascendens stent peritonitis: two distinct animal models for polymicrobial sepsis. *Shock Augusta Ga* **21,** 505–511 (2004).
120. Unsinger, J., McDonough, J. S., Shultz, L. D., Ferguson, T. A. & Hotchkiss, R. S. Sepsis-induced human lymphocyte apoptosis and cytokine production in 'humanized' mice. *J. Leukoc. Biol.* **86,** 219–227 (2009).
121. de Pablo, R., Monserrat, J., Prieto, A. & Alvarez-Mon, M. Role of circulating lymphocytes in patients with sepsis. *BioMed Res. Int.* **2014,** 671087 (2014).
122. Kushimoto, S. *et al.* The impact of body temperature abnormalities on the disease severity and outcome in patients with severe sepsis: an analysis from a multicenter, prospective survey of severe sepsis. *Crit. Care Lond. Engl.* **17,** R271 (2013).
123. Stearns-Kurosawa, D. J., Osuchowski, M. F., Valentine, C., Kurosawa, S. & Remick, D. G. The Pathogenesis of Sepsis. *Annu. Rev. Pathol.* **6,** 19–48 (2011).
124. Schulte, W., Bernhagen, J. & Bucala, R. *Cytokines in Sepsis: Potent Immunoregulators and Potential Therapeutic Targets—An Updated View*. **2013,** (2013).
125. Giannini, E. G., Testa, R. & Savarino, V. Liver enzyme alteration: a guide for clinicians. *CMAJ Can. Med. Assoc. J. J. Assoc. Medicale Can.* **172,** 367–379 (2005).
126. Adams, D. H., Ju, C., Ramaiah, S. K., Uetrecht, J. & Jaeschke, H. Mechanisms of immune-mediated liver injury. *Toxicol. Sci. Off. J. Soc. Toxicol.* **115,** 307–321 (2010).
127. Souto, F. O. *et al.* Essential role of CCR2 in neutrophil tissue infiltration and multiple organ dysfunction in sepsis. *Am. J. Respir. Crit. Care Med.* **183,** 234–242 (2011).
128. Brown, K. A. *et al.* Neutrophils in development of multiple organ failure in sepsis. *Lancet Lond. Engl.* **368,** 157–169 (2006).
129. Davies, M. J., Hawkins, C. L., Pattison, D. I. & Rees, M. D. Mammalian heme peroxidases: from molecular mechanisms to health implications. *Antioxid. Redox Signal.* **10,** 1199–1234 (2008).
130. van der Veen, B. S., de Winther, M. P. J. & Heeringa, P. Myeloperoxidase: molecular mechanisms of action and their relevance to human health and disease. *Antioxid. Redox Signal.* **11,** 2899–2937 (2009).
131. Hotchkiss, R. S. *et al.* Apoptotic cell death in patients with sepsis, shock, and multiple organ dysfunction. *Crit. Care Med.* **27,** 1230–1251 (1999).
132. Takao, K. & Miyakawa, T. Genomic responses in mouse models greatly mimic human inflammatory diseases. *Proc. Natl. Acad. Sci.* **112,** 1167–1172 (2015).
133. Liu, Y. & Ma, T. Metabolic regulation of mesenchymal stem cell in expansion and therapeutic application. *Biotechnol. Prog.* **31,** 468–481 (2015).
134. Ball, S. G., Shuttleworth, A. & Kielty, C. M. Inhibition of platelet-derived growth factor receptor signaling regulates Oct4 and Nanog expression, cell shape, and mesenchymal stem cell potency. *Stem Cells Dayt. Ohio* **30,** 548–560 (2012).
135. Kubo, H. *et al.* Identification of mesenchymal stem cell (MSC)-transcription factors by microarray and knockdown analyses, and signature molecule-marked MSC in bone marrow by immunohistochemistry. *Genes Cells Devoted Mol. Cell. Mech.* **14,** 407–424 (2009).

136. Xu, L. *et al.* Sox11-modified mesenchymal stem cells (MSCs) accelerate bone fracture healing: Sox11 regulates differentiation and migration of MSCs. *FASEB J. Off. Publ. Fed. Am. Soc. Exp. Biol.* **29,** 1143–1152 (2015).
137. Jones, B. J., Brooke, G., Atkinson, K. & McTaggart, S. J. Immunosuppression by placental indoleamine 2,3-dioxygenase: a role for mesenchymal stem cells. *Placenta* **28,** 1174–1181 (2007).
138. Nasef, A. *et al.* Identification of IL-10 and TGF-beta transcripts involved in the inhibition of T-lymphocyte proliferation during cell contact with human mesenchymal stem cells. *Gene Expr.* **13,** 217–226 (2007).
139. Samuelsson, H., Ringdén, O., Lönnies, H. & Le Blanc, K. Optimizing in vitro conditions for immunomodulation and expansion of mesenchymal stromal cells. *Cytotherapy* **11,** 129–136 (2009).
140. Killer, M. C. *et al.* Immunosuppressive capacity of mesenchymal stem cells correlates with metabolic activity and can be enhanced by valproic acid. *Stem Cell Res. Ther.* **8,** (2017).
141. Ahmed, N. E.-M. B., Murakami, M., Kaneko, S. & Nakashima, M. The effects of hypoxia on the stemness properties of human dental pulp stem cells (DPSCs). *Sci. Rep.* **6,** 35476 (2016).
142. Buravkova, L. B., Andreeva, E. R., Gogvadze, V. & Zhivotovsky, B. Mesenchymal stem cells and hypoxia: where are we? *Mitochondrion* **19 Pt A,** 105–112 (2014).
143. Ejtehadifar, M. *et al.* The Effect of Hypoxia on Mesenchymal Stem Cell Biology. *Adv. Pharm. Bull.* **5,** 141–149 (2015).
144. Roemeling-van Rhijn, M. *et al.* Effects of Hypoxia on the Immunomodulatory Properties of Adipose Tissue-Derived Mesenchymal Stem cells. *Front. Immunol.* **4,** (2013).
145. Shum, L. C., White, N. S., Mills, B. N., de Mesy Bentley, K. L. & Eliseev, R. A. Energy Metabolism in Mesenchymal Stem Cells During Osteogenic Differentiation. *Stem Cells Dev.* **25,** 114–122 (2016).
146. Laflaquière, B. *et al.* Identifying Biomarkers of Wharton's Jelly Mesenchymal Stromal Cells Using a Dynamic Metabolic Model: The Cell Passage Effect. *Metabolites* **8,** (2018).
147. Pricola, K. L., Kuhn, N. Z., Haleem-Smith, H., Song, Y. & Tuan, R. S. Interleukin-6 Maintains Bone Marrow-Derived Mesenchymal Stem Cell Stemness by an ERK1/2-Dependent Mechanism. *J. Cell. Biochem.* **108,** 577–588 (2009).
148. Liotta, F. *et al.* Toll-like receptors 3 and 4 are expressed by human bone marrow-derived mesenchymal stem cells and can inhibit their T-cell modulatory activity by impairing Notch signaling. *Stem Cells Dayt. Ohio* **26,** 279–289 (2008).
149. Opitz, C. A. *et al.* Toll-like receptor engagement enhances the immunosuppressive properties of human bone marrow-derived mesenchymal stem cells by inducing indoleamine-2,3-dioxygenase-1 via interferon-beta and protein kinase R. *Stem Cells Dayt. Ohio* **27,** 909–919 (2009).
150. Tomchuck, S. L. *et al.* Toll-like receptors on human mesenchymal stem cells drive their migration and immunomodulating responses. *Stem Cells Dayt. Ohio* **26,** 99–107 (2008).
151. Elsafadi, M. *et al.* SERPINB2 is a novel TGFβ-responsive lineage fate determinant of human bone marrow stromal cells. *Sci. Rep.* **7,** 10797 (2017).
152. Law, R. H. *et al.* An overview of the serpin superfamily. *Genome Biol.* **7,** 216 (2006).
153. Massberg, S. *et al.* Reciprocal coupling of coagulation and innate immunity via neutrophil serine proteases. *Nat. Med.* **16,** 887–896 (2010).
154. El Haddad, N. *et al.* Mesenchymal stem cells express serine protease inhibitor to evade the host immune response. *Blood* **117,** 1176–1183 (2011).
155. Bladergroen, B. A. *et al.* The granzyme B inhibitor, protease inhibitor 9, is mainly expressed by dendritic cells and at immune-privileged sites. *J. Immunol. Baltim. Md 1950* **166,** 3218–3225 (2001).
156. Belizario, J. Immunodeficient Mouse Models: An Overview. *Open Immunol. J. - OPEN IMMUNOL J* **2,** 79–85 (2009).
157. Hamers, L., Kox, M. & Pickkers, P. Sepsis-induced immunoparalysis: mechanisms, markers, and treatment options. *Minerva Anestesiol.* **81,** 426–439 (2015).
158. Anand, D. *et al.* Proinflammatory versus anti-inflammatory response in sepsis patients: looking at the cytokines. *Crit. Care* **18,** P13 (2014).

159. Jin, L. *et al.* Monoclonal antibody-mediated targeting of CD123, IL-3 receptor alpha chain, eliminates human acute myeloid leukemic stem cells. *Cell Stem Cell* **5,** 31–42 (2009).
160. Shultz, L. D., Ishikawa, F. & Greiner, D. L. Humanized mice in translational biomedical research. *Nat. Rev. Immunol.* **7,** 118–130 (2007).
161. Kumar, P. *et al.* T cell-specific siRNA delivery suppresses HIV-1 infection in humanized mice. *Cell* **134,** 577–586 (2008).
162. Galle-Treger, L. *et al.* Nicotinic acetylcholine receptor agonist attenuates ILC2-dependent airway hyperreactivity. *Nat. Commun.* **7,** 13202 (2016).
163. Shultz, L. D. *et al.* Human lymphoid and myeloid cell development in NOD/LtSz-scid IL2R gamma null mice engrafted with mobilized human hemopoietic stem cells. *J. Immunol. Baltim. Md 1950* **174,** 6477–6489 (2005).
164. Tanaka, S. *et al.* Development of mature and functional human myeloid subsets in hematopoietic stem cell-engrafted NOD/SCID/IL2rγKO mice. *J. Immunol. Baltim. Md 1950* **188,** 6145–6155 (2012).
165. Rongvaux, A. *et al.* Development and function of human innate immune cells in a humanized mouse model. *Nat. Biotechnol.* **32,** 364–372 (2014).
166. Ramachandran, G. Gram-positive and gram-negative bacterial toxins in sepsis: a brief review. *Virulence* **5,** 213–218 (2014).
167. Polat, G., Ugan, R. A., Cadirci, E. & Halici, Z. Sepsis and Septic Shock: Current Treatment Strategies and New Approaches. *Eurasian J. Med.* **49,** 53–58 (2017).
168. Heumann, D. & Roger, T. Initial responses to endotoxins and Gram-negative bacteria. *Clin. Chim. Acta Int. J. Clin. Chem.* **323,** 59–72 (2002).
169. Sriskandan, S. & Cohen, J. The pathogenesis of septic shock. *J. Infect.* **30,** 201–206 (1995).

Curriculum Vitae

EDUCATION

University of Ottawa

M.Sc in Science and Medicine with Specialization in Cellular and Molecular Medicine

2016 – Present | CGPA: 10.0/10.0

B.Sc (Hons) in Biology with Specialization in Cellular and Molecular Biology with a Minor in Classical Studies

2011 – 2016 | CGPA: 9.6/10.0

RESEARCH EXPERIENCE

Ottawa Hospital Research Institute (OHRI) | Dr. W. Stanford | 2014 – Present

Masters Candidate *(Summer 2016-Present):* I am determining biomarkers and gaining mechanistic insights into mesenchymal stromal cell immunomodulatory ability. I have conducted mass spectrometry and RNA sequencing analysis from raw data and validated targets via western blotting and qPCR.

Research Assistant *(Summer 2015):* I studied early human development, specifically analysing RNA sequencing and microarray data related to early placental formation.

Honours Research Project *(Fall 2014-Spring 2015):* I elucidated and validated gene expression patterns of human embryonic stem cell (hESCs) mesendoderm differentiation from RNA sequencing data. Gained proficiency in cell culture, qPCR, R, Python, and MATlab.

Teaching Assistant | University of Ottawa | 2017

I taught the basics of MATlab coding and biological modelling, supervised lab periods, and marked assignments for *Computational Tools for Biological Sciences*.

International Genetically Engineered Machine (iGEM) | Dr. M. Kaern | 2013 – 2014

Investigator *(Jan. 2014- Nov. 2014)***:** I hired, trained, and managed a team of 5 undergraduate researchers to complete a unique research project on cell fate specification. Proficient in molecular and cellular biology techniques such as flow cytometry, PCR, and cloning.

Research Assistant *(May 2013-Nov. 2013):* I built, transformed, and tested synthetic constructs in *Saccharomyces cerevisiae*. Findings were presented at the iGEM Jamboree in Boston.

AWARDS AND SCHOLARSHIPS

2017	Frederick Banting and Charles Best Canada Graduate Scholarship (CIHR) – uOttawa | $17,500
2017	Ontario Graduate Scholarship – uOttawa (not accepted) | $15,000
2017	Stem Cell Network Till and McCulloch Meetings travel award
2016-17	University of Ottawa Excellence Scholarship | $7,729.68
2016	Queen Elizabeth II Graduate Scholarship in Science and Technology – uOttawa | $15,000
2015	Undergraduate Student Research Award – National Sciences and Engineering Research Council | $4,500
2014	Undergraduate Student Research Award – National Sciences and Engineering Research Council | $4,500
2014	Silver Medal – International Genetically Engineered Machine
2013	Undergraduate Student Research Award – National Sciences and Engineering Research Council | $4,500
2013	Gold Medal – International Genetically Engineered Machine
2011 – 2015	Dean's Honour List – University of Ottawa
2011 – 2015	Renewable Entrance Scholarship – University of Ottawa | $16,000

PUBLICATIONS

D. Siriwardena et al. Humanized Mouse Model of Sepsis Utilizing a Cecal Slurry Puncture Procedure Elicits a Consistent Human Sepsis Response. *Laboratory Investigation.* 2017. *(Under Revision)*

This study was conducted as an aim for my Masters work. I was responsible for 70% of the experiments and analysis, wrote the paper, and prepared the manuscript. In the last 30 years, the over 25 clinical trials designed to test the efficacy of sepsis therapies failed, despite each therapy showing preclinical promise. The disparity between animal models of sepsis and human sepsis patients partly contributes to the failure of sepsis therapies in clinical translation. Our goal was to develop a humanized mouse model that better recapitulates the human condition. I aided in the generation of humanized mice and characterized the cecal slurry used to induce sepsis. I analyzed the humanized mice post-surgery to characterize their response to sepsis and correlated it with the human response.

J. Beal, T. Haddock-Angelli, M. Gershater, K. de Mora, M. Lizarazo, J. Hollenhorst, R. Rettberg, **D. Siriwardena*** et al. Reproducibility of Fluorescent Expression from Engineered Biological Constructs in E. coli. *PLOS: One.* 11(3): e0150182.

Here we aimed to determine the variability introduced by differing laboratories in the expression of synthetic constructs. I participated as an iGEM Interlab Study Contributor. I transformed and validated multiple reporter constructs into E. coli. Once validated, I preformed multiple dose-response experiments using flow cytometry to characterize the promoters and reports of interests.

EXTRACURRICULAR AND VOLUNTEER EXPERIENCE

Stem Cell Talks – 2017-2018

I guided a discussion group of 5-10 high school students for a one-day conference to discuss the basic biology and ethical questions surrounding stem cell research.

Let's Talk Science – 2014-2018

Conducted in-class interactive presentations to elementary school students on scientific topics to inspire interest in science.

Ottawa Regional Science Fair Judge – 2017

Judged health science projects by students grade 7-12 for the partners in research award.

Museum of Classical Antiquities – 2016

Helped conduct research to select artifacts and create text panels for upcoming exhibits, manage the museum, and greet guests.

President of iGEM Club – 2014

I managed a team of 33 undergraduates to raise awareness about synthetic biology by working with community groups such as *Let's Talk Science.* I reached out to biotechnology companies and university faculties to raise over $15,000 for the team.

Battle Royale Lead Organizer – 2013-2014

Battle Royale is 24 hour charity gaming event that raised money for Child's Play: an organization provided hospital bound children with toys and games. I planned and ran the 10+ tournaments held during the event and organized a group of 10 volunteers.

Supplementary Primer Sequences

Model	Gene	Forward Primer (5' -> 3')	Reverse Primer (5' -> 3')
Human	*IFIT3*	AGCACAGACCTAACAGCACC	GTGACCTCACTCATGATGGC
Human	*IFIH1*	TGACCCCAGAATTCAAGGAACT	TGCACCATCATTGTTCCCCA
Human	*WARS*	CCCTTAGCTGAATGCAGGGT	GCAGACGAGTCAAGACCAGG
Human	*VCAM1*	GGACCACATCTACGCTGACA	TTGACTGTGATCGGCTTCCC
Human	*IDO*	GATGTCCGTAAGGTCTTGCC	GCGCCTTTAGCAAAGTGTCC
Human	*ADM*	TGGACTTCGGAGTTTTGCCA	CGCAGACCCTGCTAAGAGAG
Human	*CD28*	CCCCTATTTCCCGGACCTTC	TCCTCTTACTCCTCACCCAGAA
Human	*CD55*	TGAAGAGTTCTGCAATCGTAGC	CTTCTGTAACCTGGACGGCA
Human	*CD96*	AGGTGCAGGCTCAACACTTC	GGCTTATTGACCACAATACCAGT
Human	*CD160*	CCAGTCTGGTGGATGCATTA	ACACTACAAACCCCTCAGCC
Human	*GATA3*	GTCCAGCACAGAAGGCAGG	AGCCTTCGCTTGGGCTTAAT
Human	*IL7R*	AGAGAAAGCTCCAACCGGC	GATCCATCTCCCCTGAGCTA
Human	*IL18R1*	GAGATCGCTGCTTCTCACCT	TGCTTCAAATGGCTTCTCTTCA
Human	*ITK*	TAAGCCCAAGCGAAGGCTG	TGTGGTGGTCTGACAGTTCG
Human	*LAT*	GAAGCGTCTCTGGATGGCAG	CTCAGTCTTAGCCGCTCCAG
Human	*LTF*	GCCGTAGGAGGAGTGTTCAG	GCCCTGTTTTCCGCAATGG
Human	*NCF4*	ACCATCAGCACCATCAAGGAC	CAGCGTCCCGGTAATTCAGA
Human	PRF1	AGTGATGTGAGTGGTGGCTG	CATGGAGCTGGAATCCCGTA

Human	TNFAIP6	AGAATTTGTGAGCAGCCCCT	GGCTGCTCGTTCAAGCCATA
Mouse	*Adm*	AAGCCAGCAATCAGAGCGAA	CATCCATTGCTGCGGGAAC
Mouse	*CD55*	TCAGCAACCCAGCATGTACC	GGTCACCACCTGTGTTAGGC
Mouse	*CD96*	GCAACTCCTCAAACCAGCAA	GCAGTGAGTGCCATTCTGGA
Mouse	*CD160*	TGGTGGCCCTTCAAGCTCTA	ATCCGTTTTATGGACCCGGC
Mouse	*Gata3*	GCTCCTTGCTACTCAGGTGAT	GTGTGACCACACTGCACACT
Mouse	*Il7R*	ACCCAAGAATCAAGGAGGATGG	GGGGAGACTAGGCCATACGA
Mouse	*IL18R1*	AGGCAGTGCTTCACATGAGT	TTGCGACGATCATTTCCGAC
Mouse	*Itk*	TGTGGTCGTTTGGTGTACTG	GACCTCGGAATTGCTTCGGT
Mouse	*Lat*	GAGCTGGCCTCTGTGAACTC	TAGTCGGGAGCTTCCTCTCC
Mouse	*Ltf*	GCTGCTTGACCAACAGGTTC	CGGTCGCTATGACGTACTCC
Mouse	*Ncf4*	TGAACTCGGCCTGGATCTGG	CTGCTCAAAGTCGCTCTCTGAT
Mouse	Prf1	TCGCATGTACAGTTTTCGCC	CAGCCGTGATAAAGTGCGTG
Mouse	Tnfaip6	GTCCACGGCTTTGTAGGAAGATAC	GCAGGATCCACTGTGACGTA
Human	GAPDH	TTCTTTTGCGTCGCCAGCCG	TGACCAGGCGCCCAATACGA
Human	EF1α	GCTGGCTTCACTGCTCAGGTGATT	TGCAATGTGAGCCGTGTGGCA
Mouse	Gapdh	CATGGCCTTCCGTGTTCCTA	ACTTGGCAGGTTTCTCCAGG
Mouse	Ef1α	TGGCTTCACTGCTCAGGTGATT	CAGAACAGGAGCGTAGCCAG